VLÁKNA a TEXTIL

FIBRES AND TEXTILES

Ročník 19.
2012

ISSN1335-0617

Indexed in:

Chemical Abstracts,

World Textile Abstracts

EMDASE

Elsevier Biobase

Elsevier GeoAbstracts

Fibres and Textiles (3) 2012
Vlákna a textil (3) 2012

Content

Obsah

Textile materials

Textilné materiály

Za odbornú a jazykovú úroveň príspevkov zodpovedajú autori a prekladatelia.
Príspevky boli prijaté do tlače bez recenzie.

EFFECT OF SODIUM CHLORIDE ON ELECTROSPINNING OF POLY(ETHYLENE OXIDE) FIBERS

Adnan Mazari and Oldřich Jirsák

Faculty of Textile Engineering, Technical University of Liberec
Studentska 2, 461 17 Liberec, Czech Republic
adnanmazari86@gmail.com

Abstract: *Poly(ethylene oxide) (PEO) is one of the most popular polymers used as a raw material for nanofibres production via electrospinning. It is commonly processed from water solutions. PEO nanofibres find many end uses including medical applications because of its non-toxicity. PEO electrospinning process and its throughput can be influenced by various additives. Influence of NaCl on PEO electrospinning is studied in the paper and the results are discussed as a contribution to the understanding of electrospinning mechanism. In this work, water solutions of poly(ethylene oxide) 400 g/mol, with 6% weight percentage, was tested on needle and needle-less electrospinning whereas the ambient parameters (temperature and humidity) were kept constant. The results were examined on SEM and show the impact of NaCl salt on electrospinning fibers and process. Some characteristics of those solutions were measured such as surface tension, electric conductivity and viscosity.*
Keywords: *Sodium chloride effect on electrospinning, Poly(ethylene oxide) fibers, roller electrospinning, needle electrospinning.*

1 INTRODUCTION

The use of electric charge to break up liquids into small particles has been well known and extensively studied for over a century. This is true for both electro spraying, in which low viscosity liquids can be atomized into droplets, and electro spinning, in which viscoelastic liquids can be transformed into filaments of nanometer dimensions. With the emergence of nanotechnology, researchers become more interested in studying the unique properties of nanoscale materials. Electrospinning, an electrostatic fiber fabrication technique has evinced more interest and attention in recent years due to its versatility and potential for applications in diverse fields. The notable applications include in tissue engineering, biosensors, filtration, wound dressings, drug delivery and enzyme immobilization [1]. Using the keyword 'electrospinning' for a search on internet will return a thousand scientific papers, but almost all of them concerned on needle electro spinning technique includes many aspects as mechanism of electrospinning, materials for electro spinning, properties of nanofibers, factors effect to spinning process and to products properties etc, as summarize by in works [2, 3]. Up to now, Nanospider is the unique commercial equipment to produce nanofibrous web by needle-less electrospinning technology. This equipment patented by Jirsak [4], enable to produce membranes collected fibers in a range from 100 to 600 nm of diameter.

2 EXPERIMENTS

PEO with molecular weight 400 g/mol from ALDRICH Company were taken and solutions of 6% weight concentrations are made in water solvent. The polymer samples were then tested on needle-less electrospinning and temperature and relative humidity are kept constant. Different amount of NaCl (ALDRICH quality p.a) is added and polymer solutions are then tested on needle and needle-less electrospinning. Deionized distilled water is taken to make solution. Before electrospinning, some properties of solutions have been measured such as viscosity, surface tension and conductivity. Surface tensions of solutions were measured

by Kruss apparatus using plate method. The conductivities of solutions were measured by conductivity meter OK-102/1 branded Radelkis and viscosity were measured on ROTOVISCO RV1. For all experiments relative humidity is maintained at 65% and temperature was kept at 25°C.

3 RESULTS AND DISCUSSION

Results are evaluated with the pictures from electron microscope, which is then observed on image analysis software to detect the fiber diameter and non-fibrous area. Observations and calculations are done to make a comparison between needle and needle-less electro spinning regarding, conductivity, viscosity, surface tension, fiber quality, throughput, non-fibrous area and effect of NaCl, fiber diameter and fiber diameter distribution.
A very minor difference is noted on the surface tension of sample solutions with different amount of NaCl salt (Table1).

Table 1 Surface tension of 6 wt% PEO (400 g/mol) polymer solution with various content of NaCl at 24°C and RH 65%

NaCl-salt percentage (%)	surface tension (mN/m)
0	69.5
0.1	69.7
0.3	69.4
0.5	69.3
1.0	68.7
1.5	68.9
2.0	69.2

The conductivity of sample solutions rises with the increase of the NaCl salt solution (Figure 1).
The zero shear viscosity of sample solutions rises slightly with the increase of NaCl salt percentage (Figure 2).
The addition of NaCl salt to sample solution caused a huge decrease in throughput of the needle electrospinning process. Huge amount of ions added into solution with addition of NaCl causes a decrease in throughput for needle-less spinning.

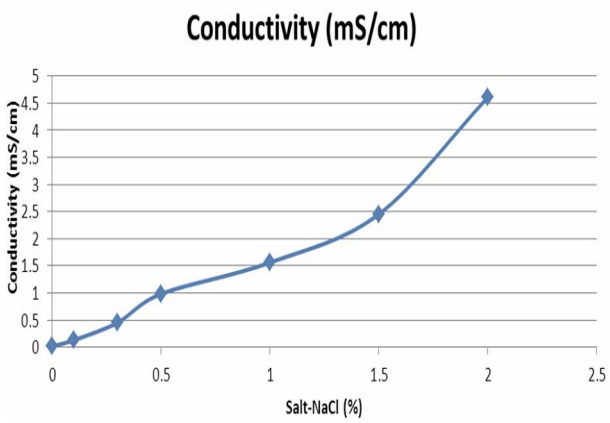

Figure 1 NaCl effect on solution conductivity

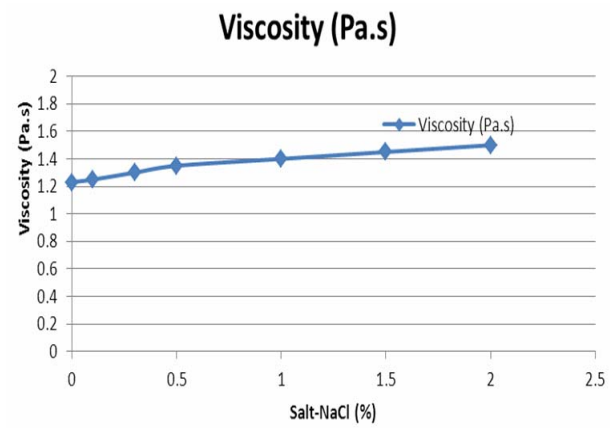

Figure 2 NaCl effect on zero shear viscosity

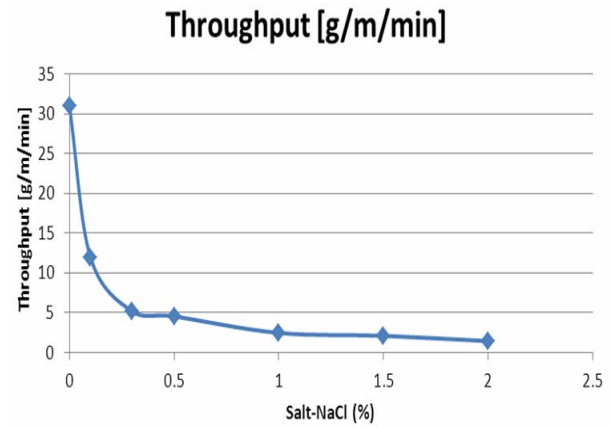

Figure 3 NaCl effect on throughput PEO

Addition of salt caused a major decrease in the non fibrous areas as with the increase percentage of salt, greater number of ions are introduced to the solution and throughput is decreased (Figure 3) which causes better

time for the nanofibers to dry up then to stick together and form a non fibrous areas (Figure 4).

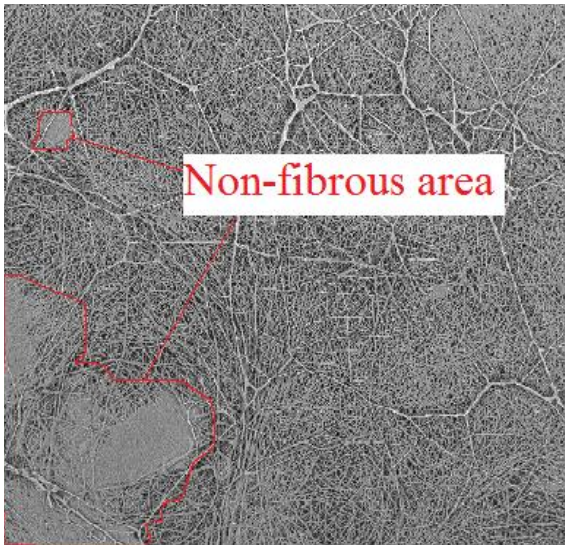

Figure 4 Non-fibrous area

The NFA are decreased with the increased with the increase of NaCl percentage (Figure 6) which is caused by the decrease in throughput (Figure 5).

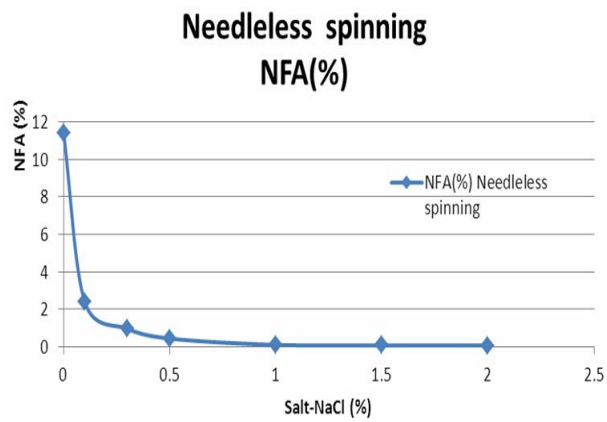

Figure 5 NaCl effect on NFA in needle-less electrospinning

The fiber diameter is much finer in the needle electrospinning with the addition of NaCl salt but the throughput is decreased, where as the needle-less electrospinning shows bigger diameter of nanofibers and high deviations of diameter (Figure 6).

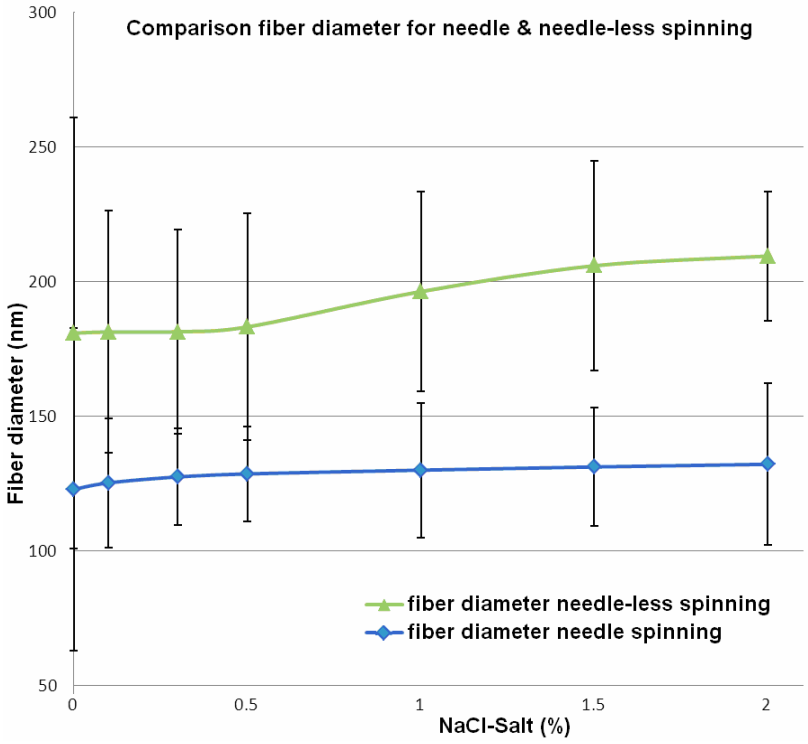

Figure 6 NaCl effect on fiber diameter of needle and needle-less electrospinning

Electron microscope images of individual samples are shown in Figure 7 a-f.

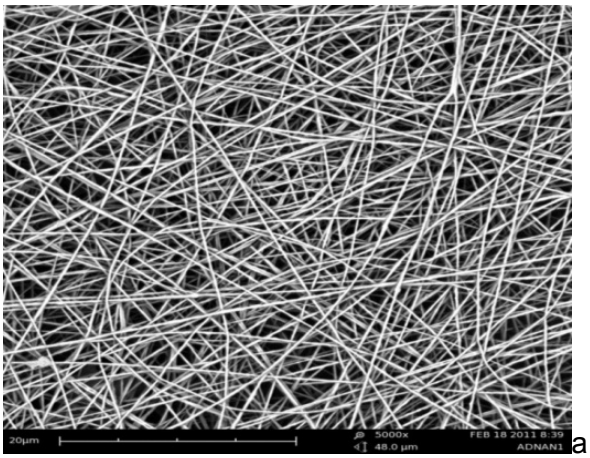

a.

0% NaCl, needle electrospinning

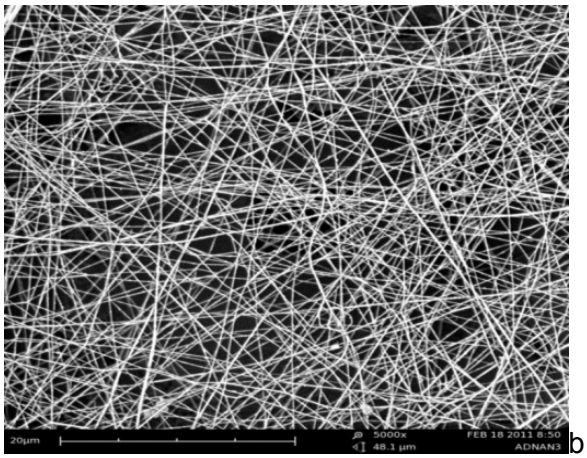

b.

1% NaCl, needle electrospinning

c.

0%NaCl needle-less electrospinning

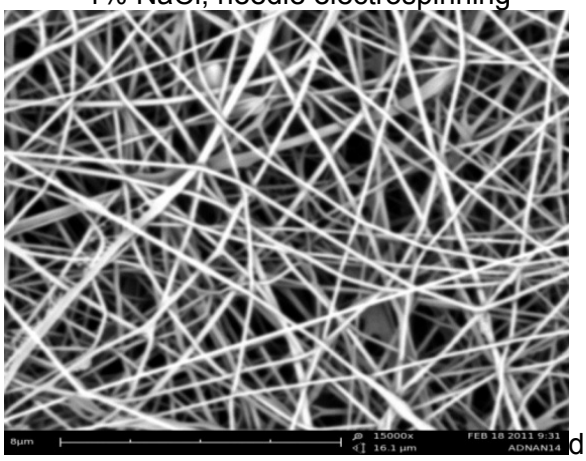

d.

1%NaCl needle-less electrospinning

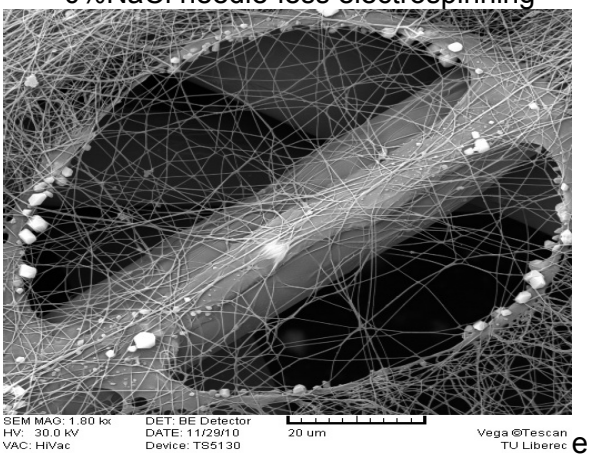

e.

2% NaCl, needle-less electrospinning
(NaCl crystals are clearly visible)

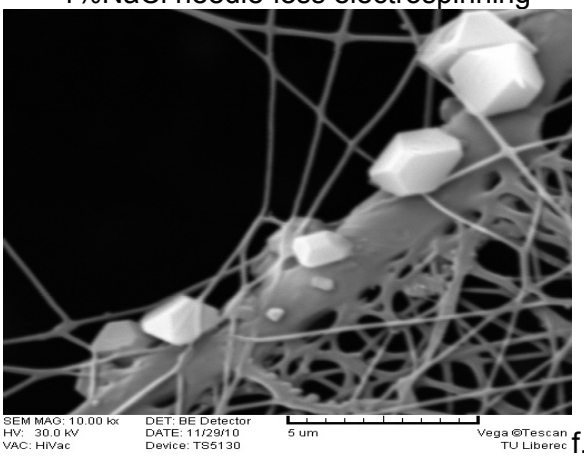

f.

2 %NaCl needle-less electrospinning
(NaCl crystals are clearly visible)

Figure 7 Electron microscope images of individual samples of PEO

Histograms characterizing fiber diameter distribution for individual samples is shown in Figure 8 a-f.

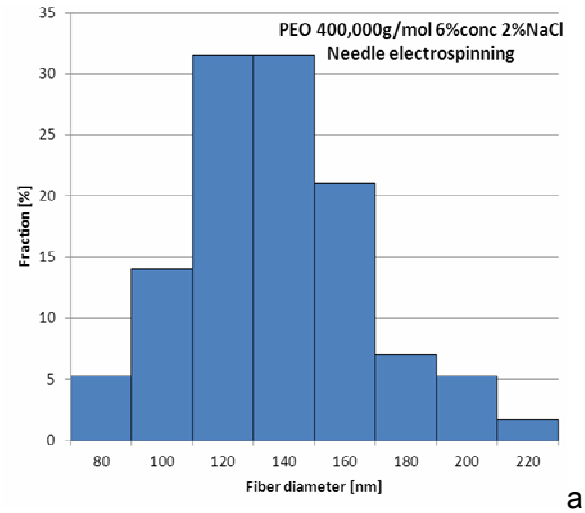

a.

2% NaCl, needle spinning

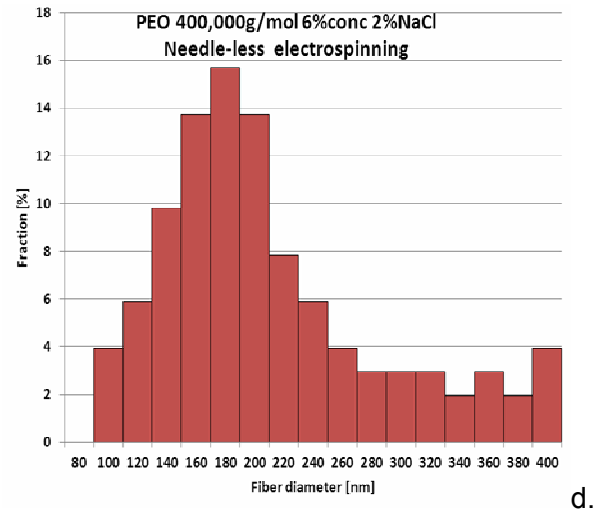

d.

2% NaCl, needle-less spinning

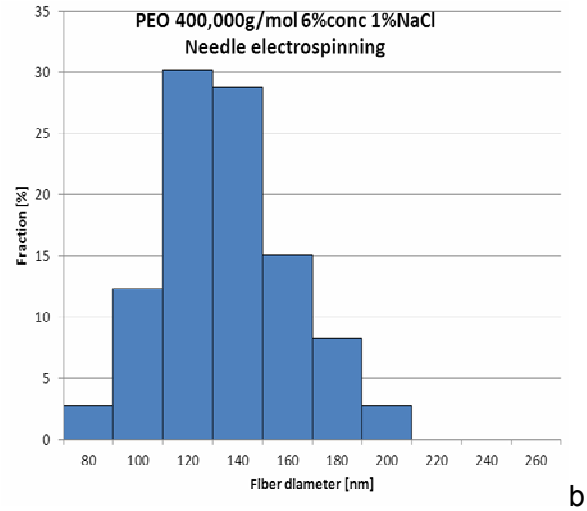

b.

1%NaCl, needle spinning

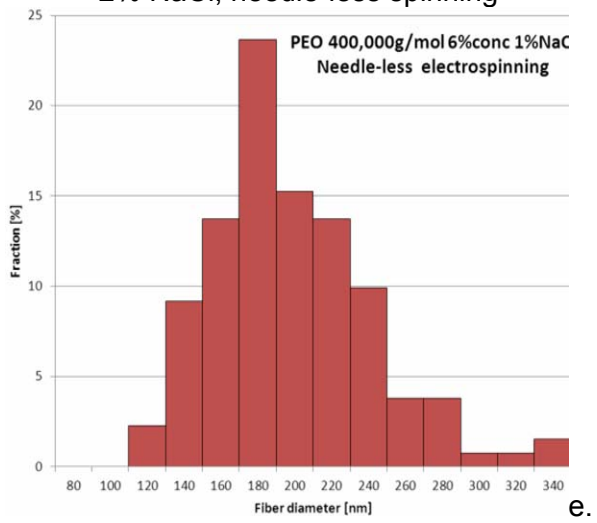

e.

1%NaCl, needle-less spinning

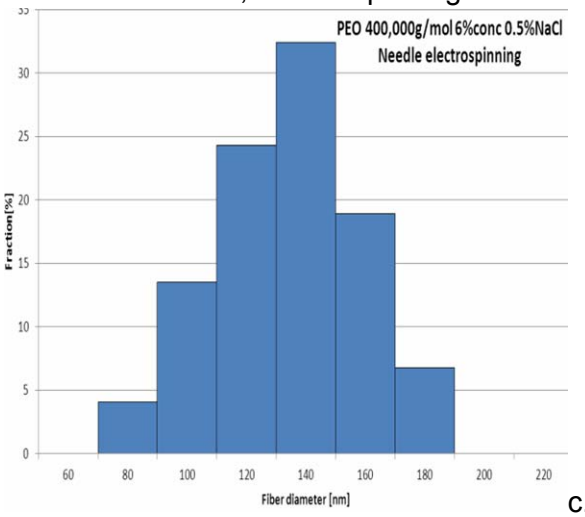

c.

0.5%NaCl, needle spinning

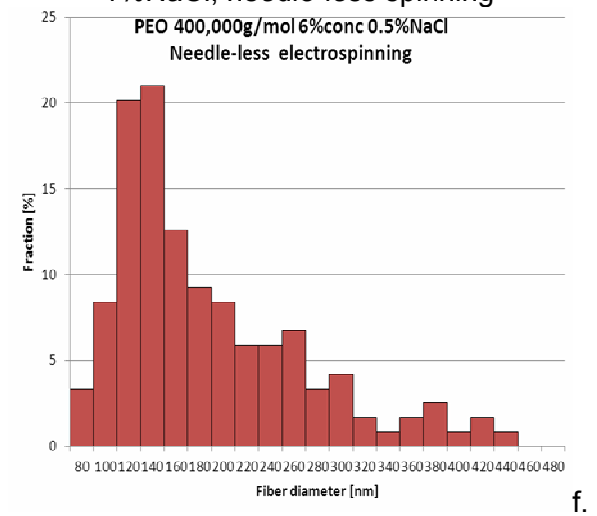

f.

0.5%NaCl, needle-less spinning

Figure 8 Fiber diameter distribution or individual samples of PEO

Based on the above presented graphs and tables the following conclusion can be stated:

- By adding various concentration of sodium chloride, the surface tension and viscosity of PEO polymer solution do not change significantly (Table 1). On the contrary, conductivity of the solution increases strongly with increasing concentration of sodium chloride (Figure 1). It means that sodium chloride does not affect the structure of PEO solutions. This slightly increases the friction coefficient between molecules inside solution. On the other hand, it brings a huge amount of ions into solution which causes conductivity of solution increase strongly.
- Conductivity of spinning solution affects strongly electrospinning dependent parameters, especially the throughput (Figure 3). As huge amount of ions are added in to solution with addition of NaCl that causes a decrease in throughput for needle-less spinning.
- The fiber quality of needle electrospinning is better than needle-less electrospinning, and fiber diameter is less as compare to needle-less electrospinning (Figure 6).
- Adding NaCl decreases the non-fibrous area and fiber diameter distribution in both needle and needle-less electrospinning (Figures 4 and 5).
- Diameter distribution of needle-less electrospinning has higher variability as compared to needle electrospinning (Figure 8)
- Salt percentage above 2% makes the throughput very little with huge amount of salt crystals on the PEO fiber web (Figures 7e and 7f).

4 CONCLUSION

The additive sodium chloride NaCl almost does not affect to surface tension and rheological properties of PEO. In fact it strongly affects electrical properties of PEO. After adding the NaCl the conductivity of PEO solution is increased significantly which causes it's through put to decrease at electrospinning process. Finer and better quality nanofibers are obtained whereas the nonfibrous areas are also reduced with the increase of the NaCl salt percentage. In comparison, the needle electrospinning makes more fine nanofibers than the needle-less electrospinning with the addition of NaCl. Addition of NaCl salt influence the fiber diameter of fibers, higher the concentration higher is the fiber diameter distribution.

5 REFERENCES

1. Fujihara R.K., Teo W., Lim T., Ma Z.: *An introduction to electrospinning and nanofibres*, World Scientific Publishing Co., Singapore, 2005
2. Anthony L.A.: *Science and Technology of Polymer Nanofibers*; John Wiley & Sons, Inc., Hoboken, New Jersey, 2008
3. Stanger M.J., Tucker N., Staiger M.: Electrospinning, Rapra Technology, Report 190, 2005.
4. Jirsak O., Sanetrnik F., Lukas D., Kotek V., Martinova L., Chaloupek J.: EP 1673493

VLIV CHLORIDU SODNÉHO NA ELEKTROSTATICKÉ ZVLÁKŇOVÁNÍ POLYETYLÉNOXIDOVÝCH VLÁKEN

Translation of the article
Effect of sodium chloride on electrospinning of poly(ethylene oxide) fibers

Abstrakt: Polyetylénoxid (PEO) je velmi často používán jako surovina pro přípravu nano vláken technikou elektrostatického zvlákňování. Standardně se používá vodných roztoků PEO a výsledná nanovlákenná spleť se hodí vzhledem k netoxicitě pro medicínské účely. Kvalita elektrostatického zvlákňování PEO závisí na přídavku různých aditiv. V této práci je sledován vliv NaCl na proces elektrostatického zvlákňování PEO. Pro jehlové a bez jehlové zvlákňování je použit vodný roztok PEO o koncentraci 6% s různými přídavky NaCl za jinak konstantních podmínek. Jsou měřeny základní vlastnosti zvlákňovacího roztoku, jako je povrchové napětí, elektrická vodivost a viskozita. Vliv obsahu soli na výslednou nanovlákennou spleť je demonstrován na obrázcích z elektronového skenovacího mikroskopu.

BARRIER PROPERTIES OF POLY LACTIC ACID PACKAGING FILMS REINFORCED WITH JUTE MICRO/NANO PARTICLES

Vijay Baheti[1], Rehan Abbasi[1], Jiří Militký[1] and Jaroslav Dobiáš[2]

[1]Department of Textile Materials, Faculty of Textile Engineering; Technical University of Liberec, Studentská 2, 461 17 Liberec, Czech Republic
[2]Department of Food Preservation and Meat Technology, Institute of Chemical Technology, Technicka 3, 166 28 Prague, Czech Republic
vijaykumar.baheti@gmail.com

Abstract: *Textile industry generate significant amount of waste fibres in form of short lengths during mechanical processing. However these short fibres possess excellent properties suitable for many other applications. The objective of this work was to use the short fibres for the preparation of nanoparticles as fillers in nanocomposite applications. In the given research paper, jute fibres were at first refined to micro/nanoscale particles by high energy planetary ball milling in dry condition and wet condition. Wet milling was observed more efficient than dry milling in terms of unimodality of size distribution but no significant reduction in size below 500 nm was obtained even after milling for 3 hours. These particles were then added into the matrix PLA and composite films were produced by hand casting method to evaluate the reinforcement performance of jute micro/nano particle for thermal and barrier properties in food packaging applications.*
Keywords: *Short waste fibres, Planetary ball milling, Particle size distribution, Food packaging.*

1 INTRODUCTION

Natural fibres are cheap, renewable and biodegradable materials. They are known for high aspect ratio, low density, good tensile strength and modulus. These properties make them attractive class of textile materials traditionally used in manufacture of yarn by spinning process. However due to certain limitations of the spinning process, shorter fibres generated during mechanical processing are not suitable to reuse in yarn manufacture and consequently result into the waste. Presently various ways are being explored to utilise these short fibres as they possess some useful intrinsic properties. One such interesting way is to separate the nanofibrils or nanocrystals from these short fibres and use it as fillers in composites [1-4].
Among all natural fibres, use of plant based fibres is more common in textile industry. Cellulose is the main fibril component of plant cells with many nanofibrils packed together. At the nanoscale, there exist only small number of defects to provide modulus and strength close to Kevlar in range of 130 and 7 GPa respectively [5-7]. Previous work on composites made from cellulose nanofillers showed improved strength and stiffness with a little sacrifice of toughness, reduced gas/water vapour permeability, lower coefficient of thermal expansion, and increased heat deflection temperature [1, 8, 9]. These properties could promise in replacement of conventional petroleum based composites by new, high-performance, and lightweight green nanocomposite materials.
The nanofibrils or nanocrystals of cellulose are extracted in previous research work from several natural sources like cotton [10], sisal [6], jute [11-13], soybean [14], wheat straw and soy hulls [15], hemp [9], etc by mechanical [16, 17], chemical [6], enzyme [18] or combination of techniques [2,19]. The chemical method employs strong acid hydrolysis treatment to remove the amorphous regions of cellulose fibres and separate nanocrystalline cellulose (NCC) whereas mechanical method involves high-pressure shear refining treatment to produce nanofibrillar cellulose (NFC) together with crystalline and amorphous regions [20].

However the use of acid treatment over mechanical treatment has number of drawbacks, such as longer time of separation of nanocrystals, potential degradation of cellulose, corrosivity, and environmental incompatibility [18, 20, 21]. Therefore some researchers preferred the alternative route of mechanical treatment through various ways like grinding [16, 17, 20, 22], high pressure homogenizing [23, 24], cryo-crushing [9, 14, 17], ultrasonic treatment [19, 21, 25], etc to obtain NFC rather than NCC.

The present study focused on novel method for preparation of NFC by pulverisation of short jute fibres to nano/micro jute particles using high energy planetary ball milling in wet conditions. This technique has many advantages over other mechanical treatments as it easily provides nanocellulose in bulk quantity at room temperature. The barrier property of obtained jute nano/micro particles were then evaluated in terms of oxygen and water vapour in Poly lactic acid (PLA) hand cast films to be used in food packaging.

2 PARTICLES AND COMPOSITE FILMS PREPARATION

Jute fibres were obtained from Textile Technology Department of IIT Delhi, India. Poly lactic acid (PLA 2002D) was purchased from NatureWorks LLC, USA through local supplier Resinex, Czech Republic.

Chemical pre-treatment of fibres was carried out before pulverisation to remove lignin and hemicelluloses. Jute fibres were sequentially treated with 4% sodium hydroxide (NaOH) at 80°C for 1 hour and with 7 $g.l^{-1}$ sodium hypochlorite (NaOCl) at room temperature for 2 hours under pH 10-11. The fibres then antichlor treated at the end of bleaching with 0.1% sodium sulphite at 50°C for 20 min and transferred in ball mill for pulverisation in dry and wet conditions. Ball milling process relies on the principle of energy release at the point of impact between balls as well as on the high grinding action created by friction of balls on the wall [20].

High-energy planetary ball mill of Fritsch pulverisette 7 was used with sintered corundum container of 80 ml capacity and zirconia balls of 10 mm diameter for initial 3 min of dry milling. The bigger balls were replaced by smaller balls of 3 mm diameter for further extended milling in wet condition in distilled water up to 3 hours. The ball mill was loaded with ball to material ratio (BMR) of 10:1. The rotation speed of the disc was kept at 850 rpm with reverse rotation of containers.

Particle size distributions of milled jute particles was carried out after each one hour of milling on Malvern zetasizer nano series based on dynamic light scattering principle of brownian motion of particles. The deionised water was used as dispersion medium and ultrasonicated for 5 min with Bandelin ultrasonic probe before characterisation. Refractive index of 1.52 was used to calculate particle size of milled jute particles.

In addition morphologies of jute particles after each stage of ball milling was observed on scanning electron microscope TS5130-Tescan SEM at 30 KV accelerated voltage. Jute particles of 0.01 g were dispersed in 100 ml acetone, and then a drop of the dispersed solution was placed on aluminium foil and gold coated after drying.

At the end of wet milling, the nano/micro particles of jute were separated from water by centrifugation at 4000 rpm with simultaneous transfer in solvent isopropanol to avoid hornification. The solvent isopropanol helped to dry the jute particles without clustering.

PLA/nanocellulose composite films with 1, 5 and 10% filler content were prepared by mixing the calculated amount of jute particles with 5% PLA in chloroform using a magnetic stirrer. The stirring was performed at room temperature for 30 minutes. The composite mixture further ultrasonicated for 10 min on Bandelin Ultrasonic probe mixer with 50 horn power. The final mixtures then cast on a Teflon sheet. The films were kept at room temperature for 2 days until they were completely dried and then removed from the Teflon sheet. One neat PLA film was also prepared without addition of nanocellulose as reference sample to compare.

3 COMPOSITE FILMS TESTING

The viscoelastic behaviour of the composite materials was measured on dynamic mechanical analysis DMA DX04T RMI. The test was performed in tension mode (gauge length and sample width of 10 mm and 10 mm respectively) at a frequency of 1 Hz. The samples were subjected to an oscillating frequency of 1 Hz and 100 % oscillating amplitude in the temperature ranges of 35°C to 60°C at the heating rate of 3°C/min.
Oxygen barrier property (ml/m^2.24 h.0.1 MPa) of 10 cm circular sample was measured by manometric method using permeameter Lyssy L100-5000 on Systech Instrument, USA at 0% RH and 23°C temperature. Water vapour barrier property (g/m^2.d) of 6.5 cm circular sample was measured using gravimetric method ZM-23 at 85% RH and 38°C temperature.

4 RESULTS AND DISCUSSIONS

Under one hour dry milling, jute fibres were pulverised to microparticles with average size of 1480 nm in wider particle size distribution as shown in Figures 1(a) and 2(a). The reason behind multimodal distribution of particles was due to increase in temperature within the mill because of continuous impact of balls. The increased temperature of mill rendered the jute particles to undergo cold welding and deposited a layer on the surface of container and balls as milling progressed. The growth of deposited layer on the milling media changed the impact force of balls on the material with least impact on particles at bottom of layer. In case of wet milling, the increase in temperature was slowed down by deionised water which consequently resulted in narrow particle size distribution with significant reduction in average particle size to 640 nm after one hour of wet milling as shown in Figures 1(b) and 2(b). This can be attributed to uniformity in impact action of balls on every individual particle in wet condition.
To further refine the jute particles to smaller size, wet milling was performed for extended duration. The average particle size reached to 443 nm after 3 hours of wet milling and the particle size distribution changed slowly from multimodal nature to unimodal nature as shown in Figure 3(a) and Figure 3(b). This showed the consistency and homogeneity in milling action on every individual particle as milling continued for longer time. However the rate of refinement became slower while grinding the smaller particles in addition to the severe damage of milling balls due to direct collision. This could have introduced some inorganic contaminations from mill to the material, so further pulverisation was stopped and jute particles in 500 nm range were used as nano/micro fillers.
The storage modulus of jute particles reinforced PLA composite films are higher than that of neat PLA film (Figure 4). The stiffness effects introduced by jute particles enable the PLA to sustain high storage modulus value. These improved properties were ascribed to a mechanical percolation phenomenon [26], yielded by jute micro/nano particles interactions through hydrogen bond forces. This also suggests that the jute particles behave as good reinforcement and allow homogeneous stress transfer from the matrix to the particles.

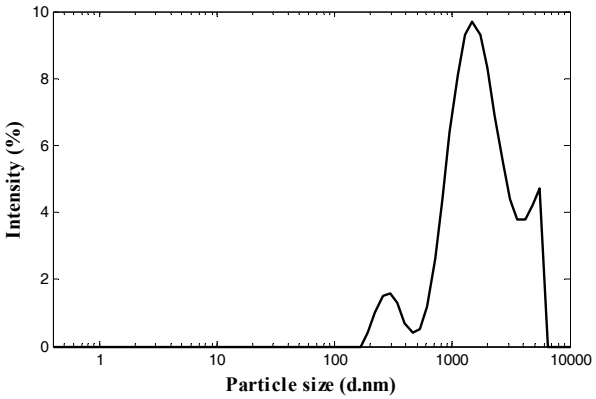

(a) One hour dry milling

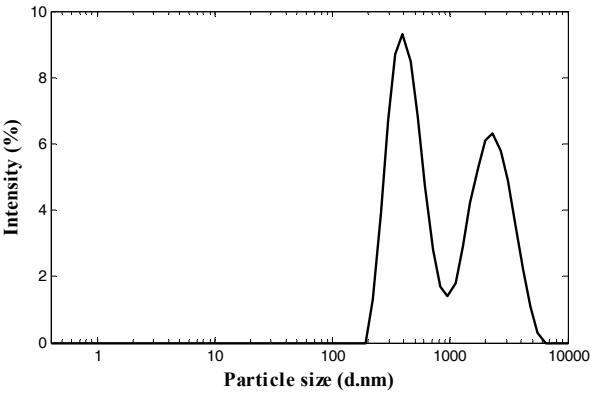

(b) One hour wet milling

Figure 1 Particle size distribution of jute particles after ball milling action

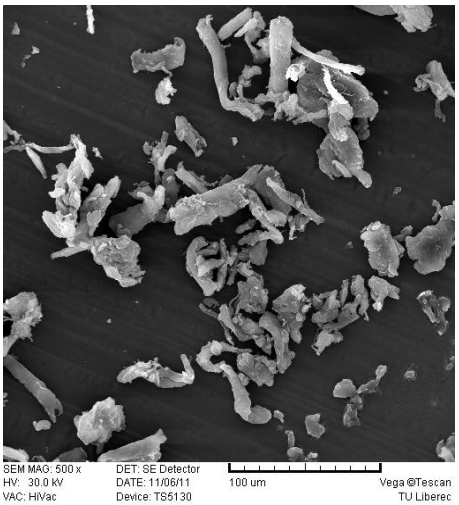

a) One hour dry milling

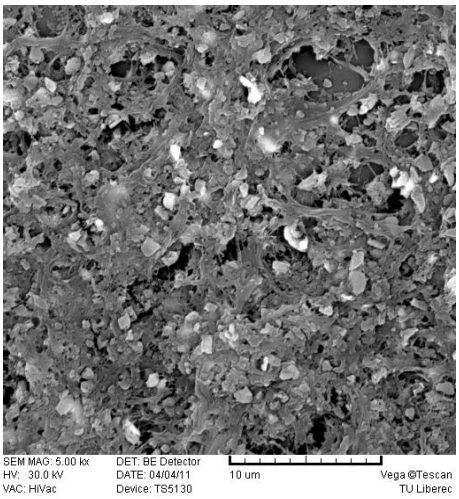

b) One hour wet milling

Figure 2 SEM images of jute particles

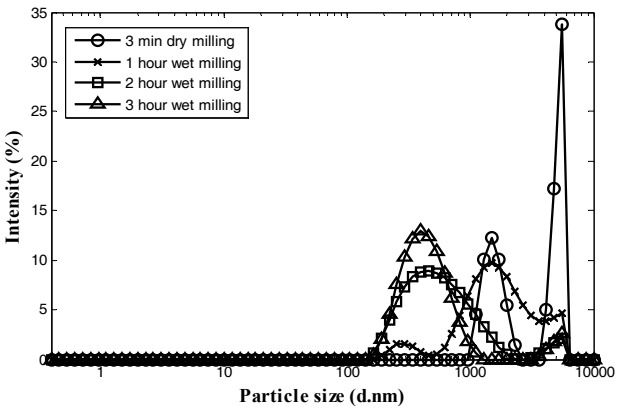

Figure 3(a) Effect of extended wet milling time on pulverisation

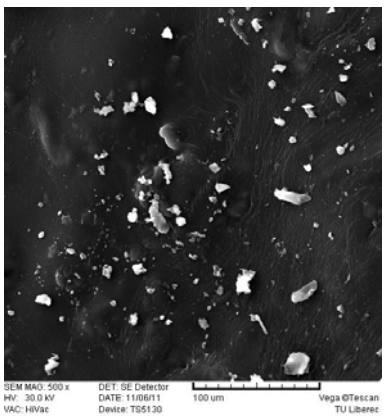

Figure 3(b) Particle size after 3 hour wet milling and solvent exchange

It was expected that barrier to penetration of water vapour and gas molecules would improve due to addition of jute particles. But no clear trend was observed in composite films loaded with jute particles. Water vapour barrier found to decrease in all composite PLA films loaded with 1, 5 and 10 wt% jute particles as compared to neat PLA films. This behaviour can be related to hydrophilic nature of jute particles which tend to absorb moisture in the composite films. However reduction in oxygen barrier performance in case of 1 and 5 wt% loaded films was not expected. Only PLA films loaded with 10 wt% jute particles showed improvement in oxygen barrier by 10% from 900 to 800 ml/m^2.24 h.0.1 MPa as compared with neat PLA films.
Previous studies reported that improvement in barrier properties is directly related to tortuosities created by nanoparticles. However the tortuous nature of path depends on many other factors like shape and aspect ratio of the filler, degree of exfoliation or dispersion, filler loading and orientation, adhesion to the matrix, moisture activity, filler-induced crystallinity, polymer chain immobilisation, filler-induce solvent retention, degree of purity, porosity and size of the permeant. The main reason behind poor barrier properties in our case can be related to hydrophilic nature of jute particles in comparison with hydrophobic nature of PLA matrix which provided poor dispersion within matrix, non adhesion to the matrix and non improvement in crystallinity of matrix. Further research is needed on adjusting compatibility between filler and matrix by surface modification treatments like silylation, acetylation, etc.

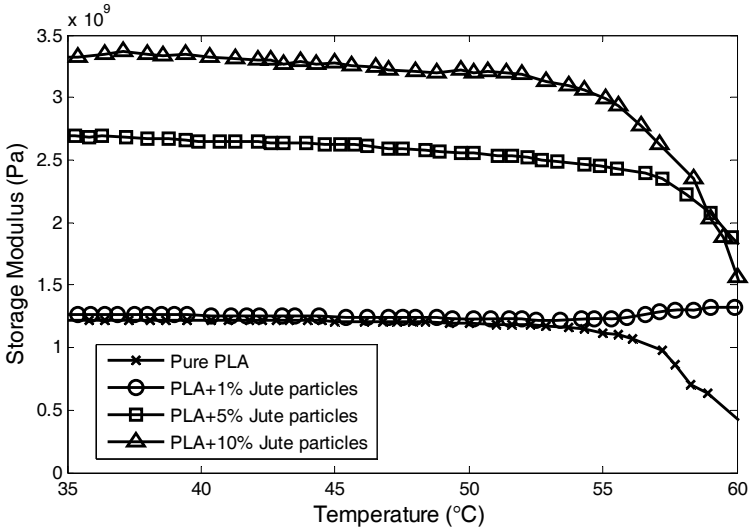

Figure 4 Storage modulus of NFC/PLA film

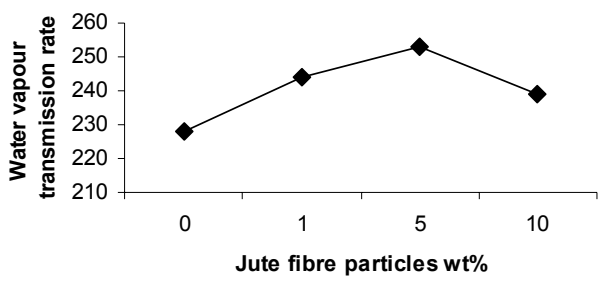

Figure 5 Moisture Barrier of NFC/PLA film

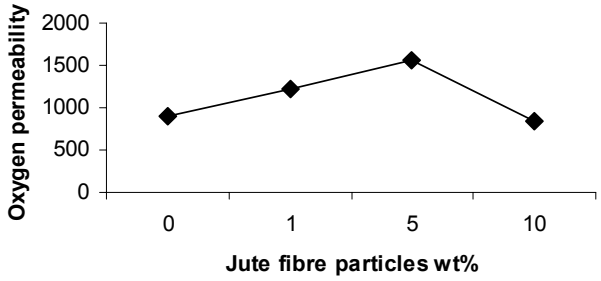

Figure 6 Oxygen barrier of NFC/PLA film

5 CONCLUSION

Jute fibres were successfully pulverised into powder form below 500 nm with narrow size distribution after 3 hours of wet milling in deionised water. Dry milling was difficult due to sticking of material to milling media. Thermal properties of PLA films loaded with micro/nano particles of jute were improved to some extent than that of neat PLA films due to mechanical percolation phenomena.
Improvement in oxygen barrier properties was observed by 10% from 900 to 800 ml/m^2.24 h.0.1 MPa only in case of 10 wt% jute particle loading. Both oxygen and water vapour barrier properties started to increase only under higher loadings of jute particles. The reduction in barrier properties in 1 and 5% loadings of jute particles was due to inability in generation of complex tortuous path from poor compatibility between hydrophilic jute particles and hydrophobic PLA matrix.

Acknowledgement: *Authors are thankful to Department of Food Preservation and Meat Technology at Institute of Chemical Technology in Prague to allow measurement of barrier properties. The research was supported by SGS-4857 grant.*

6 REFERENCES

1. Khalil H.P.S., Bhat A.H., Yusra A.F.: *Carbohydrate Polymers* 87, 2012, 963-979
2. Jonoobi M., Khazaeian A., Tahir P., Azry S., Oksman K.: *Cellulose* 18, 2011, 1085-1095
3. Qua E.H., Hornsby P.R., Sharma H.S., Lyons G., McCall R.D.: *Journal of Applied Polymer Science* 113, 2009, 2238-2247
4. Klemm D., Schumann D., Kramer F., Hebler N., Hornung M., Schmauder H., Marsch S.: *Adv Polym Sci* 205, 2006, 49-96
5. Lu J., Wang T., Drzal L.: *Composites A* 39, 2008, 738-746
6. Moran J.I., Alvarez V.A., Cyras V.P., Vazquez A.: *Cellulose* 15, 2008, 149-159
7. Zimmermann T., Bordeanu N., Strub E.: *Carbohydrate Polymers* 79, 2010, 1086-1093
8. Siro I., Plackett D.: *Cellulose* 17, 2010, 459-494
9. Wang B., Sain M., Oksman K.: *Appl Compos Mater* 14, 2007, 89-103
10. Yuen C.W.M., Cheng Y.F., Li Y., Hu J.Y.: *Journal of Textile Institute* 100, 2009, 165-172
11. Wang H., Huang L., Yafei L.: *Fibers and Polymers* 10, 2009, 442-445
12. Jahan M.S., Abrar S., Zhibin H., Yonghao N.: *Cellulose* 18, 2011, 451-459
13. Das K., Ray D., Bandyopadhyay N.R., Sahoo S., Mohanty A.K., Misra M.: *Composites B* 42, 2011, 376-381
14. Wang B., Sain M.: *Composites Science and Technology* 67, 2007, 2521-2527
15. Alemdar A., Sain M.: Bioresour. Technol 99, 2008, 1664–1671
16. Chang F., Lee S., Toba K., Nagatani A., Endo T.: *Wood Sci Technol* 46, 2012, 393-403
17. Prasad B.M., Sain M.M., Roy D.N.: *Journal of Material Science* 40, 2005, 4271-4278
18. Satyamurthy P., Jain P., Balasubramanya R., Vigneshwaran N.: *Carbohydrate Polymers* 83, 2011, 122-129
19. Chen W., Yu H., Liu Y., Chen P., Zhang M., Hai Y., *Carbohydrate Polymers* 83, 2011, 1804-1811
20. Baheti V.K., Militky J.: *World Journal of Engineering*, 9, 2012, 45-50
21. Li W., Yue J., Liu S.: *Ultrasonics Sonochemistry*, 19, 2012, 479-485
22. Liimatainen H., Sirvio J., Haapala A., Hormi O., Niinimaki J.: *Carbohydrate Polymers* 83, 2011, 2005-2010
23. Leitner J., Hinterstoisser B., Wastyn M., Keches J., Gindl W.: *Cellulose* 14, 2007, 419–425
24. Bruce D.M., Hobson R.N., Farrent J.W., Hepworth D.G.: *Composites A* 36, 2005, 1486–1493
25. Cheng Q., Wang S., Rials T.: *Composites A* 40, 2009, 218-224
26. Favier V., Canova G.R., Cavaille J.Y., Chanzy H., Dufresne A., Gauthier C.: *Polymer for Advanced Technologies* 6, 1995, 351-355

BARIÉROVÉ VLASTNOSTI OBALOVÉ FÓLIE Z KYSELINY POLYMLÉČNÉ ZESÍLENÉ JUTOVÝMI MIKRO/NANO ČÁSTICEMI

Translation of the article

Barrier properties of Poly lactic acid packaging films reinforced with jute micro/nano particles

Abstrakt: Textilní průmysl generuje značné množství vlákenných odpadů zejména v mechanických procesech přípravy textilií. Tyto krátké vlákenné odpady jsou však stále kvalitním zdrojem pro některé aplikace. Cílem této práce bylo využití těchto vlákenných odpadů pro přípravu nano částic jako plniv do nano kompozit. Byla použita odpadní jutová vlákna, která byla převedena na mikro/nano částice pomocí planetového kuličkového mletí za mokra a za sucha. Mletí za mokra se ukázalo jako výhodnější s ohledem na unimodalitu částic. Na druhé straně ani po mletí po dobu 3 hod. nevedlo ke zjemnění částic pod 500 nm. Získané částice celulózy byly přidány do matrice z kyseliny polymléčné a byly vytvořeny fólie vhodné jako obaly. Byly zkoumány vybrané tepelné a bariérové vlastnosti těchto zesílených obalových folií.

COMPARISON OF DRAPE PROFILES OBTAINED BY VARIOUS TECHNIQUES

Rajesh Mishra, Jiří Militký, B.K.Behera[1] and Dana Křemenáková

Faculty of Textile Engineering, Technical University of Liberec, Czech Republic
[1] Department of Textile Technology, IIT Delhi, India
rajesh.mishra@tul.cz

Abstract: *Drape is an essential parameter to decide both appearance and handle of fabrics. It is a secondary determinant of fabric mechanical properties and influenced by the low stress mechanical properties like bending rigidity, formability, tensile and shear properties & compressibility of the fabric. The principal objective of this research is to analyze and compare drape profile of woven fabrics using various modeling methods especially FEM and polar coordinate technique. To compare the above discussed computational methods for prediction of drape profile of woven fabrics the ten carefully selected samples of cotton woven fabrics are used.*
Key words: *Drape evaluation, finite element method, polar coordinate method, comparison of drape characteristics.*

1 INTRODUCTION

With the improvement in life style and economic conditions, today's consumers are much more quality conscious than ever before. Consumers now prefer to have less clothing but of high quality. Among various properties, aesthetic characteristics of clothing have become the primary consideration in determining serviceability of apparel fabrics. Normally fabric appearance is determined from several traditional attributes like wrinkle, crease, texture, pilling, color and drape characteristics. In fact, among all these parameters drape ability of a fabric plays an important role particularly when the garment is required to provide an elegant look to make the wearer presentable in the occasion [1]. Drape is an essential parameter to decide both appearance and handle of fabrics. It is a secondary determinant of fabric mechanical properties and influenced by the low stress mechanical properties like bending rigidity, formability, tensile and shear properties & compressibility of the fabric [2-5]. All these mechanical properties have a direct bearing with basic fibre properties and fabric construction. It is observed over a decade that the consumers prefer to wear light weight fabrics. At the same time fabric comfort has gained priority over fabric durability. When fiber composition is changed along with fabric areal density, fabric drape ability is expected to be influenced significantly. With decrease in fabric areal density, the fabric becomes more flexible and may loose structural stability. The drape parameters such as: number of folds, depth of folds, evenness of folds together with the drape coefficient need to be examined. The relationship between these parameters and fabric mechanical properties is already established [6-10].

In the textile and clothing industries, because of the increasingly individual and customer-oriented production, the sample collections of the firms extend more and more, whereas the quantities for the production decrease. At present, the stage of product development and product preparation of clothes require approximately three times the stage of consumption. In order to compensate the high time consumption, efforts are made to react quickly for the product preparation and flexibly to latest fashion. The use of complex CAD-CAM solution is one of the solutions but does not help fully to characterize the drape. The primary objective is to simulate the garment/home furnishing by using the fundamental properties of fabrics. The

simulation must be sufficiently realistic for the garment designer's need and to be carried out quickly enough for the designer to work. In engineering, great progress has been made in developing theories to explain and predict the deformation behavior of nearly rigid materials like steel and stiff plastics. Unfortunately the same is not true for the flexible materials such as cloth.

The finite element method (FEM) has become a powerful tool for the numerical solution of a wide range of engineering problems [7-8]. Applications range from deformation and stress analysis of automotive, aircraft, building, and bridge structures to field analysis of heat flux, fluid flow, magnetic flux and other flow problems. In the recent years, finite element analysis is also applied in the flexible materials like fabric for the modeling and simulation [7-8]. Several alternative configurations can be tested on a computer before the prototype is built. So we need to keep pace with the developments by understanding the basic theory, modeling techniques, and computational aspects of finite element method.

Apart from FEM, statistical methods are used for years to predict the product and process parameters. So this method can be employed for the prediction of the drape coefficient.

The principal objective of this research is to analyze and compare drape profile of woven fabrics using various modeling methods especially FEM and polar coordinate technique.

To compare the above discussed computational methods for prediction of drape profile of woven fabrics the ten carefully selected samples of cotton woven fabrics are used.

2 METHODOLOGY

Ten cotton fabric samples with a wide range of areal densities and structures were used for this study. The constructional specifications of these fabrics are given in Table 1.

The drape parameters for all the fabric samples are evaluated by using the digital image processing based drapemeter as discussed in the work [11]. In this image analysis system, the shadow projected from the fabric is quantified into a binary image after being digitized. The threshold value that sets the criteria for converting a grey scale image into a black and white image is controlled at the user interface of the system. For this reason, this image analysis method is not influenced by the fabric color.

The digitized binary image is processed with a closing operation which removes noise and segmentizes the shadow image of the draped fabric from the background image. The closing operation is a dilation operation followed by an erosion operation. This operation fills in single pixel object abnormalities. After digitizing the image of the draped fabric, the image analysis system searches the boundary between the fabric shadow and the central disk on the drape meter and the boundary between the fabric shadow and the outer region of the fabric shadow.

Table 1 Parameters of tested fabrics

Fabric_ID	Fabric Name	Yarn Count	Fabric count	GSM [g.m^{-2}]
1	Sheeting	45 x 45	139 x 94	121
2	Shirting	14x14	060x60	200
3	Drill	20 x 20	108 x 58	193
4	Drill	20x 16	128 x 60	236
5	Drill	16x 12	108 x 56	266
6	Corduroy	20x 16	122 x 60	229
7	Drill	7x07	070 x 42	372
8	Cambric	30 x 30	068 x 68	106
9	Cambric	20x 20	060x60	140
10	Twill (2/3)	32 x 32	130 x 70	146

By using this boundary description, the software calculates the different drape parameters such as drape coefficient DC, Drape Distance Ratio DDR, Fold Depth Index FDI, Amplitude to Radius Ratio ARR and number of Nodes NI.

3 DRAPE PREDICTION BY FINITE ELEMENT ANALYSIS

Finite element method is a numerical method used to solve real world problems that involve complicated physics, geometry, and/ or boundary conditions. In the finite element method, a given domain is viewed as a collection of sub-domains, and over each sub-domain the governing equation is approximated by any of the traditional variational methods. The main reason behind the seeking the approximate solution on a collection of sub-domains is the fact that it is easier to represent a complicated function as collection of simple polynomials. In this study ABAQUS 6.6 was used for the simulation and analysis of the fabrics.

3.1 Domain discretisation

In this step, the complex fabric domain is represented as a collection of simple sub-domains or elements. These elements are the cross-over points of the warp and weft. Each finite element is viewed as an independent domain by itself. The discretisation of the fabric is illustrated in the Figure 1.

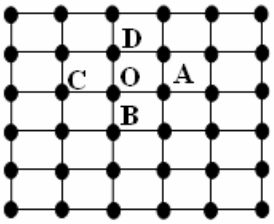

Figure 1 A typical grid-point "O" and its four neighborhoods in the fabric mesh.

The elements are connected to each other point called nodes and in this case it is 4 with 24 degrees of freedom. The domain is assumed to be a uniform mess.

3.2 Constitutive equations

In formulating FEM equations for elements, a local coordinate system was used in reference to global coordinate system that is defined for the entire structure. In this study, the model is assumed to be a linear elastic model. So the total stress is defined from the total elastic strain is

$$\boldsymbol{\sigma} = \mathbf{D}^{el}\ \boldsymbol{\varepsilon}^{el} \tag{1}$$

where, $\boldsymbol{\sigma}$ is the total stress, $\boldsymbol{D}^{el}$ is the fourth-order elasticity tensor and $\boldsymbol{\varepsilon}^{el}$ is the total elastic strain.

To define the material properties, the fabric is considered to be an orthotropic material which has two principal directions warp and weft and the fabric is discretised to quadrilateral shell elements. In this study E_1 (Young's modulus in warp direction), E_2 (Young's modulus in weft direction), v_{12} (Poisson's ratio in bias direction), G_{12} (Shear modulus in X-Y direction), G_{13} (Shear modulus in X-Z direction) and G_{23} (Shear modulus in Y-Z direction) are used to define the orthotropic material. In this study (1, 2) surface is the surface of plane stress, so that the plane stress condition is $\sigma_{33} = 0$. The shear moduli G_{13} and G_{23} are included because as they are required for modeling of transverse shear deformation in the shell [4].

For an orthotropic material the engineering constants define the $\boldsymbol{D}$ matrix is shown in equations 2 to 9.

$$D_{1111} = E_1\left(1-\vartheta_{23}\vartheta_{32}\right)\gamma \tag{2}$$

$$D_{2222} = E_2\left(1-\vartheta_{13}\vartheta_{31}\right)\gamma \tag{3}$$

$$D_{3333} = E_3\left(1-\vartheta_{12}\vartheta_{21}\right)\gamma \tag{4}$$

$$D_{1122} = E_1\left(\vartheta_{21}-\vartheta_{31}\vartheta_{23}\right)\gamma \tag{5}$$

$$D_{1133} = E_1\left(\vartheta_{31}-\vartheta_{21}\vartheta_{32}\right)\gamma \tag{6}$$

$$D_{2233} = E_2\left(\vartheta_{32}-\vartheta_{12}\vartheta_{31}\right)\gamma \tag{7}$$

$$D_{1212} = G_{12} \tag{8}$$

$$D_{1313} = G_{13} \tag{9}$$

where

$$\gamma = \frac{1}{1-\vartheta_{12}\vartheta_{21}-\vartheta_{23}\vartheta_{32}-\vartheta_{31}\vartheta_{13}-2\vartheta_{31}\vartheta_{32}\vartheta_{13}} \tag{10}$$

The restrictions on the elastic constants due to the material stability are shown in equations 11 to 15.

$$D_{1111}, D_{2222}, D_{3333}, D_{1212}, D_{1313}, D_{2323} \geq 0 \quad (11)$$

$$\left|D_{1122}\right| \leq \sqrt{D_{1111} D_{2222}} \quad (12)$$

$$\left|D_{1133}\right| \leq \sqrt{D_{1111} D_{3333}} \quad (13)$$

$$\left|D_{2233}\right| \leq \sqrt{D_{2222} D_{3333}} \quad (14)$$

$$\det\left(\mathbf{D}^{el}\right) \geq 0 \quad (15)$$

That last relation turns to equation

$$D_{1111}D_{2222}D_{3333} + 2D_{1122}D_{1133}D_{2233} - \\ - D_{2222}D_{1133}^2 - D_{1111}D_{2233}^2 - D_{3333}D_{1122}^2 \geq 0 \quad (16)$$

These restrictions in terms of the elastic stiffness are equivalent to the restrictions in terms of the engineering constants.

The final equilibrium equation is formed using the principle of total potential energy which is the sum of the total strain energy and work done due to gravitational forces. The non-linearity of the final equation was approximated using Newton-Raphson's method.

The input to the ABAQUS software is D matrix which can be calculated from the above cited equations from the Young's moduli (**E**), Shear moduli (**G**) and Poission's ratio (v) of the fabric. The other inputs are thickness of the fabric and for the boundary condition the diameter of the fabric (24 cm) was applied. The Poission's ratio (v) for all the fabrics assumed to be 0.3.

The output of the ABAQUS software is the virtual draped images. The draped images are fed to the image processing software to get the drape parameters.

4 DRAPE PREDICTION BY POLAR COORDINATE TECHNIQUE

A fabric drape profile can be captured in a two dimensional image projected from a three dimensional draped fabric sample by a digital camera and the image can be transferred to the computer CPU for the observation [14]. Software was developed using Matlab 7.0 to estimate the drape parameters. The input parameters of the software are the boundary coordinates of the draped profile.

The algorithm used to determine the drape parameters are image capturing by a digital camera and then conversion of the image into a binary image (from an intensity based luminance threshold). The centroid and the boundary of the binary image were traced by 8 connected neighbored principles. After boundary tracing, the radii of the drape profile measured using eqn 17 from the drape profile. In the last step drape profile was plotted in the form of a Polar Diagram.

$$r_i = \sqrt{(x_i - x_c)^2 + (y_i - y_c)^2} \quad (17)$$

where r_i are the radius of the drape profile at 1° interval i.e. *i* varies from 1 to 360°.

x_i and y_i are the Cartesian coordinates of the boundary of the drape profile at 1° interval.

x_c and y_c are the Cartesian coordinate of the center of the drape profile.

The equation

$$r = \left(\sum_{i=1}^{360} r_i\right) / 360 \quad (18)$$

is used for calculation of the average radius of the drape profile. This r value is in terms of pixels. For conversion of pixel to cm unit, the supporting disc image was captured and then it was transformed into centimeter scale by counting the number of pixels in radial direction and then changed to the centimeter scale.

Drape coefficient *DC* is defined by relation

$$DC[\%] = \frac{r^2 - 6.25}{25 - 6.25}\ 100 = 5.33\ (r^2 - 6.25) \quad (19)$$

because $A_s = \pi r^2$, $A_1 = \pi\ 2.5^2$ and $A_2 = \pi\ 5^2$ where, 5 and 10 are the diameters of the supporting disc and the undraped fabric in inches. Drape distance ratio *DDR* is defined as

$$DDR\ [\%] = \frac{r_2 - r_s}{r_2 - r_1}\ 100 \quad (20)$$

Fold depth index *FDI* is defined as

$$FDI\ [\%] = \frac{r_{max} - r_{min}}{r_2 - r_1}\ 100 \quad (21)$$

Amplitude *ARR* is characterized by relation

$$ARR = \frac{r_{max} - r_{min}}{2} \quad (22)$$

The drape parameters can be therefore simply estimated from predicted drape profiles.

5 RESULTS AND DISCUSSION

The drape coefficients measured by image captured by a digital camera are then processed by the software developed in Matlab 7.0. The results are listed in the Table 2 with the drape coefficient measured by Cusik method [5].

The GSM, thickness of the fabric, initial Young's modulus, shear rigidity and Poisson's ratio of the fabric are considered for the input parameters for the finite element analysis. These parameters are listed in the Table 3 and the virtual draped images obtained from finite element analysis are given in Figure 2. The result obtained from this method is tabulated in Table 4.

The drape parameters measured by polar coordinate technique are listed in the Table 5 and the predicted images are shown in Figure 3.

Table 2 Drape parameters measured by digital image processing and Cusik's method

Sample No	DC [%]	DDR [%]	FDI [%]	ARR [cm]	NI	DCc [%] (Cusik's)
S_1	75.69	48.82	56.82	1.05	6	74.58
S_2	72.12	54.19	57.32	1.17	5	70.45
S_3	74.02	52.76	59.86	1.28	6	69.28
S_4	68.18	59.02	64.26	1.22	6	66.38
S_5	67.76	62.37	66.04	1.40	5	69.69
S_6	64.80	65.53	70.91	1.25	6	62.26
S_7	57.38	71.82	76.31	1.52	5	59.85
S_8	57.51	70.46	76.05	1.40	6	56.92
S_9	51.86	76.87	79.42	1.58	5	52.48
S_{10}	54.65	79.41	78.51	1.74	5	52.72

Table 3 Input parameters used for finite element analysis

Sample No	Thickness (mm)	GSM gm^{-2}	$E_1(e^7)$ gm/cm^2	$E_2(e^7)$ gm/cm^2	$E_3(e^7)$ gm/cm^2	$G_{12}(e^3)$ gm/cm^2	$G_{13}(e^3)$ gm/cm^2	ν
S_1	0.64	190	4.8	4.36	4.57	1.36	1.36	0.3
S_2	0.71	200	4.1	4.00	4.10	1.58	1.23	0.3
S_3	0.73	215	4.6	4.10	4.34	1.27	1.18	0.3
S_4	0.78	226	3.8	4.24	4.00	1.13	1.12	0.3
S_5	0.80	240	3.5	3.51	3.50	1.19	1.15	0.3
S_6	0.40	190	2.8	3.21	3.00	1.52	1.16	0.3
S_7	0.43	210	2.4	3.65	3.00	1.41	1.09	0.3
S_8	0.47	230	1.8	2.89	2.28	1.16	1.11	0.3
S_9	0.53	240	1.9	2.74	2.28	1.17	1.02	0.3
S_{10}	0.59	255	1.6	2.14	1.85	0.98	0.97	0.3

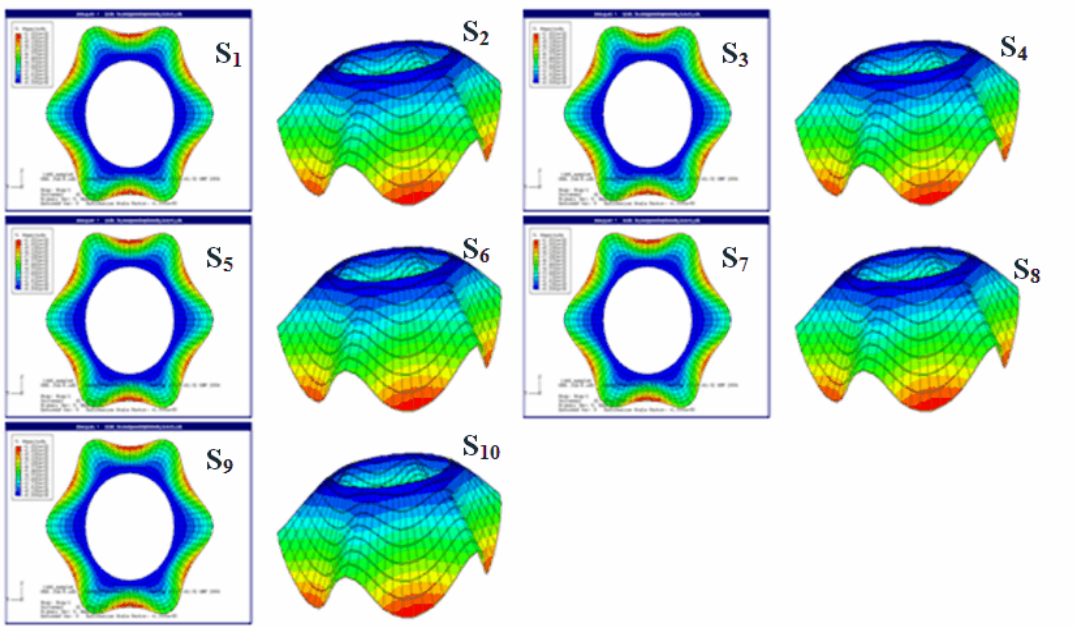

Figure 2 Virtual Draped Images of Fabric Samples (FEM)

Table 4 Drape parameters obtained from finite element profiles

Sample No	DC	DDR	FDI	ARR	NI
S_1	73.81	47.65	56.28	1.15	6
S_2	72.24	51.12	54.32	1.25	5
S_3	71.76	52.71	60.69	1.30	6
S_4	67.79	60.23	65.49	1.2	6
S_5	66.89	63.04	68.52	1.4	5
S_6	62.28	66.34	72.64	1.25	6
S_7	61.56	71.68	73.09	1.75	5
S_8	60.58	70.2	76.38	1.5	6
S_9	53.12	75.24	80.59	1.65	5
S_{10}	59.28	74.67	81.79	1.8	5

Table 5 Drape parameters measured by Polar coordinate technique

Sample No	DC	DDR	FDI	ARR	NI
S_1	73.25	48.47	54.37	1.39	6
S_2	69.37	53.35	56.72	1.45	5
S_3	63.25	49.97	63.09	1.17	6
S_4	61.46	63.26	68.57	1.22	6
S_5	74.29	61.65	71.36	1.45	5
S_6	59.38	62.08	69.97	1.29	6
S_7	56.03	71.68	72.05	1.73	5
S_8	59.25	73.55	73.19	1.51	6
S_9	53.86	78.78	78.29	1.45	5
S_{10}	54.19	72.19	83.76	1.80	5

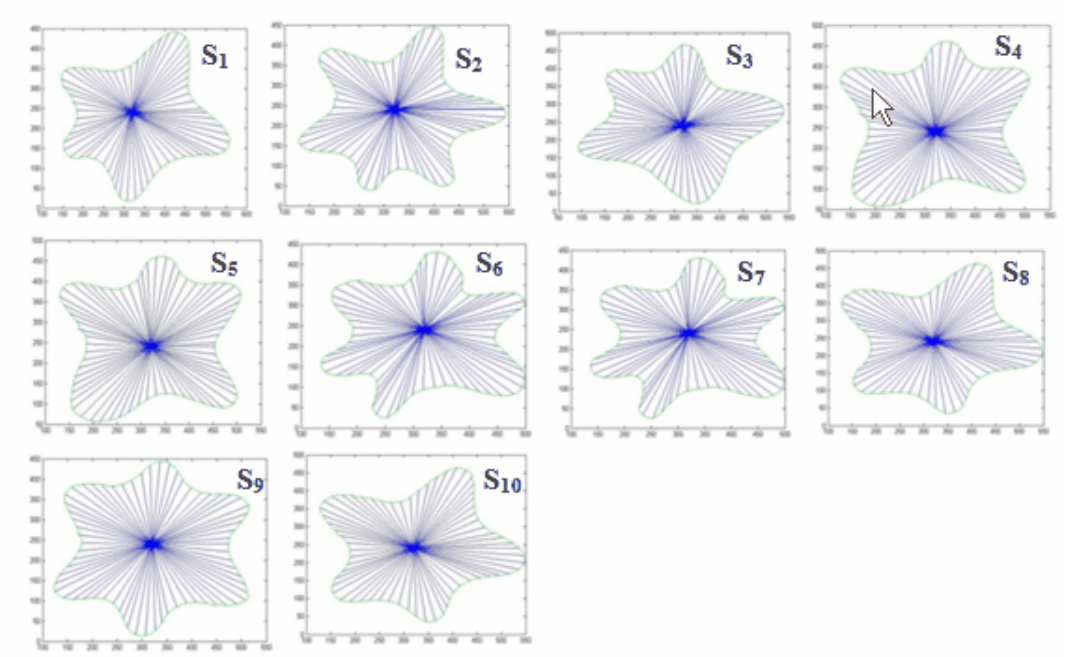

Figure 3 Virtual Draped Images of Fabric Samples (polar coordinate technique)

Drape coefficient measured Cusik's method *DCc*, image analysis *DCd*, from FEM profiles *DCf* and from polar coordinates profiles *DCp* were compared. The correlation matrix between drape coefficient *DCc, DCd, DCf and DCp* is shown in Table 6. The paired dependencies between drape coefficients are shown in the Figure 4.

Table 6 Correlation between drape coefficients

	DCc	DCd	DCf	DCp
DCc	1	0.9692	0.9504	0.8998
DCd	0.9692	1	0.9690	0.8198
DCf	0.9504	0.9690	1	0.8072
DCp	0.8998	0.8198	0.8072	1

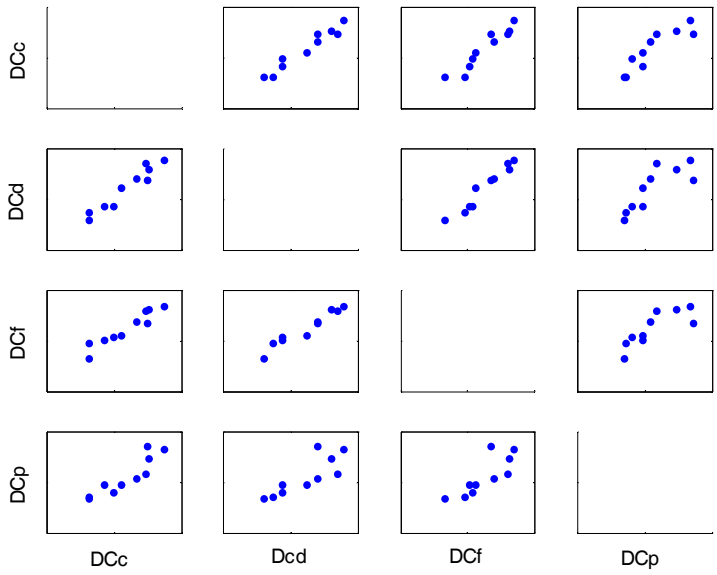

Figure 4 Paired relations between drape coefficients

From the above results it can be seen that there is a best correlation between drape coefficient *DCc* measured by Cusick's method and from the digital image processing *DCd*. Very good correlation is between *DCd* and *DCf* from FEM profiles as well.
Results of liner regression between *DCf* and *DCd* with criterion orthogonal least squares (i.e. minimization of sum of squared distances - because both variables are subjected with random errors [12]) are shown in the Figure 5. Results of liner regression between *DCp* and *DCd* with criterion orthogonal least squares are shown in the Figure 6.

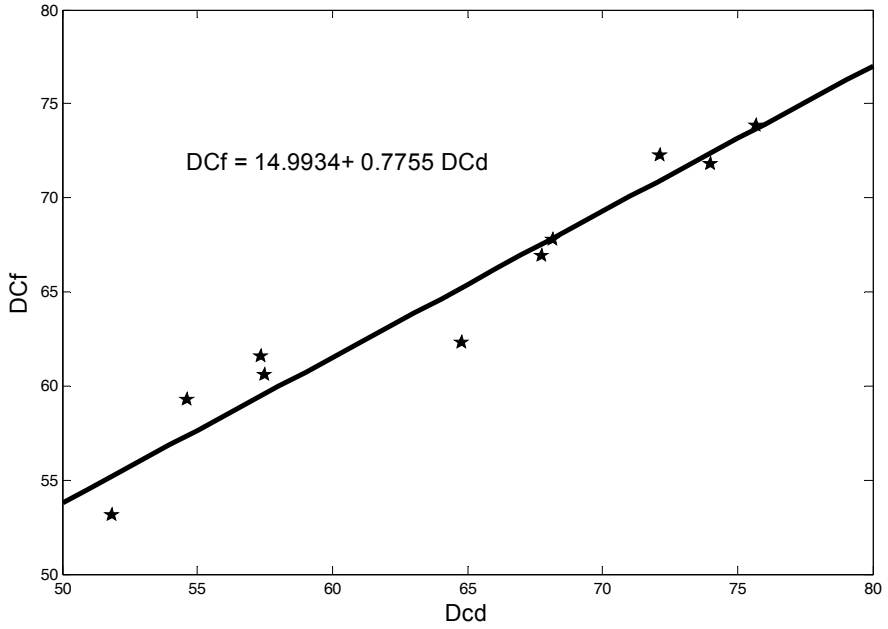

Figure 5 Regression between *DCf* and *DCd* by using orthogonal least squares criterion

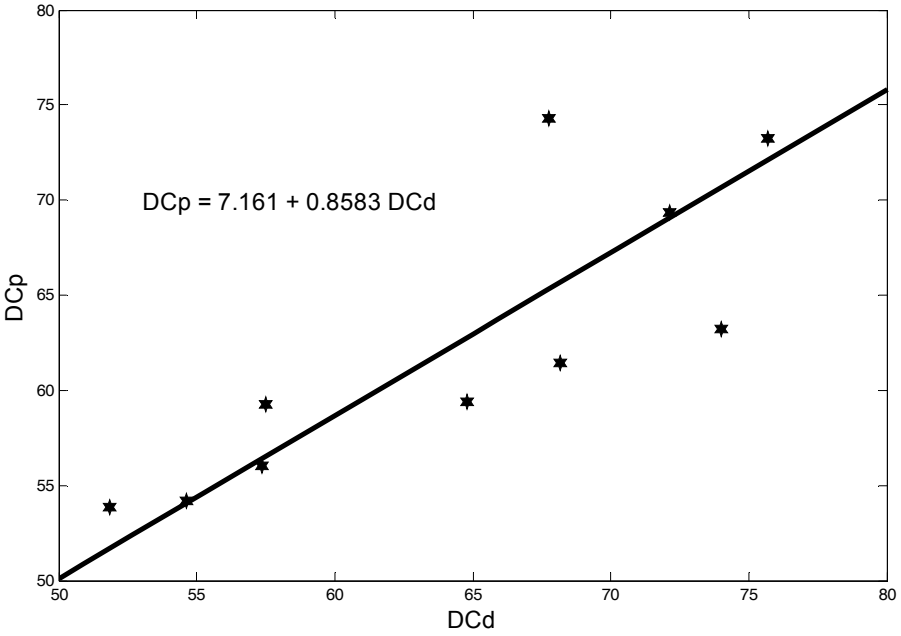

Figure 6 Regression between *DCp* and *DCd* by using orthogonal least squares criterion

6 CONCLUSION

In this study, a trial has been made to predict the drape of woven fabrics by finite element analysis as well as polar coordinate technique. The drape coefficient as measured by four methods viz. Cusik method, FEM profiles method and polar coordinate method are correlated with drape coefficient measured by digital image processing. The correlation coefficient between digital image processing and finite element profiles method gives very good result. The new drape evaluation system enables to quantitatively understand the drape ability of materials in more detail along with shape parameters and measurement technology and, therefore, it is very useful for high quality textile and garment manufacturing.

7 REFERENCES

1. The assessment of drape of fabrics, British Standard Institute, B.S Handbook 4, 1973, 29-31
2. Behera B.K. and Mishra R.: Objective Measurement of Fabric Appearance using Digital Image Processing, *J. Text. Inst.* 97(2), 2006, 142-153
3. Behera B.K. and Pangadiya A.: Drape Measurement by Digital Image Processing, *Tex. Asia* 34(11), 2003, 45-50
4. Bhatti M.A.: Advance Topics in Finite Element Analysis of Structures, John Willey & Sons Inc., Chapter 6, 2006, 331-336
5. Cusik G.E.: The measurement of fabric drape, *J Text Inst* 59(6), 1965, T253-60
6. Cusik G.E.: The Dependence of Fabric Drape on Bending and Shear Stiffness, *J. Tex. Inst.* 56(1), 1965, T596-606
7. Chen S.F. et al.: A finite volume method for contact drapes simulation of woven fabrics and garments, *Finite Element in Analysis & Design* 37, 2001, 513-531
8. Collier R. et al.: Drape prediction by means of finite element analysis, *J. Tex. Inst.* 82(1), 1991, 96-107
9. Hu J. and Chan Y.F.: Effect of Fabric Mechanical Properties on Drape, *Text. Res. J.* 68(1), 1998, 57-64
10. Jedda H. et al.: Prediction of fabric drape using the FAST system, *J. Tex. Inst.* 98(3), 2007, 219 – 225
11. Mishra R. et al.: Measurement of Drape Using Digital Image Processing Technique, Vlákna a Textil 19(3), (2012) in print
12. Meloun M., Militký J.: *Experimental Data Treatment*, Woodhead Publ. New Delhi 2011

POROVNÁNÍ SPLÝVAVÝCH PROFILŮ ZÍSKANÝCH RŮZNÝMI METODAMI

Translation of the article
Comparison of drape profiles obtained by various techniques

Abstrakt: Splývavost patří mezi základní charakteristiky textilií, které rozhodují o jejich vzhledu a omaku. Souvisí úzce s mechanickými projevy textilií při nízkých úrovních zatížení jako jsou ohybová tuhost, tahové a smykové namáhání a stlačitelnost . Cílem tohoto příspěvku je analýza porovnání profilů splývavosti získaných pomocí různých technik matematického modelování jako je analýza konečných prvků a metoda polárních souřadnic. Pro porovnání těchto technik je využito deseti speciálně vybraných bavlnářských textilií.

MEASUREMENT OF DRAPE USING DIGITAL IMAGE PROCESSING TECHNIQUE

Rajesh Mishra, Jiří Militký, B.K. Behera[1] and Dana Křemenáková

Faculty of Textile Engineering, Technical University of Liberec, Czech Republic
[1] Department of Textile Technology, IIT Delhi, India
rajesh.mishra@tul.cz

Abstract: *Fabric drape is one of the most important properties of flexible material. The drape ability of a fabric is usually characterized by dimensionless value called "drape coefficient", which is defined as the percentage of the area from an angular ring of the fabric covered by a vertical projection of the draped fabric. The main aim of this contribution is description of an instrument based on the basic idea of Cusik's drapemeter and using image processing technique for evaluating of standard and special drape characteristics like number of nodes, drape distance ratio, fold depth index, minimum/maximum/average radius etc. The applicability of this approach was tested by the analysis of commercial apparel grade cotton fabrics.*
Key words: *Fabric drape, drape characterization, image processing, cotton fabrics drape ability*

1 INTRODUCTION

Fabric drape is one of the most important properties of flexible material. It is also one of many factors that influence the aesthetic appearance of a fabric and has an outstanding effect on the formal beauty of the cloth. Drape is important for the selection and development of textile material for apparel industries. Studies of drape were first begun by Chu, when he established a measuring method for fabric drape using FRL drapemeter [1]. Chu quantified the drapability of a fabric into a dimensionless value called "drape coefficient", which is defined as the percentage of the area from an angular ring of the fabric covered by a vertical projection of the draped fabric. The apparatus was further studied by Kaswell and later revised by Chu [2]. Finally Cusik investigated the experimental method again by using a parallel light source that reflects the drape shadow of a circular specimen from hanging disc into a piece of ring paper to calculate drape coefficient [3, 4].

The most widely accepted method of drape test, according to IS 8357:1977, uses the drapemeter. In this test, a circular cloth sample whose diameter is 10 inches is placed on a disk of diameter of 5 inches. The cloth drapes and compresses internally owing to gravity, finally resulting in a flared shape. Then the drape coefficient, described as the ratio of the vertical projection area to the entire sample area, is used to evaluate cloth drapeability [5]. All these methods have several disadvantages; the testing is time consuming, tracing of the pattern by hand is highly dependent on the skill of the operator, the light source needed is of special type, the mass variation in the paper or presence of wrinkles to wet treatment may cause error in the calculation of the drape coefficient. Improved measurement of drapeability based on the use of drapemeter and digital imaging is described in the work of Glombikova [12].

The drape coefficient only is not sufficient to describe the aesthetic appearance. This may be influenced by such geometrical factors as the number of nodes and the curvature of the draped fabric. Equivalent drape coefficient is possible for two different fabrics, depending on the node values. Thus it may be better to use the distribution of the number of nodes with the drape values to describe the aesthetic appearance [6]. According to Matsudaria & Zhang [7], drape constant is not always constant for each fabric. The coefficient changes mostly with the number of nodes. Therefore, more reliable and

meaningful methods to measure the drape coefficient are necessary.
As discussed above, drape is an essential parameter to decide both appearance and handle of fabrics [14]. It is also a secondary determinant of fabric mechanical properties and influenced by the low stress mechanical properties like bending rigidity, formability, tensile and shear properties & compressibility of the fabric [8]. All these mechanical properties have a direct bearing with basic fiber properties and fabric construction [9]. It is observed over a decade that the consumers prefer to wear light weight fabrics. At the same time fabric comfort has gained priority over fabric durability. When fiber composition is changed along with fabric areal density, fabric drape ability is expected to be influenced significantly. With decrease in fabric areal density, the fabric becomes more flexible and may get loose structural stability. The drape parameters such as: number of folds, depth of folds, evenness of folds together with the drape coefficient need to be examined. The relationship between these parameters and fabric mechanical properties is already established [10-11].
It is therefore thought worthwhile to make a study on drape ability of some fabrics produced from various non-conventional fiber blends. Besides new blends, some conventional fabrics of identical constructions were also prepared for comparison and analysis purpose. The various drape parameters like Drape coefficient, Number of nodes, Drape distance ratio, Fold depth index & Amplitude were correlated to the fabric low stress mechanical properties tested on the Kawabata Evaluation System (KES) [12, 14].

2 MATERIALS

Cotton being the most used fiber in apparel sector. A wide range of mostly used commercial apparel grade fabrics are used for this study. This study is mainly focused on sixty five samples. These samples were collected from various reputed industries. The constructional parameters of these fabrics were tested according to the ASTM standard. All the sixty five samples were conditioned for 24 hours in the 200 ± 20°C and 65 ± 5 % RH prior to testing. The testing of the samples was carried out in accordance with the ASTM standard.
The type of fabric, the weave, and yarn count of each of the selected fabrics were collected. Variation of areal mass was in the range from 78 to 372 g m^{-2}.

3 DRAPE MEASUREMENT BY CONVENTIONAL METHOD

A circular fabric specimen of 10 inches diameter is supported on a circular disk of 5 inches diameter and the unsupported area drapes over the edge. Here the drape is the extent to which the fabric will deform when it is allowed to hang under the influence of gravity only. A planner projection of contour of the draped specimen was marked on a uniform paper. The drape pattern obtained was cut along the outline. Then on weighing balance it was weighted. Let its weight be W_s. Similarly the paper was cut according to edges of larger and smaller discs of the drape meter and they were weighted. Let their weights are W_D and W_d respectively. Then the drape coefficient D is: [6]

$$D = \frac{W_s - W_d}{W_D - W_d} \quad (1)$$

4 DESIGN OF THE DIGITAL DRAPEMETER

To measure the drapeability of the fabric using image processing technique, an instrument was fabricated based on the basic idea of Cusik's drapemeter. It is designed in such a way that it can be used for conventional as well as for image processing technique for accurate results.
The schematic diagram of the drapemeter is shown in Figure 1. In this design, the draped shadow image was captured at top glass plate (2). For this a bulb (3) was lightened up which throws the light on concave mirror (5) placed underneath. Then light reflected from the concave mirror, would be parallel rays.

Thus gives an exact shadow of the draped fabric. For capturing the image without the background a thin uniform density paper was placed on the top glass plate. Thus the digital camera (1) mounted above, operated by the computer captures the clear image formed. This image was then saved in computer (6 and 7) and processed by the program to give the various drape parameters such as drape coefficient, drape distance ratio, amplitude to radius ratio, fold depth index, number of nodes.

The acquired image is a color image having the format of JPEG. The standard dimension of the image is xxx X xxx and the depth of the image is 36 bit.

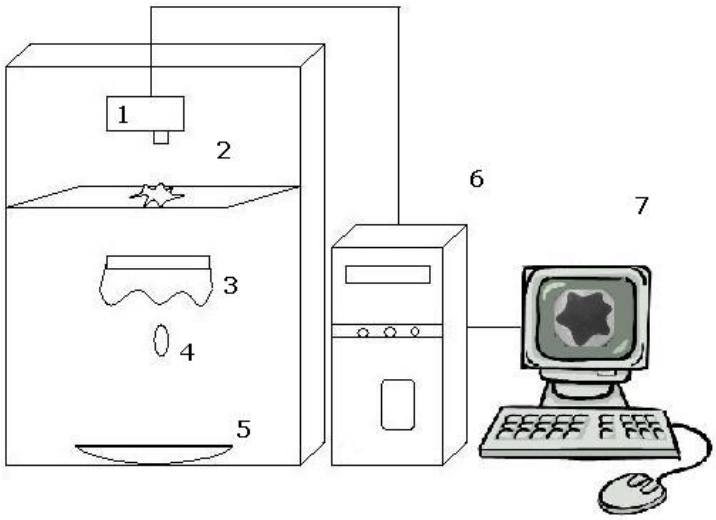

Figure 1 The schematic diagram of the Digital Drapemeter

In this measurement technique, first image is grabbed by the CCD camera and that image is processed by the software developed in the MATLAB to calculate the various drape parameters. The sequence of image processing operations used for determination of drape parameters, are given below in Figure 2.

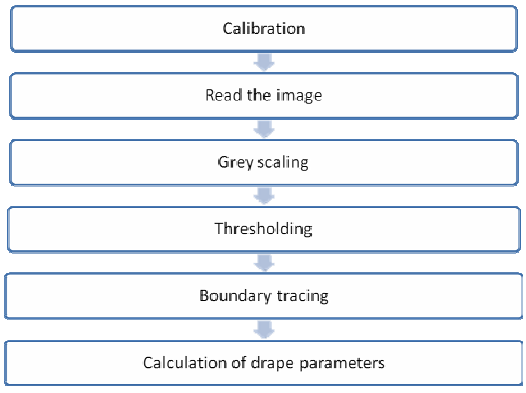

Figure 2 The flow chart of the working principle of the Digital Drapemeter

4.1 Calibration

Before the measurement of drape parameters of a new fabric, a fabric of the same dimension of the supporting disc is estimated for the calibration of the digital camera. The main objective of this process is to convert the pixel values of the radii to centimeter scale. As it is already mentioned that the diameter of the supporting disc is 5 inches and the dimension of the image is in pixels. The calculated radii are in pixels. So the radii are converted into centimeter scale by multiplying the conversion factor. The other objective of the calibration process is to eliminate the digital camera settings as the digital camera settings are subject to change with every mounting.

4.2 Read Image

The acquired image is a color image having the format of JPEG. A suitable code is developed to read the image and stores the

image into a matrix form of the same dimension of the acquired image.

4.3 Grey Scaling

In this process the color image is converted into a digital image having the value of each pixel is a single sample and carries only intensity information. Images of this kind are composed exclusively of shades of grey, varying from black at the weakest intensity to white at the strongest. The conversion of grey scale image from the color image is carried by the standard procedure of Matlab. To convert any color to a grayscale representation of its luminance, first one must obtain the values of its red, green, and blue (RGB) primaries in linear intensity encoding, by gamma expansion. Then, add together 30% of the red value, 59% of the green value, and 11% of the blue value (these weights depend on the exact choice of the RGB primaries, but are typical). Regardless of the scale employed (0.0 to 1.0, 0 to 255, 0% to 100%, etc.), the resultant number is the desired linear luminance value; it typically needs to be gamma compressed to get back to a conventional grayscale representation.

4.4 Threshold

Threshold is the simplest method of image segmentation. From a grayscale image, threshold can be used to create binary images. During the threshold process, individual pixels in an image are marked as “object” pixels if their value is greater than some threshold value (assuming an object to be brighter than the background) and as “background” pixels otherwise. This convention is known as threshold above. Typically, an object pixel is given a value of “1” while a background pixel is given a value of “0.” Finally, a binary image is created by coloring each pixel white or black, depending on a pixel's label. The threshold value is set by choosing the mean value of the image. If the brightness of the object pixel is greater than the mean value of the brightness then the value is considered 1 otherwise it is set to 0. This method is simple but vulnerable to noise. To avoid this problem the following iterative method is used.

The mean threshold (T) is chosen. The image is segmented into object and background pixels as described above, creating two sets: G_1 = {f m,n) > T}, where, G_1 is the object pixels and: G_2 = {f (m,n) <= T}, where, G_2 is the background pixels.

Here, f (m,n) is the value of the pixel located in the m^{th} column, n^{th} row.

The average of each set is computed: m_1 = average value of G_1; m_2 = average value of G_2.

A new threshold is created that is the average of m_1 and m_2 i.e. T’ = (m_1 + m_2)/2

Then these steps are repeated by using the new threshold until the new threshold matches the one before it (i.e. until convergence has been reached).

5 CALCULATION OF DRAPE PARAMETERS

The image boundary of a draped fabric consists of a number of discrete points, and the discrete points define a polygon, which is used to calculate the drape characteristics. Thus an image consists of (n-1) triangles, where n is the number of points that form the boundary of the image.

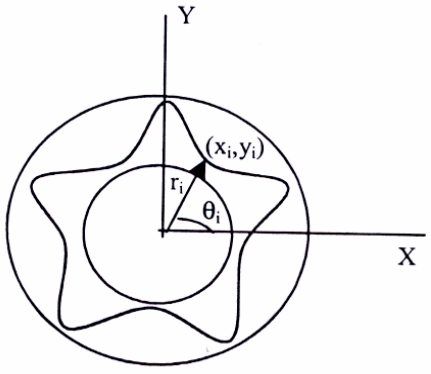

Figure 3 Draped fabric image

Hence from Fig. 3, $X_i = r_i \cos \theta_i$ and $Y_i = r_i \sin \theta_i$. Average radius is $R_a = (1/n)\Sigma r_i$

Area for the triangle (A) of (0,0), (X_1,Y_1) and (X_2,Y_2) points can be given by

$$A = \frac{1}{2} r_1 \, r_2 \, \sin\theta \quad (2)$$

Therefore total area for the boundary curve (S) can be given by

$$A_S = \frac{1}{2} \sum_{i=1}^{n-1} r_i \, r_{i+1} \, \sin\theta \quad (3)$$

Thus we need angle and radius at different points to get the area. For this first of all centre point of the binary image is located and then it is rotated by a constant angle and radius is calculated at all points. For the calculation, boundary of fabric shadow is approximated by 1 degree Thus we have 360 points on the boundary of the image, so θ = 1° and n = 360.

With these parameters now we can calculate different drape parameters such as drape coefficient *DC*, average radius *r*, maximum radius (r_{max}), minimum radius (r_{min}), drape distance ratio (*DDR*), amplitude, number of nodes (*N*), and fold depth index (*FDI*).

Drape coefficient *DC* is defined by standard manner

$$DC[\%] = \frac{A_s - A_1}{A_2 - A_1} \, 100 \quad (4)$$

Drape distance ratio *DDR* is defined as

$$DDR \, [\%] = \frac{r_2 - r_s}{r_2 - r_1} \, 100 \quad (5)$$

Fold depth index *FDI* is defined as

$$FDI \, [\%] = \frac{r_{max} - r_{min}}{r_2 - r_1} \, 100 \quad (6)$$

Amplitude *ARR* is characterized by relation

$$ARR = \frac{r_{max} - r_{min}}{2} \quad (7)$$

In these equations are: the area of the draped fabric image A_S, area of the fabric supporting disc A_1, the area of the undraped fabric sample A_2, radius of the fabric supporting disc r_1, the radius of the undraped fabric sample r_2, the maximum radius of the draped fabric image profile r_{max}, the minimum radius of the draped fabric image profile r_{min}, the average radius of the draped fabric image profile r_{avg}.

6 RESULTS AND DISCUSSION

The fabric samples were measured using the new developed digital image processing technique and also by the conventional technique (British Standard Institute: BS5058, 1974 using the Cusick Drapemeter) discussed earlier. The correlation matrix between drape coefficient *DCc* measured by the conventional technique, drape coefficient *DCd* evaluated by digital image processing technique, drape distance ratio *DDR,* fold depth index *FDI,* number of nodes *NI* and amplitude *ARR* is shown in Table 1. The paired dependencies between drape characteristics are shown in the Figure 4.

The results for drape coefficients for the different fabric samples obtained by image processing technique and conventional method are given in Figure 4. There is visible practically linear dependence between *DCc* and *DCd* which is logical. Interesting are also the correlations between *NI* and *CDd* or between *FDI* and *DDR.*

Table 1 Correlation between drape parameters measured by conventional technique and the digital image processing technique

	DCc	***DCd***	***DDR***	***ARR***	***FDI***	***NI***
DCc	1	0.9919	0.4309	0.2280	0.3168	-0.5484
DCd	0.9919	1	0.4067	0.3385	0.3003	-0.6170
DDR	0.4309	0.4067	1	0.0087	0.7452	-0.5436
ARR	0.2280	0.3385	0.0087	1	0.0571	-0.6249
FDI	0.3168	0.3003	0.7452	0.0571	1	-0.4523
NI	-0.5484	-0.6170	-0.5436	-0.6249	-0.4523	1

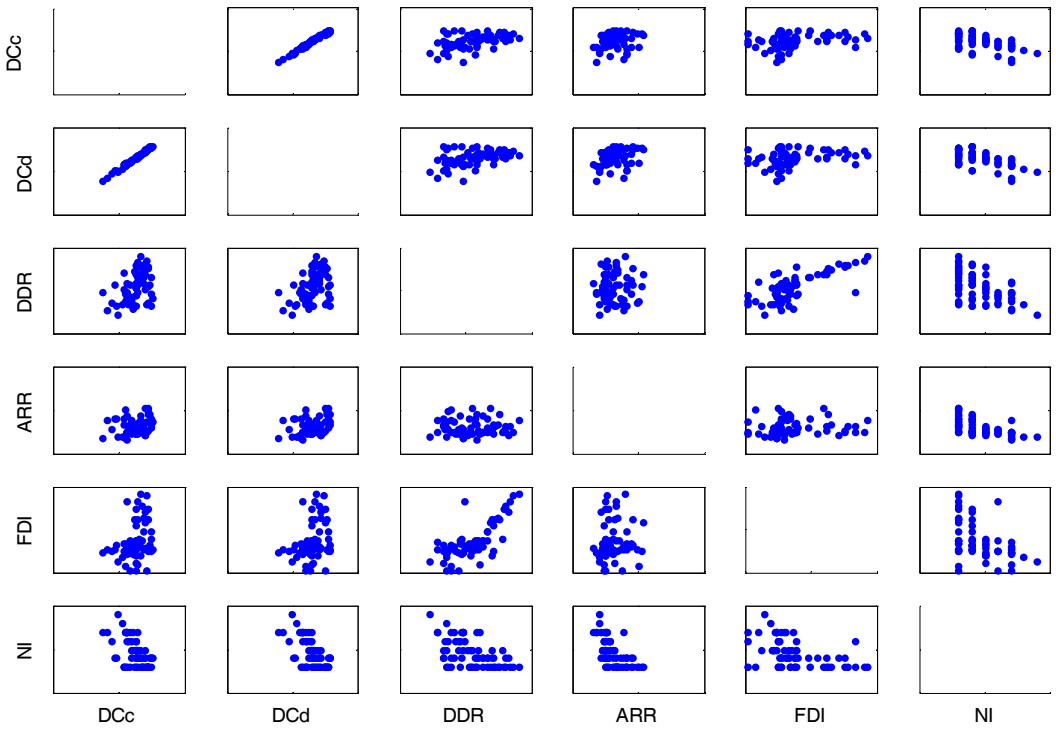

Figure 4 Paired relations between drape characteristics

Very good correlation (r = 0.9919) between drape coefficients *CDc* measured by Cusick's method and *CDd* from image processing technique shows that the new measurement method can replace the conventional technique. Results of liner regression with criterion orthogonal least squares (i.e. minimization of sum of squared distances - because both variables are subjected with random errors [15]) are shown in the Figure 5.

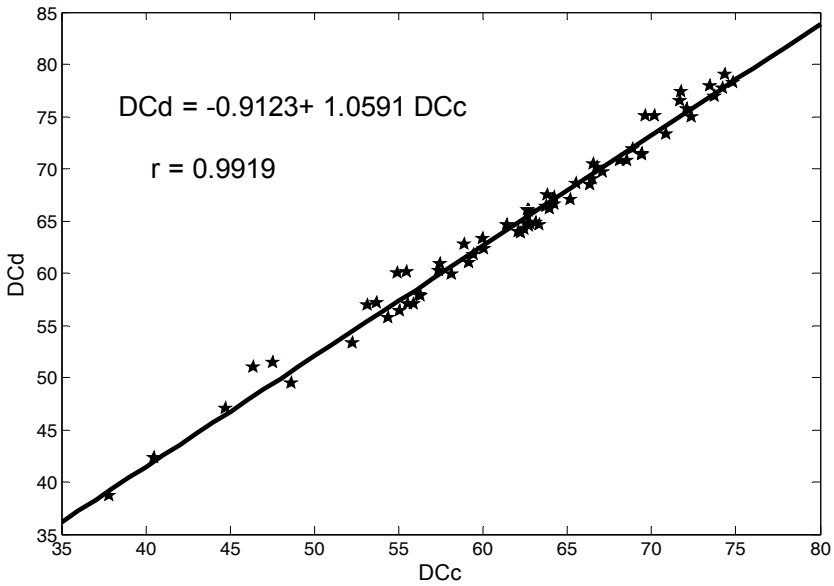

Figure 5 Comparison between standard *DCc* and *DCd* obtained by image processing by using orthogonal least squares criterion

The slope equal practically to one is indication that there is not bias between both techniques of drape coefficient evaluation.
Apart from the drape coefficient, this new technique is able to measure the other important parameters for the complete understanding of the drape profile.

7 CONCLUSION

The problems involved in measuring and making an analysis of draping behavior of textile fabrics are discussed. It is proposed that progress can be made by making the measuring principle more accurate. Design and development of such a drapemeter based on image processing technique is discussed in this chapter. Some new parameters are defined.
A drapemeter has been developed for the measurement of drape values by image processing. It was observed that the results obtained by this instrument are not significantly different from those obtained by the conventional method. This method does not require as much time and skill. With the image analysis system, new measures of drape such as the drape distance ratio, number of nodes, fold depth index and amplitude, were defined. However it is cumbersome to measure drape values many times with the conventional method. But with image analysis system it is quite easier to have multiple measurements.

8 REFERENCES

1. The assessment of drape of fabrics, British Standard Institute, B.S Handbook 4, 1973, 29-31
2. Behera B.K. and Mishra R.: Objective Measurement of Fabric Appearance using Digital Image Processing, *J. Text. Inst.* 97(2), 2006, 142-153
3. Behera B.K. and Pangadiya A.: Drape Measurement by Digital Image Processing, *Tex. Asia* 34(11), 2003, 45-50
4. Bhatti M.A.: Advance Topics in Finite Element Analysis of Structures, John Willey & Sons Inc., Chapter 6, 2006, 331-336
5. Cusik G.E.: The measurement of fabric drape, *J Text Inst* 59(6), 1965, T253-60
6. Cusik G.E.: The Dependence of Fabric Drape on Bending and Shear Stiffness, *J. Tex. Inst.* 56(1), 1965, T596-606
7. Chen S.F. et al.: A finite volume method for contact drapes simulation of woven fabrics and garments, *Finite Element in Analysis & Design* 37, 2001, 513-531
8. Collier R. et al.: Drape prediction by means of finite element analysis, *J. Tex. Inst.* 82(1), 1991, 96-107
9. Hu J. and Chan Y.F.: Effect of Fabric Mechanical Properties on Drape, *Text. Res. J.* 68(1), 1998, 57-64
10. Jedda H. et al.: Prediction of fabric drape using the FAST system, *J. Tex. Inst.* 98(3), 2007, 219 – 225
11. Kawabata S.: HESC standard evaluation, *The Text. Mach. Soc. of Japan*, 2nd edition, 1984, 130-141
12. Lo W.M. et al.: Modeling a Fabric Drape Profile, *Text. Res. J.,* 72(5), 2002, 454-463
13. Glombíková V.: The 3D Drape Scanner, *Proc 15th Int. conference STRUTEX*, Liberec December 2008
14. Militký J.: „Application of statistical methods in evaluation of fabric hand“, chap. 4 in book: *Effect of mechanical and physical properties on fabric hand*, Woodhead Publisher 2005
15. Meloun M., Militký J.: *Experimental Data Treatment*, Woodhead Publ. New Delhi 2011

HODNOCENÍ OMAKU POMOCÍ OBRAZOVÉ ANALÝZY

Translation of the article
Measurement of Drape Using Digital Image Processing Technique

Abstrakt: Splývavost patří mezi důležité charakteristiky flexibilních materiálů. Schopnost splývání se obyčejně charakterizuje bezrozměrnou veličinou „koeficient splývavosti“ což je relativní rozdíl původní plochy textilie a plochy kolmé projekce textilie upnuté do přístroje. Cílem této páce je popsat přístroj pro měření splývavosti, který vychází ze základního uspořádáni Cusikova drapemetru. Pro určování standardních a speciálních charakteristik splývavosti jako je počet záhybů, podíl vzdáleností deformovaného vzorku, index hloubky záhybů, poměr poloměrů minimum/maximum/průměr atd. je použito informací získané z analýzy digitálního obrazu textilie deformované vlivem splývání. Použitelnost tohoto přístupu je ověřena analýzou splývavosti komerčně dostupných bavlnářských tkanin.

MECHANICAL AND FUNCTIONAL CHARACTERIZATION OF FIBER REINFORCED NANOCOMPOSITES

Rajesh Mishra, Richa Tiwari, B. K. Behera[1] and Jiří Militký

Faculty of Textile Engineering, Technical University of Liberec, Czech Republic
[1] Department of Textile Technology, IIT Delhi, India
rajesh.mishra@tul.cz

Abstract: *This work presents an insight into the effect of preparation procedure and the filler content on functional and mechanical properties of glass fabric reinforced nanocomposite systems. For the preparation of the nanocomposites unidirectional glass fabrics was used. Methyl siloxane is the reins used in the study. As fillers, carbon black (CB) nanoparticles having size <50 nm were used. The characterization of nanocomposite systems was done using Thermal Mechanical Analysis (TMA), low velocity impact testing, tensile testing, thermal conductivity and electrical conductivity measurements. The morphology of composite was characterized by Scanning Electron Microscopy (SEM). The thermal conductivity of the composite was measured by Differential Scanning Calorimetry (DSC) and Alambeta thermal conductivity tester. The electrical conductivity was measured by 2 probe electrode method.*

Key words: *Nano-composites, Scanning Electron Microscopy (SEM), Differential Scanning Calorimetry (DSC), Knife penetration resistance*

1 INTRODUCTION

Traditional fiber-reinforced composites have improved over the years with respect to their material properties and have gained considerable acceptance in the aerospace industry. The inplane properties of the fiber/polymer composite system are defined by the fiber properties, while the properties along thickness dimension are defined by the characteristics of the matrix resin [1]. The use of an additional phase (e.g. inorganic filler) have been proven to improve the mechanical properties of the resin as well as some nanofillers can be used to get some additional functional properties to the composite material [2].

Nano-phased matrix based on organic polymers and inorganic particles such as carbon nanoparticle have attracted great interest because they frequently exhibit unexpected properties including reduced gas permeability, improved solvent resistance, superior mechanical and enhanced flame retardant properties. Different polymer/carbon nanocomposites have been successfully synthesized by incorporating various polymer matrixes such as epoxy [6, 7].

The primary interest of this paper was to characterize the effect of carbon nanoparticles on the thermal, electrical and mechanical properties of Methyl Siloxane. An ultrasonicator was used to disperse carbon nanoparticles in the resin.

The dependence of heat flow Q ,thermal expansion coefficient, α, the dynamic mechanical parameters, E', E'', tanδ, Tg, thermal and electrical parameters (λ, R and ρ),impact energy are associated with the filler content and is controlled by the employed curing conditions. Experimental results show that some functional properties can be enhanced by the incorporation of nanoparticles. The mechanical strength enhancement can be attributed to the intrinsic characteristics of the nanoparticles based on the rule of mixture. Electrical conductivity, which is observed at about 1% w/w of nanoparticles, indicates the creation of conducting paths and is associated with the Maxwell Wagner Sillars (MWS) relaxation, probably due to the formation of aggregated microstructures in the bulk composite [3, 5, 6]. The results of DSC show that the heat flow rate through nanocomposite is higher than the pure resin composite.

2 EXPERIMENTAL PART

The resin used in this study is commercially available Polymethyl Siloxane (Lukosil). It is a low viscosity resin. The Carbon nanoparticles used in the study were obtained from Sigma Aldrich USA having particle size < 50 nm.
The pre calculated amount of carbon nanoparticles and resin were carefully weighted and mixed together in a beaker. The mixing is carried out through a high intensity ultrasound irradiation by a probe type of sonicator (Bandelin Sonoplus Sonicator, UK) for 10 minutes with the maximum energy of 30 KJ.
The glass fabric sample was coated with the prepared carbon/siloxane resin and left for room temperature curing for 16 hrs. The test samples were again coated with the same carbon/siloxane resin and post cured at 200°C for 6 hrs. Finally test samples were cut from the original one for thermal, electrical and mechanical characterization.
Hewlett Packard (hp) 4339B high resistance meter was used to measure the surface resistance and volume resistance of the composite. The environmental condition for the measurement was 22°C temperature and 29.5% relative humidity and voltage used was 100 V.
A Perkin Elmer Differential Scanning Calorimeter (Pyris 6, DSC) was used under nitrogen atmosphere. The measurements were performed from room temperature to 400°C at a scanning rate of 10°C/min
A RMI Thermomechanical Analyzer TMA CXO 3RA-T was used. The measurements were performed from room temperature to 800°C , static force of 100 mN and frequency 5°C/min.
Thermal conductivity of the sample was measured on Alambeta Thermal conductivity tester (hot plate method).
Knife penetration resistance of the composite samples was measured on Impact tester.

3 RESULTS AND DISCUSSION

Volume resistivity of the composite samples is shown in Figure 1. Volume resistivity and the surface resistivity of the nanocomposite sample were found lesser than the neat resin composite.

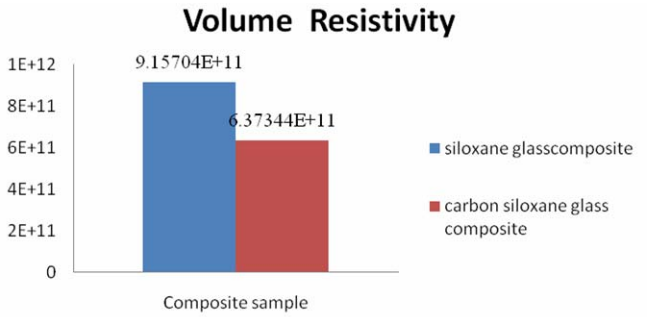

Figure1 Volume resistivity fo the composite samples

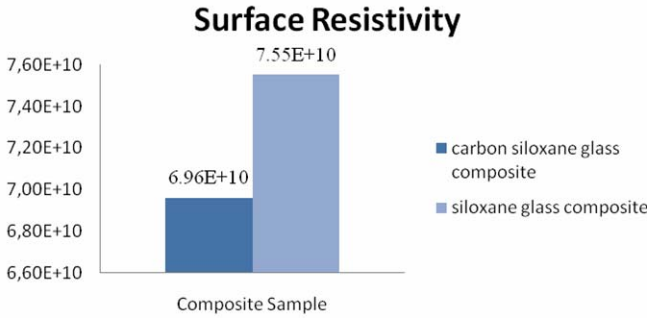

Figure 2 Surface resistivity of the composite

Higher electrical conductivity of the carbon nanocomposite is due to the formation of conductive path inside the composite according to Maxwell Wagner and Sillars. The simplest model for describing an inhomogeneous structure is a double layer arrangement, where each layer is characterized by its permittivity $\varepsilon_{1,2}$ and its conductivity $\sigma_{1,2}$. The relaxation time *TMW* is then:

$$TMW = \varepsilon_0 \frac{\varepsilon_1 + \varepsilon_2}{\sigma_1 + \sigma_2} \quad (1)$$

Importantly this shows that an inhomogeneous material may have frequency dependent response, even though none of the individual inhomogeneities severally are frequency dependent.
A more sophisticated model for treating interfacial polarization was developed by Maxwell, and later generalized by Wagners and Sillars. Maxwell considered a spherical

particle with a dielectric permittivity ε'_2 and radius *R* suspended in an infinite medium characterized by ε_1.
Figures 3 and 4 show heat flow rate through the composite and thermal expansion coefficient of the composite .Heat flow rate through the nanocomposite was higher than the neat resin composite .Thermal expansion coefficient of the nanocomposite was lesser than the neat resin composite.

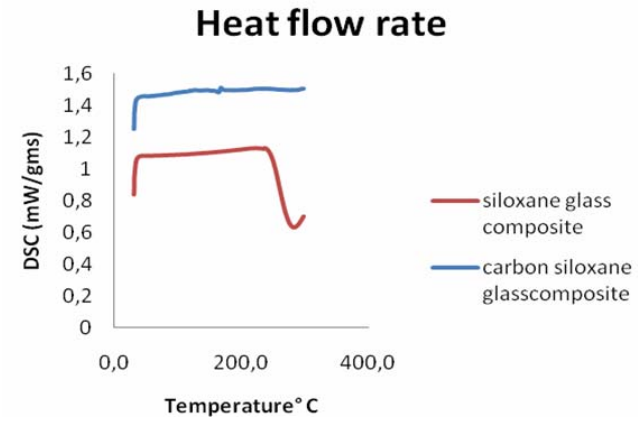

Figure 3 Heat flow rate through the composite

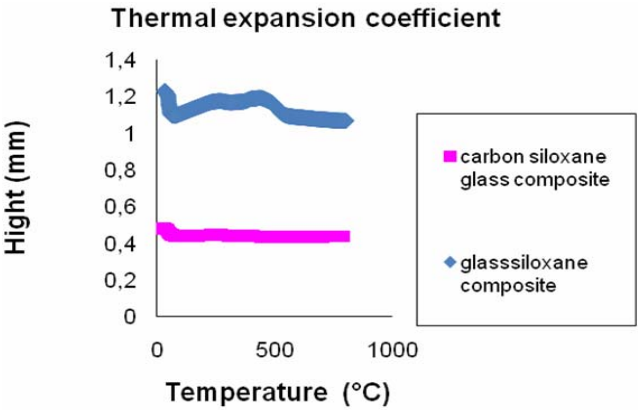

Figure 4 Thermal expansion coefficient

Nanoparticles when reinforced in to the polymer matrix create restrictive environment of the polymer chains inside the clay gallery which greatly effects molecular relaxation, mobility, and also their crystallization. Hence carbon nanoparticles induce a crystalline phase transition. Polymer molecules are sensitive to the local environment because of the characteristic long-chain morphology. Therefore, the values of Thermal expansion coefficient and normalized change of heat capacity (ΔCp) of a polymer at glass transition are important parameters that provide information about the structural changes undergone by the polymer during the transition. Nanoparticles are known to induce phase transitions in some polymer systems by providing nucleation sites.
Figure 5 shows thermal conductivity, thermal diffusivity and heat flow density of the composites and Figure 6 shows thermal absorptivity and thermal resistivity of the composites. Thermal conductivity , peak heat flow density and thermal absorptivity of nanocomposite was found higher than the neat resin composite .Thermal diffusivity and thermal resistivity of the nanocomposite was lesser than the neat resin composite.

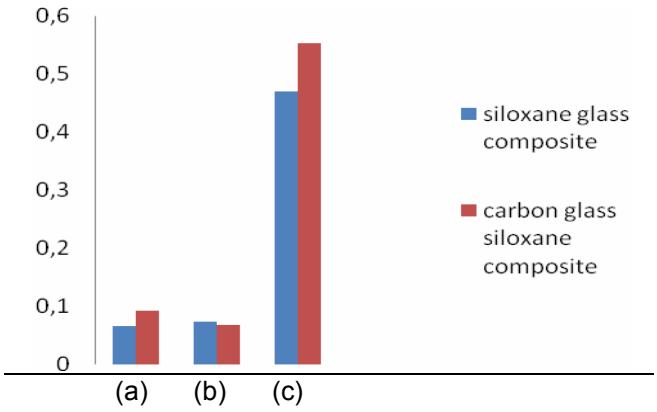

Figure 5 Comparison of (a) thermal conductivity λ ($Wm^{-1}k^{-1}$), (b) thermal diffusivity a (m^2s^{-1}), (c) Peak heat flow density q (wm^{-2}) of siloxane glass composite & carbon glass siloxane composite

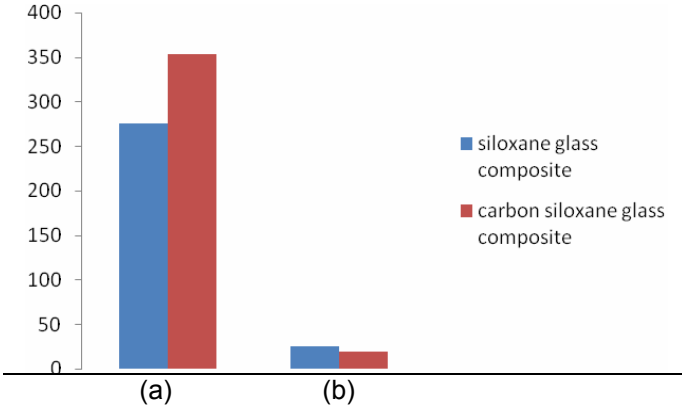

Figure 6 Thermal absorptivity (a) and thermal resistivity (b) of siloxane glass composite & carbon glass siloxane composite

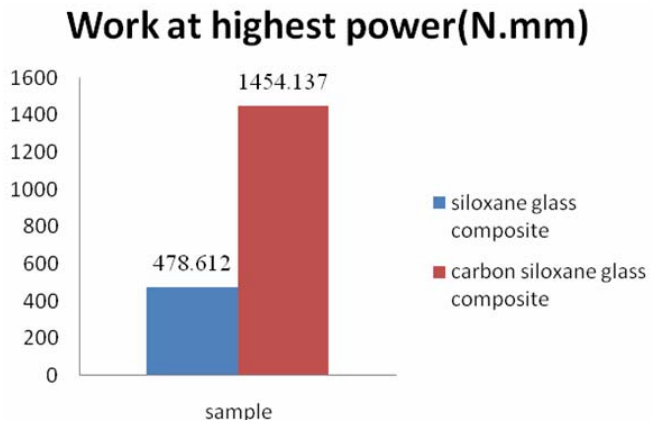

Figure 7 Comparison of work at highest penetration for the nanocomposites & neat resin composite

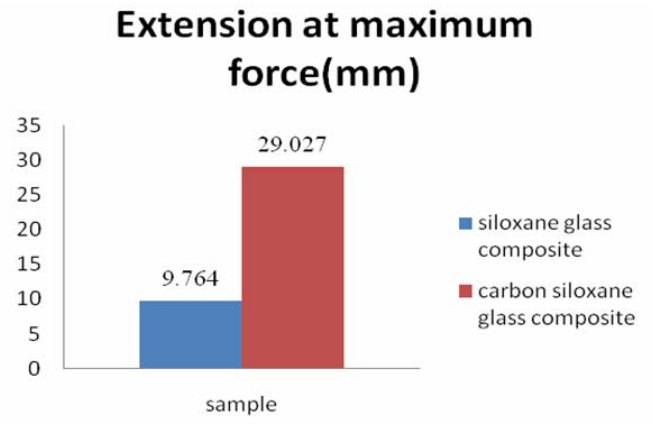

Figure 8 Comparison of Extension at maximum force for the nanocomposites and neat resin composite

Figures 7 and 8 show the work at highest power and extension at maximum force.
For nanocomposite extension and work is greater in comparison to the neat resin composite. The mechanical properties of the polymeric material are attributed to good compatibility b/w nanoparticles and matrix material. This compatibility improves the interfacial adhesion b/w nanoparticles and matrix, which can enhance interlamellar shear strength and alleviate stress concentration. This will prevent the cohesion chain between matrix and filled particles from damaging and restrain crack propagation at the interface so that the composite toughness is improved. This is particularly effective for restraining crack propagation and adsorbing fracture energy, which leads to improved mechanical properties of the composites.

SEM micrographs of the nanocomposite surface are shown in the Figure 9(a-b). SEM investigation of the surface of the nanocomposite and its statistics shows that the particle size distribution was almost uniform. Since the electrical conductivity of our composite system is related to the presence of microstructures. It is expected that the samples with more compactness and incorporation should show higher electrical conductivity.
Particle size distribution statistics on the composite surface for 10 μm magnification is shown in the Figure 10 and for 5μm magnification in the Figure 11.

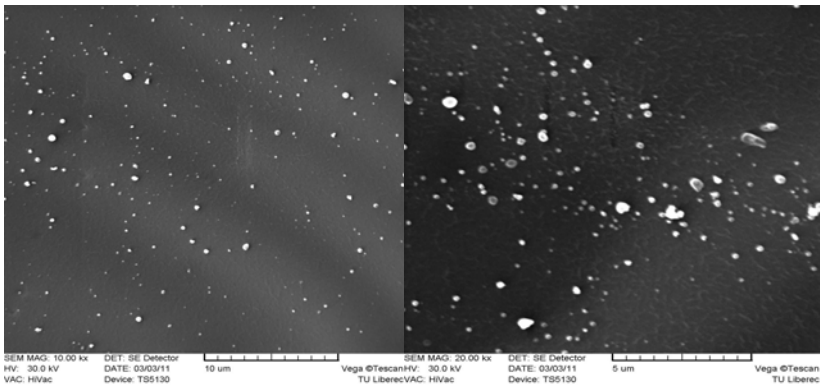

(a) (b)

Figure 9 SEM images of nanocomposite surface, (a) 10μm magnification, (b) 5μm magnification

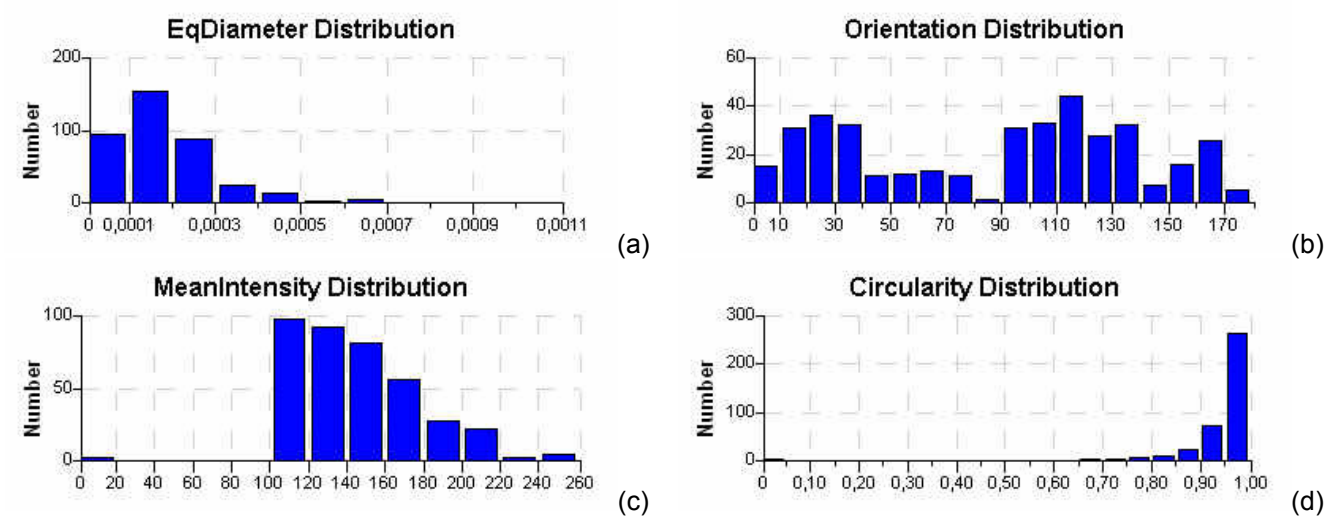

Figure 10 Statistics of carbon nanoparticles distribution on the surface of composite at 10 μm magnification, (a) equivalent diameter distribution, (b) orientation distribution, (c) Mean intensity distribution, (d) circularity distribution

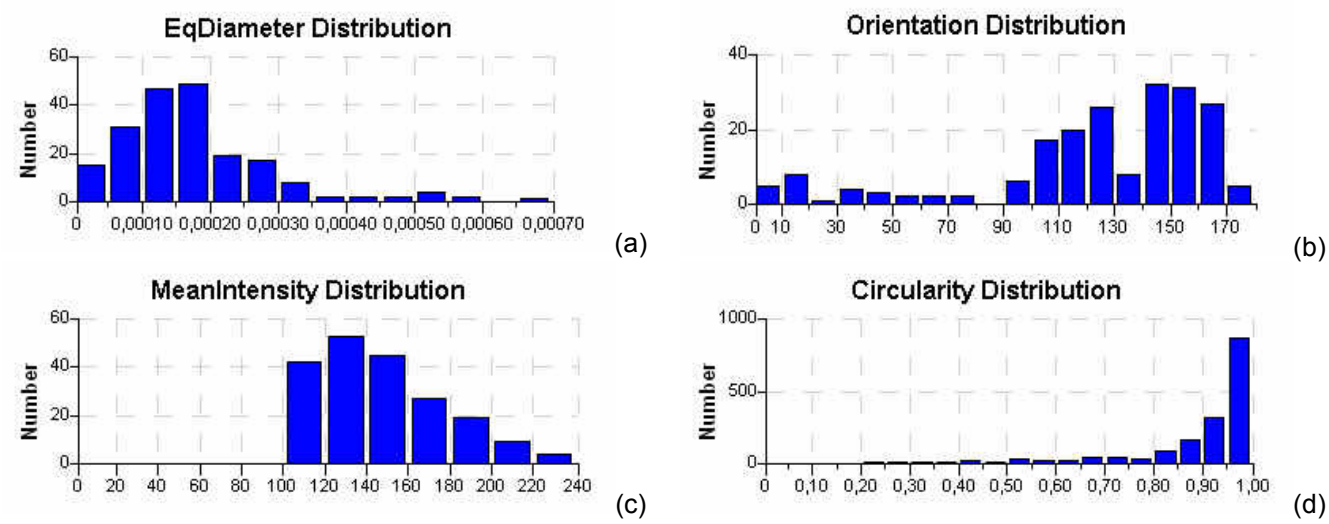

Figure 11 Statistics of carbon nanoparticles distribution on the surface of composite at 5 μm magnification, (a) equivalent diameter distribution, (b) orientation distribution, (c) Mean intensity distribution, (d) circularity distribution

4 CONCLUSIONS

The mechanical strength enhancement can be attributed to the intrinsic characteristics of the nanoparticles based on the rule of mixture. Electrical conductivity, which is observed at about 1% w/w of nanoparticles, indicates the creation of conducting paths and is associated with the Maxwell Wagner Sillars (MWS) relaxation, probably due to the formation of aggregated microstructures in the bulk composite. The results of DSC show that the heat flow rate through nanocomposite is higher than the pure resin composite as the thermal conductivity parameters for the nanocomposite are higher for the carbon nanoparticles. Smaller thermal expansion coefficient for the nanocomposite is attributed to the induced crystalline phase inside the resin.

5 REFERENCES

1. Zhao Q. and Hoa S.V.: Toughening Mechanism of Epoxy Resins with Micro/Nano Particles, *Journal of Composite Materials* 41(2), 2007, 201-2019
2. Zheng Y., Ning R. and Zheng Y.: Study of SiO_2 Nanoparticles on the Improved Performance of Epoxy and Fiber Composites, *Journal of Reinforced Plastics and Composites* 24(3), 2005, 223-233
3. Kosmidou Th.V., Vatalis A.S., Delides C.G., Logakis E., Pissis P., Papanicolaou G.C.: Structural, mechanical and electrical characterization of epoxy-amine/carbon black nanocomposites, *eXPRESS Polymer Letters* 2(5), 2008, 364-372
4. Wang Yanbing, Huang Zhixiong, Zhang Lianmeng, Mei Qilin: Mechanical and Thermal Properties of Polysiloxanes and NBR Elastomer, *Journal of Wuhan University of Technology- Mater. Sci. Ed*. 21(4), 2006, 92-94
5. Li-Nuan Tsai, Y-T Cheng, and Wensyang Hsu: Nanocomposite Effects on The Coefficient of Thermal Expansion Modification for High Performance Electro-Thermal Microactuator, in *Proc. IEEE MEMS 2005*, Florida, U.S.A., Jan. 30 - Feb. 3, 2005, 467-470
6. Ma P.C., Liu M.Y, Zhang H., Wang S.Q., Wang R., Wang K., Wong Y.K., Tang B.Z., Hong S.H., Paik K.W., Kim J.K.: Enhanced electrical conductivity of nanocomposite containing hybrid fillers of carbon nanotubes and carbon black, *ACS Appl Mater Interfaces* 1(5), 2009, 1090-1096
7. Zhou Y., Pervin F., Biswas M.A., Rangari V.K., Jeelani S.: Fabrication and characterization of montmorillonite clay-filled SC-15 epoxy, *Materials Letters* 60(7), 2006, 869-873
8. Lihua Lv and Bohong Gu: Transverse Impact Damage and Energy Absorption of Three-Dimensional Orthogonal Hybrid Woven Composite: Experimental and FEM Simulation, J*ournal of Composite Materials* 42, 2008, 1763-1786
9. Ibeh Ch., Zhou N, and Beyle A.: Lightweight nanocomposite hierarchical structures for blast mitigation, *Plastics research online* 10.1002 /spepro .000040
10. Yokoyama T., Huang C.C.: Nanoparticle Technology for the Production of Functional Materials, KONA Powder and Particle No. 23, 2005, 7-17
11. Hu H., Zhang M., Fangueiro R. and De Araujo M.: Mechanical Properties of Composite Materials Made of 3D Stitched Woven-knitted Preforms, *Journal of Composite Materials* 44(14), 2010, 1753-1767
12. Zhang Y., Huang Z.M. and Ramakrishna S.: Tensile Behaviour of Multilayer Knitted Fabric Composites with Different Stacking Configuration, *Applied Composite Materials* 8(4), 2001, 279-295
13. Hufenbach W., Gude M., Ebert Ch.: Hybrid 3D-textile reinforced composites with tailored property profiles for crash and impact applications, *Composites science and technology* 69(9), 2008, 1422-1426
14. Uygun A., Turkoglu O., Sen S., Ersoy E., Yavuz A.G., Batir G.G.: The electrical conductivity properties of polythiophene/TiO2 nanocomposites prepared in the presence of surfactants, *Current Applied Physics* 9(4), 2009, 866-871
15. Lee S.H., Kim J.E., Song H.H., Kim S.W.: Thermal Properties of Maleated Polyethylene/Layered Silicate Nanocomposites, *International Journal of thermo Physics* 25(5), 2004, 1585-1595
16. Shahid N., Villate R.G., Barron A.R.: Chemically functionalized alumina nanoparticle effect on carbon fiber/epoxy composites, *Composites Science and Technology* 65(14), 2005, 2250-2258
17. Goutianos S., Pejis T., Nystrom B., Skrifvars M.: Development of Flax Fiber based textile Reinforcement for Composite Application, *Applied Composite Materials* 13(4), 2006, 199-215

MECHANICKÁ A FUNKČNÍ CHARAKTERIZACE NANOKOMPOZITŮ ZESÍLENÝCH VLÁKNY

Translation of the article
Mechanical and Functional Characterization of Fiber Reinforced Nanocomposites

Abstrakt: Příspěvek je zaměřen na zkoumání vlivu přípravy a obsahu plniva na funkční a mechanické charakteristiky u nanokompozitů zesílených tkaninou ze skleněných vláken. Metylsiloxanová matrice je zesílena ještě částicemi uhlíkové černí (CB) s velikostí pod 50 nm. Pro charakterizaci výsledného nanokompozita je použita termo mechanická analýza, nízko rychlostní rázové testování a měření elektrické resp. tepelné vodivosti. Morfologie nanokompozitů je sledována s využití skenovaní elektronové mikroskopie.

POLYPYRROLE COATED COTTON FABRIC: THE THERMAL INFLUENCE ON CONDUCTIVITY

Mohamed A. Ramadan[ab], A. M. Rehan Abbasi[ac], J. Wiener[a], V. Baheti[a] and J. Militky[a]

[a] *Faculty of Textile Engineering, Technical University of Liberec*
Studentská 2, 461 17 Liberec, Czech Republic
[b] *Textile Research Division, National Research Center, Egypt*
[c] *Department of Textile Engineering BUITEMS Quetta Pakistan*
rehan.abbasi@tul.cz

Abstract: *Polypyrrole (PPy), one of the most extensively investigated conducting polymers, has attracted a great deal of interest because of its good electrical conductivity, environmental stability and easy synthesis. In this study, PPy was coated by chemical oxidation through in-situ polymerization technique. Tetraethyl ammonium p-toluene sulfonate (TEAp-TS) was chosen as doping agent along with $FeCl_3$ as oxidizing agent. Six different fabric samples were prepared by varying concentration of monomer, doping agent and oxidizing agent in order to achieve different samples with electrical conductivities. Each sample was exposed to four different temperatures (80, 120, 160 and 200°C) and electrical resistance was recorded at different intervals in the range 0-600 sec. In this way the influence of temperature on electrical resistance of PPy coated fabric samples was analyzed and found that resistance decreases with the increase in temperature. IR spectrum confirms that there is no change in PPy before and after heating of samples.*

1 INTRODUCTION

In recent time, most of scientific researchers turned to prepare conductive substrate by insert metal into insulating resin or coating a plastic substrate with a conductive metal solution [10]. In this way, conductive fabrics can be prepared to obtain conductive textiles which are very interesting materials because they generally have application in different areas. Actually, the textile materials can be obtained when treated with intrinsically conducting polymers (ICPs) which have received considerable attention of scientists because of its good environmental stability and its application in different areas such as manufacturing of organic transistors and light-emitting diodes [6], functional textiles [7, 13], organic electrodes [15, 18], coatings for fuel cells and corrosion protection [4, 5] and biosensors [11]. The most prominent ICPs are polypyrrole and polyaniline, where electrical conductivity can have values comparable to those observed for poorly conducting metals and alloy [1]. These textiles are able to absorb as well as reflect electromagnetic waves [17], they have also been proposed and tested for acidity-sensing, heating devices [3], design of actuators [9, 12], flame retardation [19, 20], or for printing of conducting patterns on paper [8] and then can exhibit certain advantages over metallic materials. Furthermore, the conductive fabrics are one of the most important of smart/technical materials. ICPs are conjugated polymers, with alternating single and double bonds in the polymer backbone, a necessary condition for charge carriers to move freely along the chain when doping is provided.

Pyrrole can be polymerized by electrochemical oxidation on metallic substrates or by chemical oxidation, and its conducting properties, in terms of conductivity and environmental stability, can be adjusted by doping the polymer with anionic surfactants [14]. Furthermore, some polypyrrole properties (and those of ICPs in general) i.e. volume, surface energy and ionic conductivity depend on the polymer redox state. Polypyrrole was polymerized on the surface of cellulose fibres using a sequence

of fiber impregnation in $FeCl_3$ solutions, thickening and re-dispersion in a pyrrole solution [2]. The conductive cotton fabrics prepared by polymerization of pyrrole in presence of $FeCl_3$ as an oxidizing agent and TEAp-TS a doping agent which in turn caused a reduction in the moisture regain of the substrate, resulted in production conductive cotton fabrics in laboratory scale.
Our research aimed to prepare cotton fabric samples having different levels of electrical resistance and to study the influence of temperature on the resistance of the samples.

2 DEPENDENCE OF RESISTANCE ON THE TEMPERATURE

One of the principal characteristics of materials is their electrical conductivity *K* [$\Omega^{-1}m^{-1}$ or S m^{-1}] characterizing ability to conduct electrical current. Typical conductivity values for polymers range from 10^{-14} to 10^{-17} [S cm^{-1}]. In contrast, the metals are typically around 10^{6} [S cm^{-1}].
The inverse of the conductivity is called resistivity *r* [Ω m]. The total electric resistance *R* [Ω]of a piece of conductive material is proportional to the length *L* and is inversely proportional to its conductivity and cross sectional area *S* i.e.

$$R = \frac{L}{K\ \mathrm{S}} \tag{1}$$

The dependence of *R* on *L* is then straight line with slope $(K\ S)^{-1}$.
The metals electrical conductivity is generally decreasing function of temperature. The dependence of electrical conductivity of semiconductors is generally increasing function of temperature. This function has typical exponential form (analogy with well known Arrhenius relation). The logarithm of electrical conductivity ln σ_E is for majority of conductive polymers linear function of temperature powered on –0.25. The temperature dependence of electrical conductivity is then expressed by the empirical function

$$\ln \sigma_E = \mathrm{a} + \mathrm{b}\ \mathrm{T}^{-1/4} \tag{2}$$

where *a* and *b* are constants. Because the electrical resistivity is inverse function of electrical conductivity the increase of temperature should increase of resistivity. In the case of coated fabrics the temperature dependence of electrical conductivity or resistivity of system is usually more complicated.

3 EXPERIMENTAL PART

Bleached cotton fabric was obtained from INOTEX Czech Republic. Pyrrole monomer was obtained from Merck and Iron (III) Chloride of analytical grade from BDH Chemicals was used. TEAp-TS $[(C_2H_5)_4N(CH_3C_6H_4SO_3)]$ was obtained from Aldrich Chemicals. All the chemicals were used as received.
PPy was coated on the cotton fabric by in-situ polymerization technique by the following steps. In the first step aqueous solution of $FeCl_3$ and TEAp-TS was prepared by molar ratio 1:2, then cotton fabric sample was added into the solution by keeping the liquor ratio 1:25 for 20 min. Fabric sample was then pass through pneumatically controlled horizontal padder with 70% pick up.
Padded fabric sample was then introduced into Ahiba Nuance dye pots which contains aqueous dispersion of pyrrole by keeping liquor ratio 1:25. Pots were then placed into rapid rotary dyer for 4 hr under ambient conditions. Agitation was carried out via rotation of the pots at 25 revolutions per min. Rotation direction was changed automatically each after 1 minute. After polymerization the samples were then thoroughly washed with sufficient amount of distilled water several times to remove the excess of monomer and bi-products and allowed to dry in the air at ambient conditions. Six samples of different electrical resistance were prepared by taking different concentrations of pyrrole, $FeCl_3$ and TEAp-TS, as described in the Table 1.

Table 1 Recipes for substrates preparation

Substrate label	Pyrrole conc. [M/l]	$FeCl_3$ conc. [M/l]	TEAp-TS conc. [M/l]
A	0.2	0.1	0.05
B	0.2	0.15	0.075
C	0.2	0.2	0.1
D	0.2	0.25	0.125
E	0.1	0.25	0.125
F	0.3	0.25	0.125

4 TESTING AND ANALYSIS

The electrical resistance of the polypyrrole-coated cotton fabric was measured using the AATCC 76 two point-probe technique using FLUKA digital multimeter (uni-T, UT70C). The bulk electrical resistance of the dried PPy coated fabric samples was measured in the heating oven (Venticell) at different temperatures and different time intervals. For real time testing, special electrodes as shown in Figure 1(b), made of copper were prepared to mount polypyrrole coated cotton fabrics in order to measure electrical resistance. Figure 1(a) shows the heating oven with a narrow hole in the side wall to mount the sample along with measuring electrodes. High temperature resistant rubber seal was placed around the electrode to prevent heat loses.

The surface morphology of untreated and treated fabric was investigated by using SEM, TESCAN VEGA USA Inc. in Technical University of Liberec. Before SEM imaging the fabric samples were coated with gold particles.

The FT-IR spectra of cotton fabrics treated with polypyrrole were recorded on a FT-IR spectrometer Perkin-Elmer, in the spectra range 4000-400 cm^{-1} using the KBr disc technique.

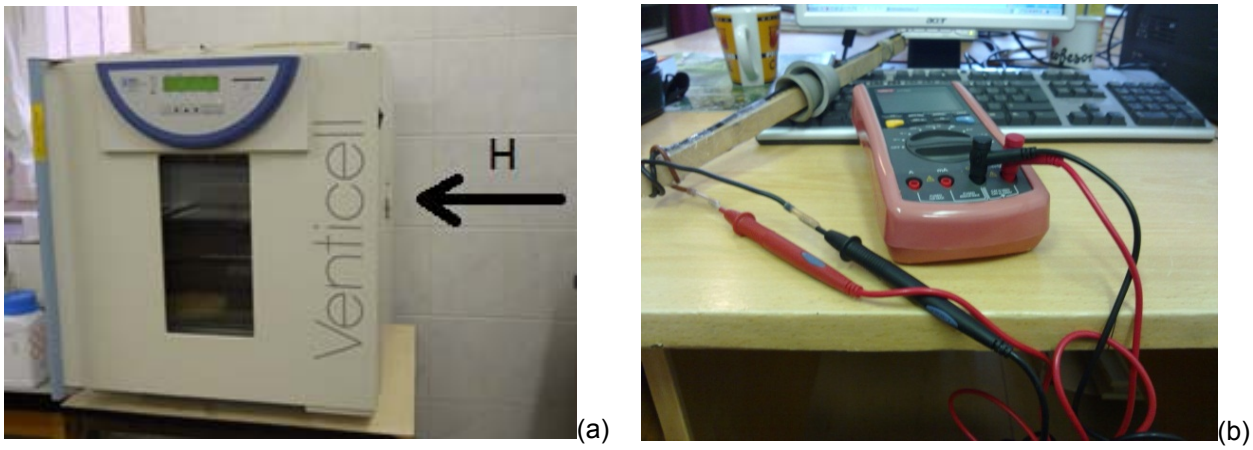

(a) (b)

Figure 1 Equipments for the experiments. (a) Heating oven with the hole “H” in the side wall, (b) Multimeter with modified electrodes

5 RESULTS AND DISCUSSION

Six samples of cotton fabric were coated by PPy by chemical oxidative polymerization of pyrrole monomer in the presence of TEAp-TS and $FeCl_3$ and their behaviors under thermal heating were recorded.

Oxidant salts such as ferric chloride ($FeCl_3$) function as both the oxidant and the dopant agent, and hence the polymer is obtained in the conducting form. Other transition metal salts can also be used as oxidizing agents for the polymerization of pyrrole. The transition metal ion is an electron acceptor. Therefore it oxidizes the π-electron system of the pyrrole ring at the initiation step. The intermediate steps of the polymerization of pyrrole initiated by $FeCl_3$ are as follows: The pyrrole molecule is oxidized to yield a radical cation as follows [16]:

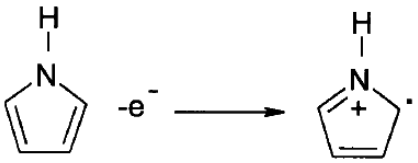

Radical cations recombine to form dications:

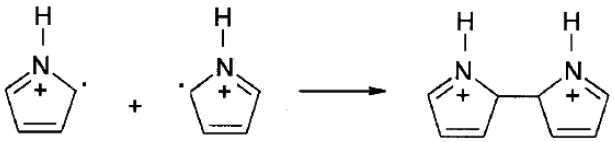

Deprotonation of dication to yield a dimer:

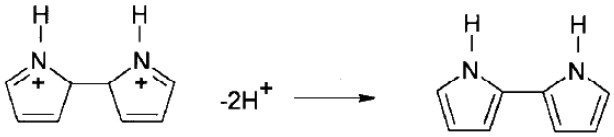

The above process continues by oxidation of the dimer to yield a radical cation of the dimer and the combination of radical cations to form trimers, tetramers, and polymers.

The electrical resistance of all the substrates was measured at different temperatures (80, 120, 160 and 200°C) at different time intervals from 0-600 sec and results are presented in Figures 2-7. In all the plots, each measurement of electrical resistance was converted into logarithmic value and plotted against time of heating. It would be probably some differences between oven temperature and real temperature of fabrics in first phases of heating but for electrical conductivity is decisive the surface effect.

All the cotton fabric samples coated by PPy initially show same behavior in terms of losing electrical resistance upon heating at different temperatures as shown in Figures 2-7.

Figure 2 shows the effect of different temperatures on electrical resistance of substrate A which has least amount of PPy coated on its surface that made it highest electrical resistive fabric among other samples. As far as influence of temperature on substrate A is concerned, there is a drastic decrease in electrical resistance in initial 100-200 sec was observed that can be seen in Figure 2 but afterwards there is no significant loss of electrical resistance was observed at all temperatures.

The results plotted in Figure 3 point up that the electrical resistance of PPy coated fabric substrate B decreases significantly up to 420 sec when heating at temperatures 80 and 120°C, after 420 sec stability in electrical resistance values can be seen. On the other hand, it is worth noticing that while heating at temperatures 160 and 200°C electrical resistance of substrate B decreases with time up to 120 sec, but afterwards values of electrical resistance started rising again till the end of experiment.

Same phenomenon can be observed in Figures 4 and 5 which depict the influence of different temperatures on electrical resistance of substrate C and D respectively at different intervals of time. Like substrate B significant drop in electrical resistance can be seen up to 420 sec for the temperatures 80 and 120°C but afterwards no substantial drop was observed. While heating at 160°C and 200°C the decrease can be seen for both the samples up to 300 sec and 120 sec respectively and keep heating at same temperatures result increase in electrical resistance.

Substrate E and F were prepared by varying in concentration of pyrrole in the recipe which was used to prepare substrate A by ±0.1 in

order to study the effect of pyrrole concentration on bulk electrical resistance of the sample. From the Figure 6 it can be perceived low concentration of pyrrole monomer produces less amount of PPy on the fiber surfaces and hence there is similar effect of different temperatures on the electrical resistance of PPy coated substrate. Like other substrates it is clear from the curves that as the temperature increases, more loss in electrical resistance is observed. Substrate F behaves in the same manner as substrate B, C and D as shown in Figure 7.

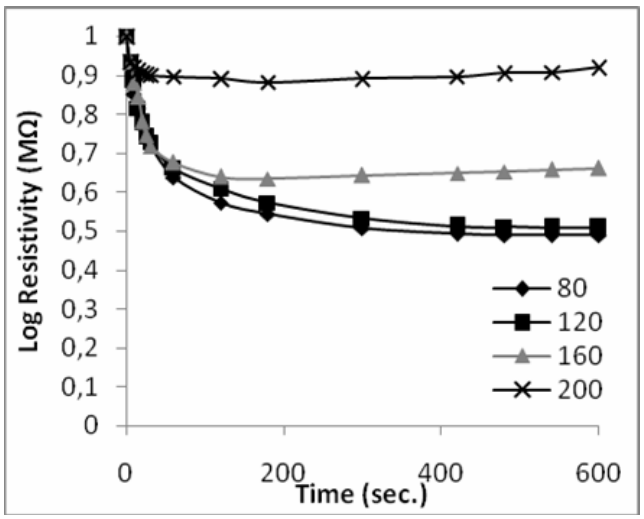

Figure 2 Effect of temperature on electrical resistance of substrate A at different intervals

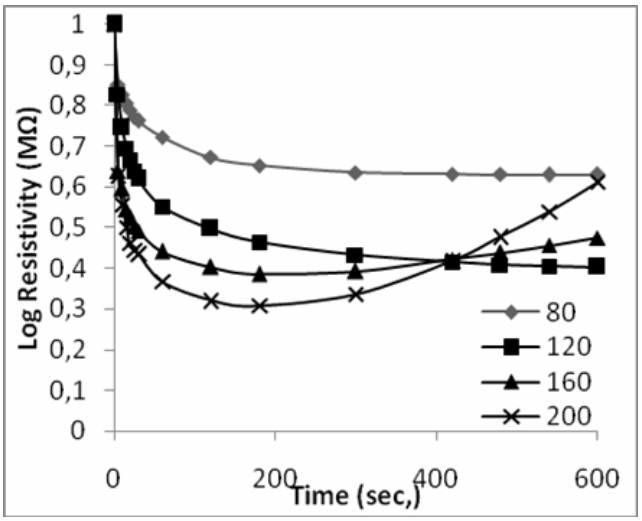

Figure 3 Effect of temperature on electrical resistance of substrate B at different intervals

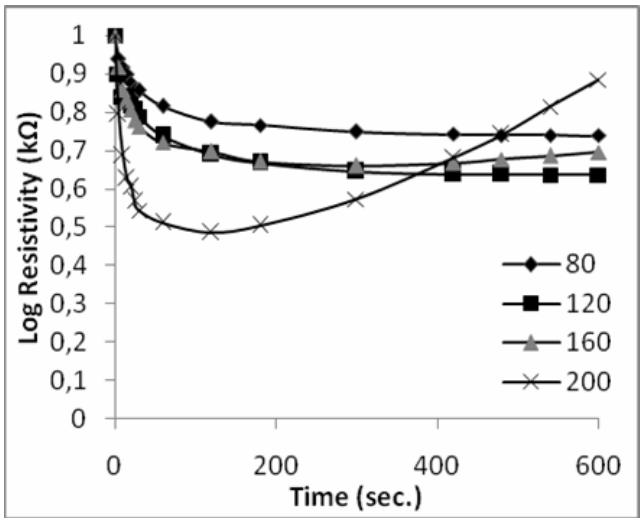

Figure 4 Effect of temperature on electrical resistance of substrate C at different intervals

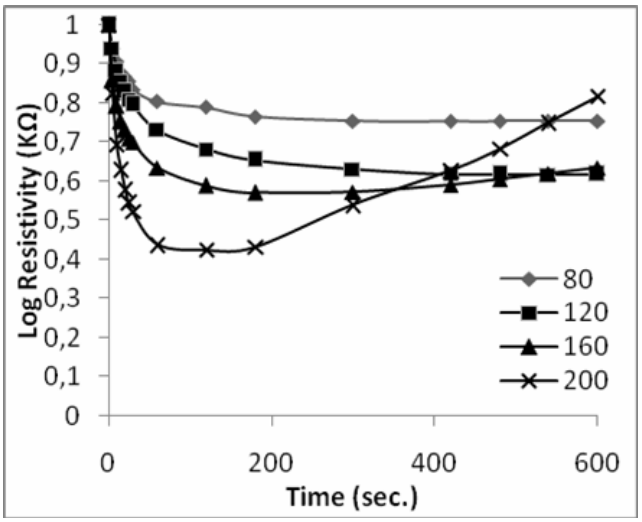

Figure 5 Effect of temperature on electrical resistance of substrate D at different intervals

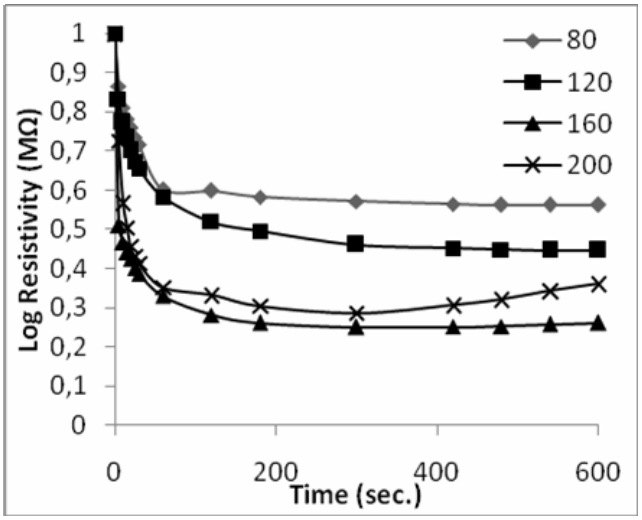

Figure 6 Effect of temperature on electrical resistance of substrate E at different intervals

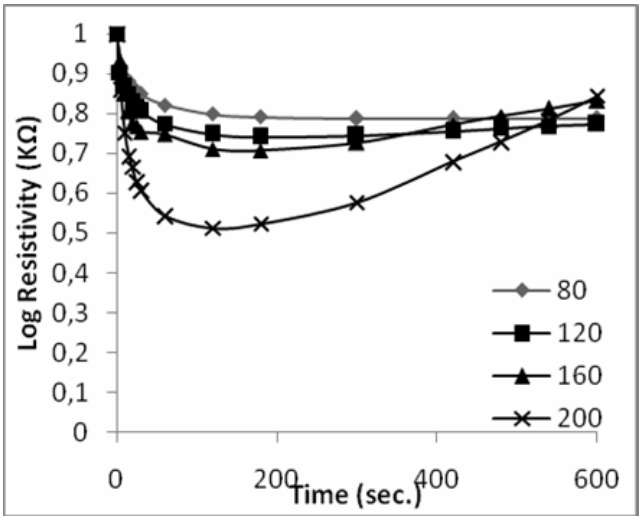

Figure 7 Effect of temperature on electrical resistance of substrate F at different intervals

The dependence of logarithm of thermal resistance y = log(R) measured at 600 sec. on the temperature powered by $-0.25x=T^{-0.25}f$ or sample A is shown in Figure 8.
The data have relative big scatter but the trend is following the empirical eqn. (2). In another samples was this trend more scattered.
The IR spectrum of the treated cotton fabric before and after heating, as shown in Figure 9 reveals the presence of a broad band at 3300-3500 cm^{-1} attributable to the OH groups, a strong absorption band at about 1566 cm^{-1} which is assigned to the C=N and C=C groups, with notice that this absorption band disappeared in case untreated cotton fabric. This IR spectrum confirms the presence of polypyrrole in the treated cotton fabric before and after heating and there is no difference between them.

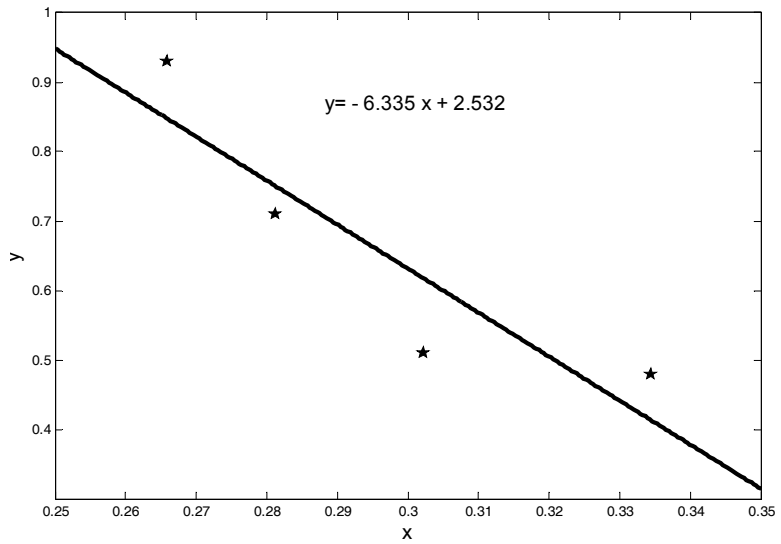

Figure 8 The dependence of y = log(R) measured at 600 sec. on the $T^{-0.25}$ for sample A

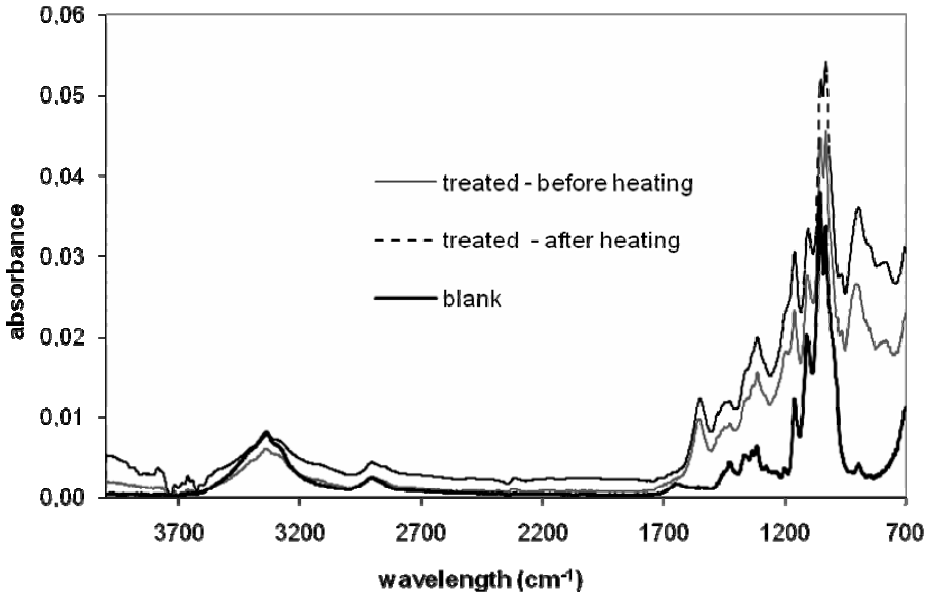

Figure 9 FT-IR spectra, of sample coated with PPy and untreated sample

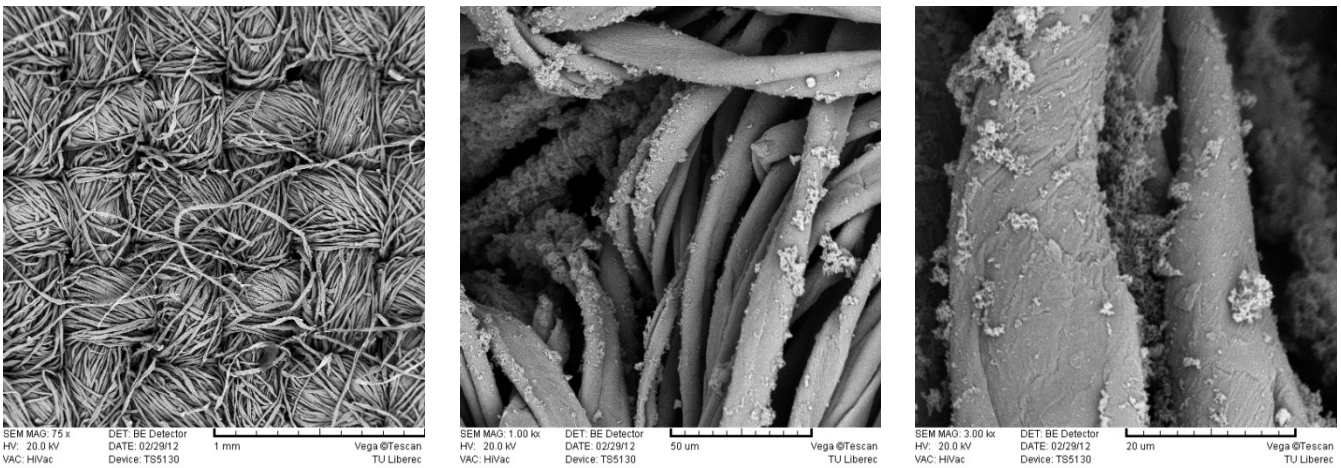

(a) (b) (c)

Figure 10 SEM micrographs analysis the morphology of cotton fiber after deposition of PPy

The morphology of cotton fibers after deposition of PPy was examined by SEM images. It can be observed from Figure 10 (a, b and c) that in this method of polymerization submicron circular particles are produced which get aggregated with the passage of time and deposit on the fiber surface.

6 CONCLUSION

Few different sample of cotton fabric were coated through in-situ polymerization of pyrrole monomer in the presence of $FeCl_3$ and TEAp-TS by varying in their concentrations. The influence of dry thermal treatment of coated fabric samples at different temperatures on electrical resistance at different time intervals was studied. It was found that electrical resistance of coated fabric samples decreases with increase in temperature. It is also worth noticing that electrical resistance decreases drastically when sample is subjected to particular temperature and when sample attains the temperature of environment, drop in resistance is no more significant. At

temperatures 80 and 120°C loss in resistance is stabilized whereas at high temperatures i.e. at 160 and 200°C electrical resistance reflected back to increase. This phenomenon is more pronounced with low resistive or highly conductive samples.
IR spectroscopy confirms the presence of PPy on the cotton fabric substrate and that dry thermal treatment of these samples causes no influence on the structure of PPy.

Acknowledgement: *This work was financed by student grant scheme SGS 2012 in Technical University of Liberec Czech Republic.*

7 REFERENCES

1. Avloni J., et al.: *Journal of Thermoplastic Composite Materials* 20(3), 2007, 241
2. Beneventi D., et al.: Polymerization of pyrrole on cellulose fibres using a $FeCl_3$ impregnation-pyrrole polymerization sequence, *Cellulose* 13, 2006, 725-734
3. Bhat N. V., et al.: Development of conductive cotton fabrics for heating devices, *Journal of Applied Polymer Science* 102, 2006, 4690-4695
4. Bouzek K., et al.: Platinum distribution and electrocatalytic properties of modified polypyrrole films, *Electrochim. Acta* 46, 2001, 661-670
5. Breslin C.B., et al.: Surface engineering: corrosion protection using conducting polymers, *Material Des.* 26, 2005, 233-237
6. Carpi F. and De Rossi D.: Colours from electroactive polymers: electrochromic, electroluminescent and laser devices based on organic materials, *Optics Laser Tech.* 38, 2006, 292-305
7. Dall_Acqua L., et al.: Performances and properties of intrinsic conductive cellulose-polypyrrole textiles, *Synth. Metals* 146, 2004, 213-221
8. de Barros R. A., et al.: Writing with conducting polymer, *Synth. Metals* 155, 2005, 35-38
9. Deshpande S.D., et al.: Studies on conducting polymer electroactive paper actuators: effect of humidity and electrode thickness, *Smart Materials and Structures* 14, 2005, 876-880
10. Edenbaum J.: *Plastics Additives and Modifiers Handbook*, Van Nostrand Reinhold, New York. 1992
11. Gerard M., et al.: Application of conducting polymers to biosensors, *Biosens. Bioelectron*.17, 2002, 345-359
12. Kim J., et al.: A comparative study of conductive polypyrrole and polyaniline coatings on electro-active papers, *Polymer Journal* 38, 2006, 659-668
13. Lin T., et al.: Polymerising pyrrole on polyester textiles and controlling the conductivity through coating thickness, *Thin Solid Films* 479, 2005, 77-82
14. Omastova M. and Mičušik M.: Polypyrrole coating of inorganic and organic materials by chemical oxidative polymerization, *Chemical Papers*, DOI: 10.2478/s11696-011-0120-4, 2011
15. Otero T.F. and Cantero I.: Conducting polymers as positive electrodes in rechargeable lithium-ion batteries, *J. Power Sourc.* 81-82, 1999, 838-841
16. Rodriguez J., et al.: in "*Handbook of Conductive Molecules and Polymers*", (H. S. Nalwa Ed.), Vol. 2, John Wiley and Sons Ltd., 1997, 415
17. Sapurina I., et al.: Electromagnetic radiation shielding by composites of conducting polymers and wood, *Journal of Applied Polymer Science* 95, 2005, 807-814
18. Schultze J.W. and Karabulut H.: Application potential of conducting polymers, *Electrochim. Acta* 50, 2005, 1739-1745
19. Stejskal J., et al.: Flame retardant effect of polyaniline coating deposited on cellulose fibers, *Journal of Applied Polymer Science* 98, 2005, 2347-2354
20. Stejskal J., et al.: Flame retardancy afforded by polyaniline deposited on wood, *Journal of Applied Polymer Science* 103, 2007, 24-30

BAVLNĚNÁ TKANINA POVRCHOVĚ UPRAVENÁ POLYPYRROLEM: VLIV TEPLOTY NA VODIVOST

Translation of the article
Polypyrrole coated cotton fabric: the thermal influence on conductivity

Abstrakt: Polypyrrol (PPy) patří mezi nejvíce využívané vodivé polymery z důvodů dobré elektrické vodivosti, stability v podmínkách používání a snadné přípravy. V této práci byl PPy povrchově navázán na bavlněnou tkaninu pomocí chemické oxidace spojené s “in situ” polymerizací. Jako dopant pro zajištění vodivosti byl použit tetraetyl amonium p-toluen sulfonát (TEAp-TS) a jako oxidační činidlo chlorid železitý. Na vzorcích s různým obsahem pyrrolu, dopantu a oxidačního činidla byl měřen elektrický odpor při teplotách 80, 120, 160 a 200°C v rozmezí ohřevu 1 - 600 s. Bylo zjištěno, že elektrický odpor klesá s teplotou. Pomocí IR spekter bylo ověřeno, že ohřev textilií nezpůsobuje chemické změny PPy.

COMPARISON OF METHODS FOR EVALUATING THE ELECTROMAGNETIC SHIELDING OF TEXTILES

Veronika Šafářová and Jiří Militký

Faculty of Textile Engineering; Technical University of Liberec
Studentská 2, 461 17 Liberec, Czech Republic
veronika.safarova@tul.cz

Abstract: *Materials with electromagnetic shielding efficiency are widely used to attenuate the strength of electromagnetic fields as functional elements in electrotechnic devices and also as supporting elements for electromagnetic interference reduction. One of modern application is not only technical protection, but also protection of human being while operating specific electric equipments. In these days, instead of metallic shields it is more common to use various types of textile materials due to their desirable flexibility and lightweight. The results of shielding effectiveness measurements depend on the method, frequency and properties of the material itself. The current state of work in the field of standardization and measurement methods for the shielding effectiveness of thin planar materials is presented in this paper. Testing of textile samples shielding was performed by different methods and scope of application, their limitations and possibilities for comparison of results are discussed.*
Keywords*: Electromagnetic shielding efficiency, measurement methods, hybrid fabrics.*

1 INTRODUCTION

According to World Health Organization [1], exposure to electromagnetic fields is not a new phenomenon. However, during the 20th century, environmental exposure to man-made electromagnetic fields has been steadily increasing as growing electricity demand, ever-advancing technologies and changes in social behavior.

Due to rapid development in commercial, military, scientific electronic devices and communication instruments, there has been an increased interest in developing materials that could shield against electromagnetic radiation to prevent interference.

Metal is considered to be the best electromagnetic shielding material due its conductivity and permeability, but it is expensive, heavy, and may also have thermal expansion and metal oxidation, or corrosion problems associated with its use. In contrast, most synthetic fabrics are electrically insulating and transparent to electromagnetic radiation [2].

In recent years, conductive fabrics have obtained increased attention for electromagnetic shielding and anti-electrostatic purposes. This is mainly due to their desirable flexibility and lightweight. One way how conductive fabrics can be created is by using minute electrically conductive fibers. They can be produced in filament or staple lengths and can be incorporate with traditional non-conductive fibers to create yarns that possess varying degrees of conductivity. Another way represents conductive coatings which can transform substrates into electrically conductive materials without significantly altering the existing substrate properties. They can be applied to the surface of fibers, yarns or fabrics. The most common are metal and conductive polymer coatings.

Whilst we are able to determine shielding effectiveness for metal shield just by knowing the materials' electrical magnetic parameters, for materials containing inserted metallic or graphite threads, metalized surfaces or composite materials, it seems we are able to determine the shielding effectiveness by actually measure it [4].

2 ELECTROMAGNETIC SHIELDING MEASUREMENT METHODS

There are several methods available for shielding effectiveness (SE) measurement. However, for thin planar structures, there are no standards defining the evaluation of small samples of only a several tens of centimeters in size. The following test methods are commonly used to measure electromagnetic shielding of a given shielding material.

1. Shielded box method
2. Shielded room method
3. Coaxial transmission line method
4. Waveguide method – modified shielded box method

Each of mentioned method has some advantages and limitations. For example coaxial transmission line method (ASTM D4935) is now the preferred method. The measurements can be made at specific frequency range (from 30 MHz to 1.5 GHz). The results obtained in different laboratories should be comparable [5]. Tests are carried out on small doughnut shaped samples, but preparation of samples is quite time consuming.

MIL-STD-285, IEEE-STD-299 and later standards (e.g. EN 61000-5-7) are based on the shielded room method, are marked as the most sophisticated ones [3], but test specimen size is typically of the order of 2.5 m^2 in area. In general, a signal source is place outside the test enclosure, whilst the measurement device is located inside. Frequency range is about 100 kHz to 10 GHz. It is expected [4] that the test results obtained for the same material tested at different laboratories can vary, even by as much as several dB. This is because the opening in the shielded wall of the chamber also affects the measurements. This opening itself forms a type of antenna with the parameters depending of several factors, one of which is its dimension.

Waveguide method was developed during this research. Basic parts of device are two waveguides. One waveguide is connected with receiving wire (antenna). Textile sample is placed on the entrance of second waveguide. The end of this waveguide is filled by foam saturated by carbon absorbing the electromagnetic field passed through sample. Sample is oriented perpendicularly the electromagnetic waves. Transmitting antenna is placed in front of first waveguide input. This method overcomes the limitations of shielded box method. No special preparation of test samples is necessary, but for particular frequency range a waveguide with specific dimensions is required.

The electromagnetic interference shielding efficiency measurement needs to use special devices. Simpler are measurements of electric characteristics of sample. It is known from theory that at sufficiently high frequencies in is possible to measure characteristics of electrical part of electromagnetic field only and therefore it should be mathematical relation between total shielding effectiveness and fabric resistivity or conductivity [6].

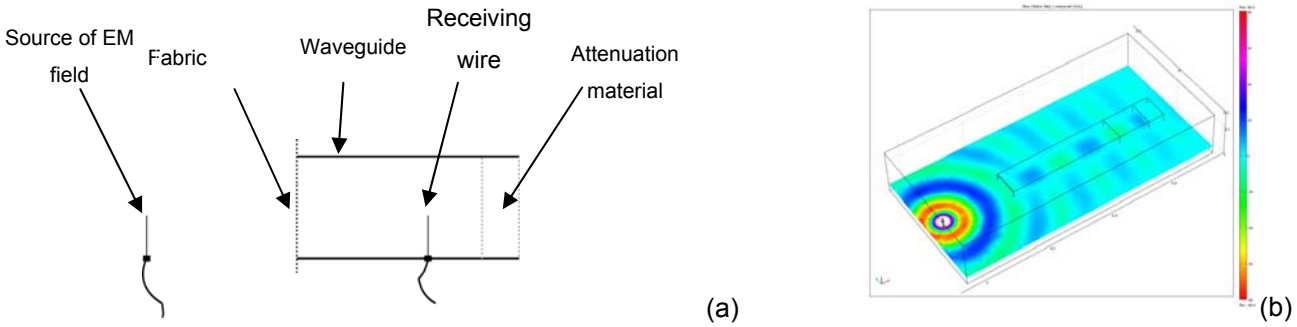

Figure 1 a) Scheme of device for measurement of electromagnetic shielding efficiency (based on waveguide method), b) simulation of electromagnetic wave entering the waveguide

Basic proposed numerical models of fabrics SE are based either on electrical properties (especially volume conductivity) of element [7-12] or on analysis of leakage through of opening in textile [13].
Shielding effectiveness S_T of the conductive materials can be expected by the following expression [8, 9]

$$S_T = 50 - 10\ \log\left(\frac{f}{K}\right) + 1.7\ t\ \sqrt{f\ K} \qquad (1)$$

where K [S cm^{-1}] is the volume conductivity of the conductive material and f [MHz] is the frequency.
The usefulness of this model can be ascertained by comparison with the model of White [7], which is usually used to predict the shielding effectiveness of a conductive sample of thickness t [cm] to an electromagnetic wave of frequency f (Hz), given as

$$S_T = 168 - 10\ \log\left(\frac{K_c f}{K}\right) + 1.315\ t\ \sqrt{\frac{K}{K_c} f} \qquad (2)$$

where K [S cm^{-1}] is the volume conductivity and K_c is copper conductivity (5.82 10^5 S cm^{-1}).
The analysis of leakage through openings in conductive yarn fabric shields is based on transmission line theory [13]. The shielding effectiveness is given by the equation

$$S_T = A_a + R_a + B_a + K_1 + K_2 + K_3 \qquad (3)$$

where A_a [dB] is attenuation introduced by a particular discontinuity, R_a [dB] is a fabric aperture with single reflection loss, B_a [dB] is a multiple reflection correction term, K_1 [dB] is a correction term to account for the number of like discontinuities, K_2 [dB] is a low-frequency correction term to account for skin depth and K_3 [dB] is a correction term to account for a coupling between adjacent holes. The empiric relations for these attenuation are published e.g. in the work of Perumalraja [1]. Only in the evaluation of term K_2 is an implicit knowledge of the electrical characteristics (conductivity and permeability) of the fabric required. Since this term is valid only for low frequencies [11] it has been omitted from the calculation at microwave frequencies.
In order to approximate the mesh nature of the fabrics the following assumptions are used:

1) The conductive fibers are wound together in a bundle in the center of the bundle of nonmetallic fibers. These two bundles together form the fabric strands.
2) The only influence of the nonmetallic fibers is to space the bundles of metallic fibers apart.
3) The pores in the fabric are square.

For effective shielding the fabric it should contain as few portions of pores as possible.
The shield effectiveness S_T of materials with (carbon) filler depends on the volume percent of the filler material V [%] [14]

$$ST = 2.46\ V \qquad (4)$$

For a single conductive layer, the theoretical value S_T can be written as [10]

$$S_T = 20\ \log\left(1 + \frac{K\ t\ Z_o}{2}\right) \qquad (5)$$

where K is conductivity; t the thickness of the sample; and Z_0 the free-space wave impedance, 377Ω. For low electrically conductive materials are these models not useful [10].
Another way is utilization of knowledge of materials complex permittivity. Attenuation of electromagnetic wave in material is possible to calculate from this value. The amount of attenuation due to shield depends on the electromagnetic waves reflection from the shield surface, absorption of the waves into the shield and the multiple reflections of the waves at various surfaces or interfaces in the shield. Following relationships stand for electric part of electromagnetic wave. Similar formulas stand for magnetic part:

$$\vec{E}_r = R\vec{E}_d \qquad (6)$$

$$\vec{E}_t = T\vec{E}_d \qquad (7)$$

where R coefficient of reflection and T coefficient of transmission are:

$$R = \frac{Z_2 - Z_1}{Z_2 + Z_1} \quad (8)$$

$$T = \frac{2Z_2}{Z_2 + Z_1} \quad (9)$$

where Z_1 and Z_2 are characteristic impedance of air and sample. A characteristic impedance of surroundings can be calculated from:

$$\hat{Z} = \sqrt{\frac{\mu}{\hat{\varepsilon}}} \quad (10)$$

where $\hat{\varepsilon}$ is complex permittivity of surroundings and μ is relative permeability.

3 EXPERIMENTAL PART

Hybrid fabrics composed of hybrid yarns containing polypropylene and different content of staple metal fiber (SS) were used [15]. The aspect ratio (length/diameter ratio, *l/d*) of the SS used in this study is 6250, since the diameter of the SS is 8 μm and the fiber length is 50 mm. Details about these fabrics are given in the Table 1. Microscopic images of samples 2 and 4 are shown in Figure 2.
Electromagnetic shielding efficiency of textiles sample set was measured by 3 different methods. These methods comprise coaxial transmission line method based on ASTM D4935 performed at two different laboratories – at Marmara University in Turkey and Czech Technical University in Prague, shielded room method (EN 61000-5-7) in certified lab VOP Šternberk and waveguide method at similar frequency range. Possibilities of modeling electromagnetic shielding efficiency based on electric properties of samples were verified. Specifically models based on volume resistivity (White model [7]) and complex permittivity were verified. Result were compared, findings and recommendations are discussed.

Table 1 Characterization of fabrics samples

Sample No.	Structure	Composition	Thickness [mm]	Yarn fineness [tex]	Mass per unit area [g/m^2]
1	woven - twill	80% POP/ 20% SS	0.71	50	220
2	woven – twill	95% POP/ 5% SS	0.77	50	220
3	woven - twill	99% POP/ 1% SS	0.78	50	220
4	knitted – flat stitch	90% POP/ 10% SS	0.64	25	182

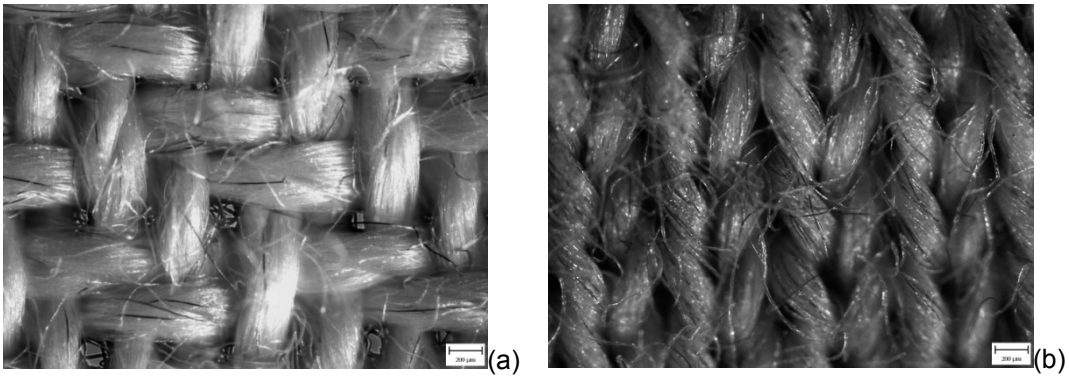
(a) (b)

Figure 2 Microscopic images of fabrics: a) sample 2, b) sample 4

4 RESULTS

The comparison of results measured by coaxial transmission line method for the same textile samples are shown in Figure 2. It is clear that the curves are not exactly the same, but they are comparable. The differences can be caused by different modification of samples before measurement (in one case, paper was mounted on textile to cause easier preparation of samples), sample holder used in Czech Technical University was not commercial (it was prepared according to the standard by researchers), screws were not used at Marmara Uni. measurement (change in impedance).

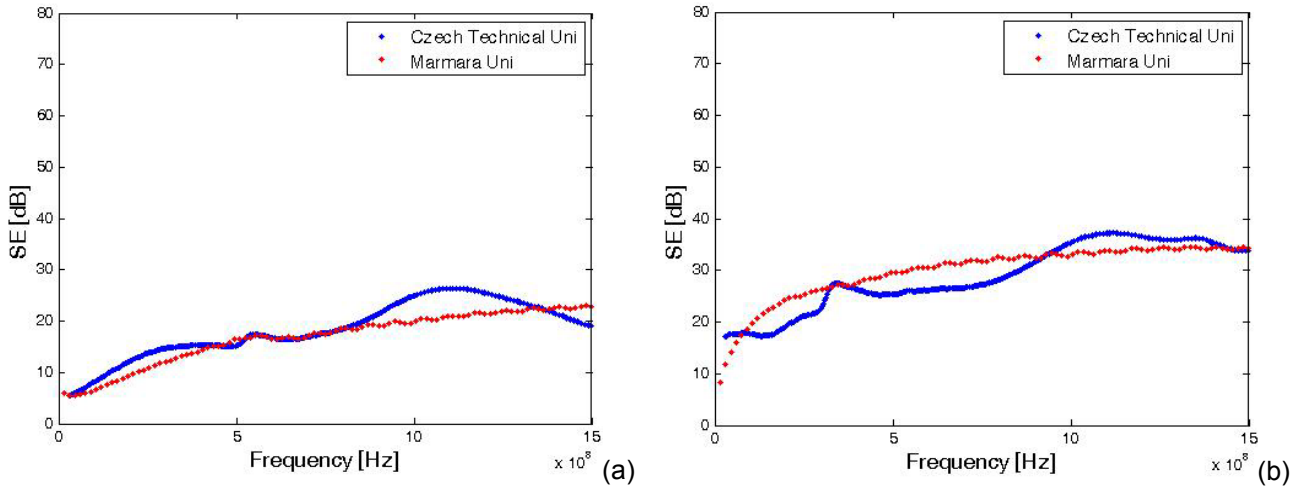

Figure 2 Comparison of measurement by transmission line method at two different laboratories: a) sample No. 2, b) sample No. 1

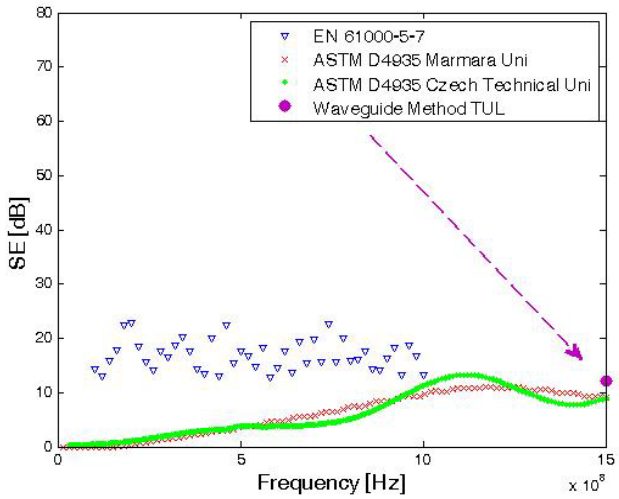

Figure 3 Comparison of shielding effectiveness measured by different methods for sample No. 4

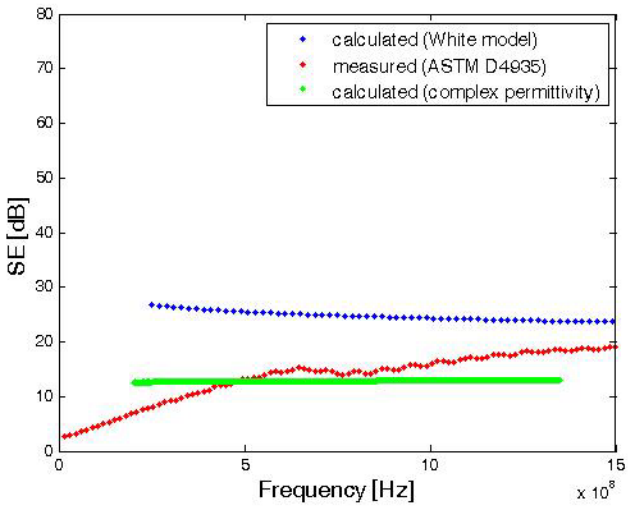

Figure 4 Comparison of measured shielding effectiveness prediction of a shielding efficiency based on electric conductivity knowledge for sample No. 3

Comparison of shielding efficiency results measured by different methods (coaxial transmission line method measured at two different laboratories, shielded room method, waveguide method) for the same sample is shown at Figure 3. It is clear that results given by shielded room method (standard EN 61000-5-7) vary widely from other results.
Comparison of results measured by coaxial transmission line with results calculated based on knowledge of electrical properties (volume resistivity, complex permittivity) for the same textile sample is shown at Figure 4.

5 CONCLUSION

It was found out that results obtained by coaxial transmission line method at two different laboratories are comparable. It is clear that the shielding effectiveness measurement results obtained using currently known methods based on different principles depend not only on the parameters of the material, but also on the size of the test sample, the geometry of the test setup and the parameters of the source of electromagnetic radiation and there is a lack of generally accepted standardized methods for measuring shielding effectiveness. Therefore the same measurement method and the same test setup geometry should be always used to be able to compare and evaluate a shielding of material. Also, when presenting research results, one should specify the measurement method used in study.
Another way how to find out shielding efficiency of textile samples is calculation based on knowledge of electrical properties of samples. Two basic approaches were demonstrated. The results are comparable with data obtained by ASTM D4935.

Acknowledgement: *This work was financially supported by the research project TIP – MPO VaV 2009 "Electromagnetic field protective textiles with improved comfort" of Czech Ministry of Industry and student project 2011 "Comparison of methods for evaluating the shielding effectiveness of textiles" of Technical university of Liberec.*

6 REFERENCES

1. World Health Organization, Establishing a Dialogue on Risks from Electromagnetic Fields, Geneva, Switzerland, 65p., 2002
2. Cheng K.B., et al.: Effects of Yarn Constitutions and Fabrics Specifications on Electrical Properties of Hybrid Woven Fabrics, *Composites Part A* 34(10), 2003, 971-978
3. Geetha S., et al.: EMI shielding: Methods and Materials - A Review, *J Appl Pol Sci* 112, 2009, 2073-2086
4. Wieckowski T.W., Janukiewicz M.J.: Methods for Evaluating the Shielding Effectiveness of Textiles, 2009, http://www.fibtex.lodz.pl/59_09_18.pdf
5. Vojtěch L., Hájek J.: Measurement of electromagnetic shielding efficiency of planar textiles in frequency range 100 kHz – 1.5 GHz, *Acces server* [online], Vol. 8, No. 3, 2010, Internet: http://access.feld.cvut.cz/view.php?cisloclanku=2010030006 (in Czech)
6. Safárova V.; Militky J.: Corelation between resistance and electromagnetic shielding of hybrid weaves, In *Aachen Dresden International Conference: Book of abstract*, Technical University Dresden, 2010, 5
7. White D.R.J.: *A Handbook Series on Electromagnetic Interference and Compatibility*, Vol. 5, Don White Consultants, Germantown, MD, 1971
8. Simon R.M.: Conductive plastics for EMI shielding, in *Thirty-Eighth Annual Technical Conference*, 1980, 207
9. Shinagawa S.: Conductive papers containing metallized polyester fibers for electromagnetic interference shielding, *J. Porous Materials* 6, 1999, 185-190
10. Colaneri N.F., Shacklette L.W.: *IEEE Trans Instrum. Meas.* 41(2), 1992, 291-297
11. Chen H.C., Lee K.C., Lin J.H., Koch M.: Fabrication of conductive woven fabric and analysis of electromagnetic shielding via measurement and empirical equation, *Journal of Materials Processing Technology* 184, 2007, 124-130
12. Vojtěch L., Neruda M., Hájek J.: Planar materials electromagnetic shielding efficiency derivation, *International Journal on Communications Antenna and Propagation* 1(1), 2011
13. Perumalraja R.: Electromagnetic shielding effectiveness of copper core-woven fabrics, *J. Text. Inst.* 100, 2009, 512-524
14. Keith J.M. et all.: Shielding Effectiveness Density Theory for Carbon Fiber/Nylon 6, 6 Composites, *Polym. Compos*. 26, 2005, 671-678
15. Militký J. and Šafářová V.: Numerical and Experimental Study of the Shielding Effectiveness of Hybrid Fabrics, *Vlákna a textil* 19, 2012, 21-27

POROVNÁNÍ METOD PRO HODNOCENÍ ELEKTROMAGNETICKÉHO STÍNĚNÍ TEXTILIÍ

Translation of the article
Comparison of methods for evaluating the electromagnetic shielding of textiles

Abstrakt: Materiály schopné výrazně omezit působení elektromagnetického pole jsou široce využívány jako prvky elektrických zařízení a pomocná zařízení pro potlačování elektromagnetických inferencí. V nových aplikacích se řeší nejen problém ochrany strojů ale také problém ochrany lidí, kteří jsou vystavení působení elektromagnetických polí. Kromě kovových ochranných zařízení se čím dál tím více uplatňují textilní materiály, které jsou lehké a snadno tvarovatelné. Výsledky měření efektivity stínění elektromagnetického pole závisí na použité metodě a zvoleném rozsahu frekvencí. V prácí jsou uvedeny současné poznatky o standardizaci a měření efektivity stínění elektromagnetického pole tenkých plošných vrstev. Stínící schopnost vybraných textilií je určena různými metodami. Na základě porovnání získaných výsledků jsou stanoveny omezení a možnosti těchto metod.

IMAGE PROCESSING BASED METHOD FOR EVALUATION OF FABRIC STRUCTURAL CHARACTERISTICS

Ebraheem Shady[1], Mounir Hassan[1&2], Khadijah Qashqary[3] and Dana Křemenáková[4]

[1]*Textile Engineering Dept, Faculty of Engineering, Mansoura University, Egypt*
[2]*Computer science Dept, Faculty of Education, King Abdulaziz University, Saudi Arabia*
[3]*Fashion Design Dept., Faculty of Art &Design, King Abdulaziz University, Saudi Arabia*
[4] *Faculty of Textile Engineering, Technical University of Liberec, Czech Republic*
monir_hassan@yahoo.com

Abstract: *Digital image processing approach is developed to evaluate fabric structure characteristics and to recognize weave pattern utilizing Wiener filter. Images of six different groups are obtained and used for analysis. The groups included three different fabric structures with two different constructions for each. The developed approach decomposed fabric image into two images each of which included either warp or weft yarns. Yarn boundaries are outlined to evaluate the fabric surface characteristics and further used to identify the areas of interlaces to detect the fabric structure. The results showed success in evaluating the surface fabric characteristics and detecting the fabric structure for the types of fabrics having same colors of warp and weft yarns. The approach was also able to obtain more accurate evaluation for yarn spacing and rational fabric cover factor compared to the analytical techniques used to estimate these characteristics.*
Keywords: *Fabric surface characteristics, Pattern recognition, Image processing, Wiener filter.*

1 INTRODUCTION

Visual analysis of a fabric sample is an essential process for reproducing this fabric and/or evaluating its structural characteristics. Basically, this analysis defines the weave pattern, the densities of warp and weft yarns and probably the counts of warp and weft yarns by using a microscope. The process is traditionally carried out by a human inspector who uses magnifier, ruler and some other simple tools to count the densities and visually define the weave pattern. Generally, a manual operation like this is tedious, time-consuming and inconvenient for inspector's eyes. Thus, the judgment may not be consistent or accurate enough because it may vary from inspector to another.

On the other hand, the dynamic development in computer speed and storage capacity open the door for more advanced digital image analysis to replace the operations that depend on human vision. Using digital image analysis enabled detailed analysis of basic structural parameters of textile products [1]. It was used earlier to estimate the cross sectional area of wool fibers [2]. Thereafter, other applications were arisen to estimate the irregularities of fiber blending on the yarn surface, to evaluate cotton maturity and to analyze the damage of wool fibers [3-7]. Other researchers utilized the digital image analysis to characterize the basic structural parameters of yarn's surface like thickness, hairiness and twist [1, 8, 9]. The digital analysis was also used to characterize the texture of carpets during usage [10]. The term image processing showed up when techniques started to be more complicated and used some image processes to suite certain applications. An image processing technique was used to assess the fabric surface after pilling by analyzing the brightness of each channel (Red, Green and Blue) of a colored fabric image. Analytical techniques were used to assign the pilling grade for each sample based on counting the pilled area obtained from the analyzed image [11]. Another image processing technique was used to measure the surface roughness of a knitted fabric. Fabric images were captured via high resolution scanner and then

analytical analysis was conducted in order to obtain the fabric roughness index [12]. Fabric wrinkle was also characterized utilizing image processing through analyzing heights of light profiles created by fabric wrinkle. Statistical parameters for the light profile were estimated to characterize the fabric wrinkle [13]. Frequency transforms were also utilized to estimate morphological features for nonwoven web [14] and to extract some of images features to classify some knitted fabric defects [15]. Correction operations, like histogram leveling and autocorrelation erosion, were also used in other applications to classify some woven fabric defects [16]. Wiener filter was used for weave pattern recognition by decomposing the fabric image into two images one contained the warp yarns and the other contained the weft yarns [17]. Then another image was initialized to define grid lines represent central axis of yarns. The points where central axis intersected were defined as the cross-over points. This technique assumed that the yarns are straight and identified the pattern by checking the intensity at each cross-over point. Depending on only one point and checking its intensity to decide which yarn is crossing over the other is not sufficient even if the yarns were straight.

The aim of this work is to use image processing analysis to estimate some of structural characteristics of woven fabric and to identify the weave pattern. Success of such an image processing approach will enable fast and accurate analysis of some of the fabric structure characteristics. The traditional procedure was known to be tedious, time-consuming and inconvenient for inspector's eyes. All these drawbacks will be vanished when the traditional procedure is replaced by a computer system that captures and processes fabric images. In this work, an image processing approach utilizing Wiener filter is presented to identify the pattern of woven fabric and estimate some of the fabric structure characteristics. Six groups of fabric samples are used in this work include three different fabric structures namely plain weave, twill 3/1 and satin 5 and each structure contains two fabric constructions in order to have different structural characteristics. Five images are captured from each sample group to be analyzed. Weave pattern, warp and weft densities and yarns' diameters are identified and compared to samples' data which are estimated using the traditional manual procedure.

2 MATERIALS AND IMAGE ACQUISITION

Three fabric structures are chosen for this study and each of fabric structure is represented by two fabric constructions. The three fabric structures are plain, twill 3/1 and five harnesses satin weave. All fabrics are manufactured from 100% cotton yarns. The six fabric samples are tested utilizing the manual traditional procedure to identify the fabric structure and densities in both directions of warp and weft. The yarn counts of each sample are tested and the results agreed with what obtained from the fabric manufacturer. The detailed specifications of each sample are listed in Table 1. The data represent the average measured values with their standard error and the data between brackets were provided by the manufacturer. All fabric samples are uni-color except sample number four which is denim fabric with dark blue warp yarns and white weft yarns.

A CCD camera equipped with attached zoom lens is used to capture the fabric images under reflected light. Five different images are captured for each sample type. The images are digitized utilizing a frame grabber and transferred to be stored in a personal computer. The image size was 512x512 pixels with resolution 6500 pixels per inch. All images are processed using histogram equalization to reassign the brightness to improve the visual appearance. Colored images are converted into two-dimensional grayscale images with 256 gray levels to improve the computer processing time and speed for the next image processing steps. Samples of images for the three structures are shown in Figure 1 after the grayscale conversion.

Table 1 Specifications of fabric samples

ID	Fabric structure	Density (thread per inch)		English yarn count	
		Warp	Weft	Warp	Weft
1	Plain 1/1	65 ± 1.038	88 ± 1.400	20 ± 1.194	28 ± 1.333
2	Plain 1/1	76 ± 1.257	66 ± 1.248	34 ± 1.637	34 ± 1.543
3	Twill 3/1	95 ± 1.427	50 ± 0.836	22 ± 1.301	16 ± 0.841
4	Twill 3/1	66 ± 1.377	80 ± 1.234	14 ± 0.778	20 ± 1.109
5	Satin 5	68 ± 1.346	45 ± 1.033	20 ± 1.261	14 ± 0.711
6	Satin 5	144 ± 1.896	74 ± 1.377	46 ± 1.977	42 ± 2.044

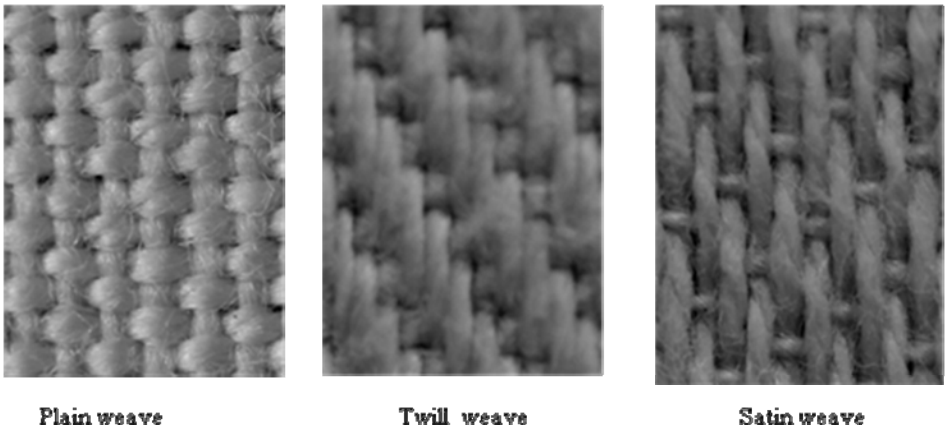

Figure 1 Grayscale images for the three fabric structures

3 IMAGE PROCESSING APPROACH

Wiener filter is applied to the grayscale fabric images to regenerate two sub-images from original image of a fabric. Each sub-image shows only one group of the basic two groups of yarns known as warp and weft. Generally, Wiener filter uses constant power spectra to reduce the noise within a local window of pixels. The Wiener filter calculates the value of each pixel using the following expression [17]

$$W(m,n) = \mu + \frac{S^2 - v^2}{S^2}\left[I(m,n) - \mu\right]$$

where

$$\mu = \frac{1}{M\ N}\sum I(m,n) \quad S^2 = \frac{1}{M\ N}\sum I^2(m,n) - \mu^2$$

and v^2 is the variance of the noise. The window's dimensions (*M*x*N*) are chosen based on application and the filtration method depends on statistical calculations in the local neighborhood of each pixel. Assuming that *I* represent the 2D matrix of a fabric grayscale image and *m*, *n* denote the indices of image's pixel. Hence, *I(m,n)* will denote the intensity of the pixels in the gray level which will vary from 0, black, to 255, white.

The shape of the texture in warp or weft direction is always long line type. Therefore, applying the filter in the horizontal direction the vertical texture is neutralized and vice versa. Choosing window with short height and long width will produce a sub-image that contains only the weft yarns group. In this case the size of the window was chosen as 5x60 pixels. On the other hand, a window with long height and short width will produce a sub-image that contains only the warp yarns group. In this case the size of the window was chosen as 60x5 pixels. Figure 2 shows sample of original grayscale plain weave fabric image under investigation and its sub-images resulting from applying Wiener filter. Histogram equalization and adjustment processes are applied to the resulted images in order to enhance the quality of the images as shown in Figures 2.

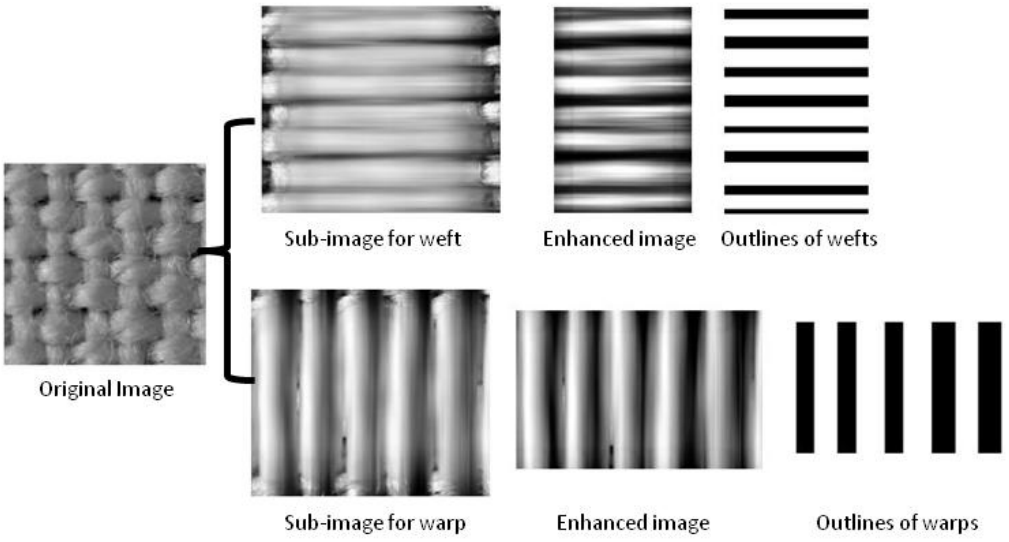

Figure 2 Applying Wiener filter on a plain weave image

Some noises are recognized at the top and bottom in the sub-images that contain warp yarns group and also on the sides in the sub-images that contain weft yarns group. Removing these parts will ease the process of detecting the outbound of yarns and will not affect the further processes. The resulting sub-images are enhanced again utilizing histogram equalization and converted into binary images. Clustering thresholding or Otsu's method is used to obtain the threshold values of fabric images in order to convert them into binary images [18]. Otsu's method is considered as one of the most referenced methods. This method establishes an optimum threshold by minimizing the weighted sum of within class variances for the foreground and background pixels. The minimization of within class variances is equivalent to the maximization of between class scatter. The method's results are considered satisfactory when the numbers of pixels in each class are close to each other. Small holes (3x3 pixels) and short-thin lines show up in binary images are considered as noise and removed. Then outbound of each yarn in both directions are outlined as shown in Figure 2.

4 STRUCTURAL CHARACTERISTICS

The outlines of yarns shown in the last step of Figure 2 are used further to calculate the mean value of the yarn diameter in each direction by relating the image resolution to the number of pixels representing each yarn width. The calculated mean diameter of warp and weft yarns can be used to calculate the English yarn count (N_e) using the following relation

$$d \approx \frac{1}{28\sqrt{N_e}}$$

Also, the number of yarns in each direction is identified and used to calculate the density in each direction using the information of the image dimensions. The same technique is used to calculate the yarn spacing.

In general, the cover factor indicates the extent to which the area of a fabric is covered by one group of yarns, *i.e.* for any fabric there are two cover factors one for the warp yarns and the other for the weft yarns. Pierce presented the following equation to calculate the cover factor CF for each group [19]

$$CF = \frac{n}{\sqrt{N_e}}$$

Where n is the number of threads in one inch and N_e is the English yarn count.

Fractional cover factor is also known to represent the fabric cover factor considering both groups of yarns. It is defined as the total area of the fabric that covered by the components yarns. A simplified approach is used to calculate the fractional cover factor assuming that the yarns have circular cross-section. If the yarn diameter is *d* and the adjacent yarn is displaced by a distance *s*, the fractional cover factor is expressed as *d/s*. in an ideal model, *s* is equivalent to *1/n* and hence the fractional cover will be *d* x *n*. if C_w is fraction cover for the warp and C_f is the fraction cover for the weft, the total fabric cover factor will be: $C_w + C_f - C_w C_f$.

5 PATTERN RECOGNITION

The outbound of yarns in each sub-image is identified as mentioned previously for each fabric image as shown in Figure 2. Only the outlines of yarns are captured in each sub-image to produce another two images contain only the lines represent the yarns' outlines and by adding up these two images an image is resulted containing grid lines. At this point, the windows represent the yarns cross-over areas are identified. Applying this information on original fabric image after converting it into a binary image utilizing Otsu's method, the windows represent cross-over areas are defined in the binary image. Then, intensities of all the pixels within the window are summed up. The analysis shows that areas where weft yarn crosses over warp yarn are much brighter compared to areas where warp crosses over weft. To this end, the fabric structures are recognized as shown in Figures 3-5 where white marks mean that weft yarn is crossing over warp yarn. This approach evaluates the weave pattern based on the intensity in each cross-over area which makes it more reliable and able to detect wide range of weave patterns.

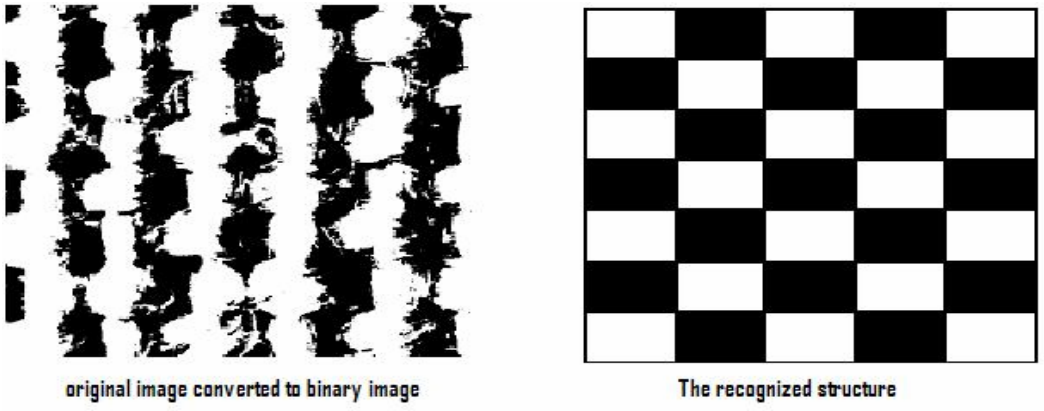

Figure 3 The original image converted to binary image and the structure was recognized

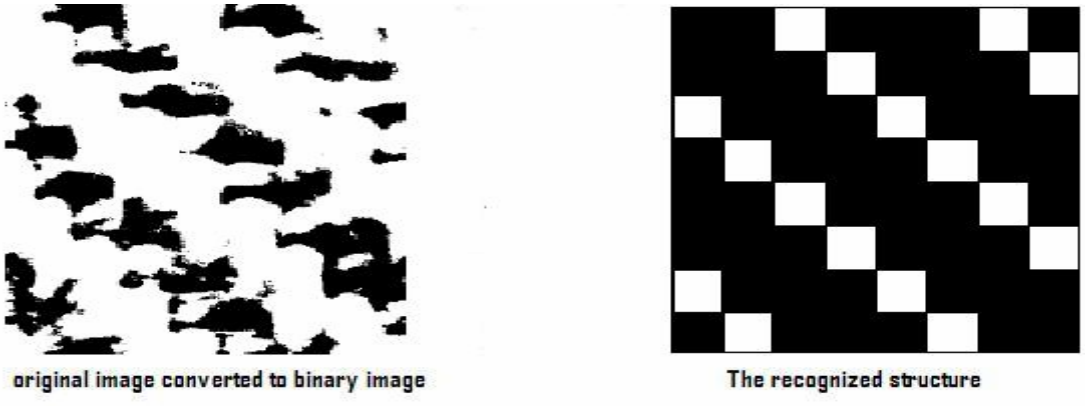

Figure 4 The original image converted to binary image and the structure was recognized

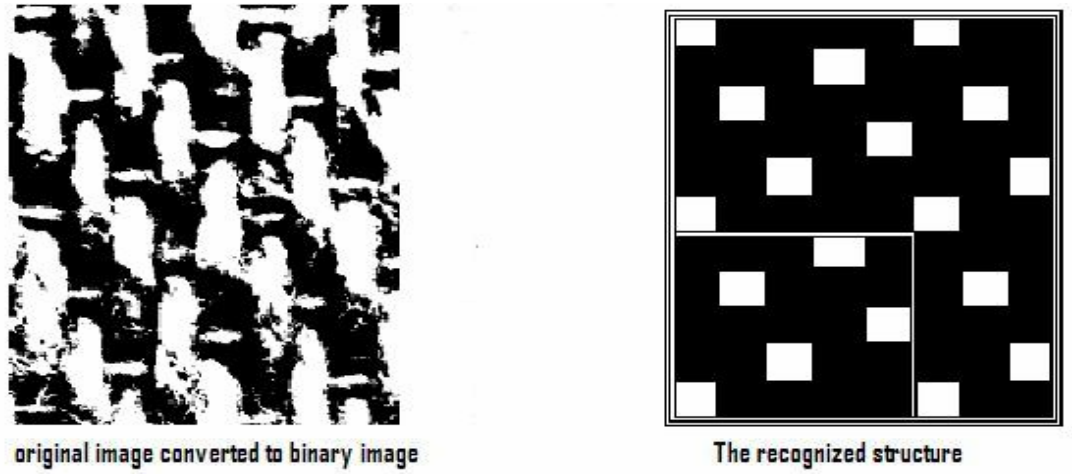

Figure 5 The original image converted to binary image and the structure was recognized

6 RESULTS AND DISCUSSION

The image processing approach is applied to various fabric images to calculate some of yarn parameters and to identify the weave pattern. The image processing approach was applied for all images and the pattern recognition results were compared to the known weave patterns. The presented approach was able to identify successfully the pattern of fabric structure for all samples except for sample number 4 (denim fabric). The main problem with that sample is the color difference between the warp and weft yarns. The color of warp yarns is dark blue (too dark) and the color of the weft yarns is white (too bright). All enhancement processes failed to decompose the yarns accurately. Because of the color difference, some yarns were merged together and some were split. Thus, image processing technique was not able to recognize the yarns' boundaries and so the cross-over areas for that sample. Figures 6 and 7 show the approach results for densities and yarn counts compared to the measured values via the traditional procedure. Results showed good agreement between the two procedures. Some differences between the counts resulting from the approach and measured counts are recognized for twill and satin weave. The reason for that based on the concept of obtaining the count from the image approach. The image approach calculates the width of yarn's projection not the yarn diameter and uses this information to calculate yarn's count. Comparing the approach results to the measured results, one can notice that the significant difference of the weft counts compared to the warp counts for both twill and satin weave. Weft yarns have less tension compared to warp yarns during the weaving process and this gives the chance of weft yarns to get flatten especially when they have the space. The space is provided in fabrics with low yarn densities and/or in fabric structures which have relatively long float length like twill and satin weave. This clarifies why there is almost no difference between weft counts for plain weave however the differences start appearing in twill and satin weaves.

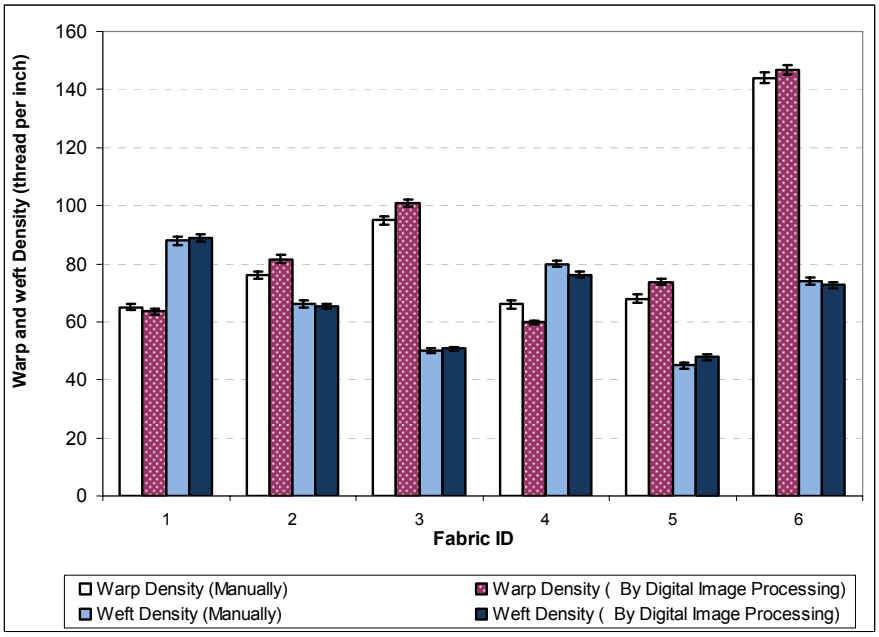

Figure 6 Comparison between the measured densities and densities' results of presented approach

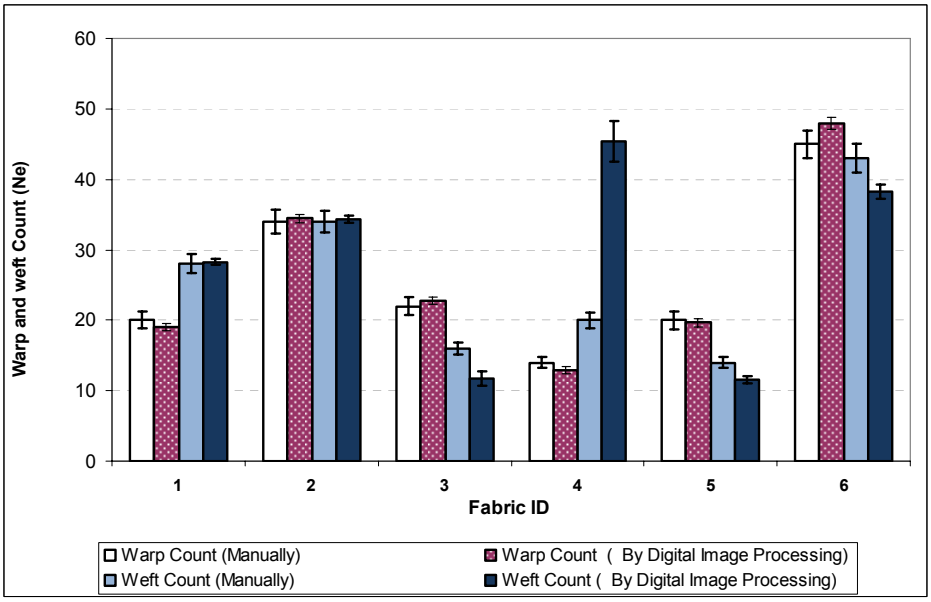

Figure 7 Comparison between the measured counts and counts' results of presented approach

Table 2 Mean yarn diameter and spacing calculated using the digital image processing approach

ID	Mean yarn diameter (inch)		Mean calculated yarn spacing (inch)	
	Warp	Weft	Warp	Weft
1	0.0082	0.0067	0.0147	0.014
2	0.0061	0.0061	0.017	0.016
3	0.0075	0.0104	0.010	0.021
4	0.0099	0.0053	0.016	0.017
5	0.0081	0.011	0.018	0.022
6	0.0052	0.0067	0.007	0.017

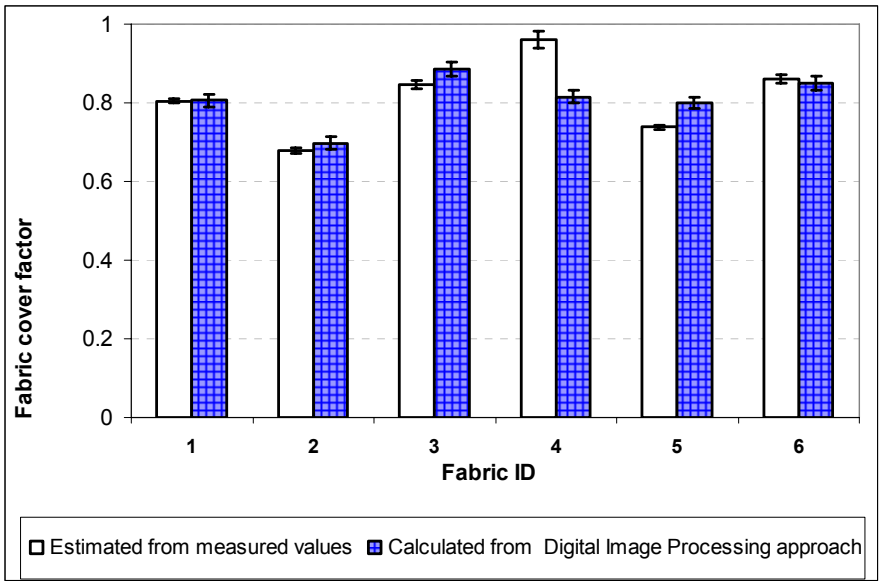

Figure 8 Comparison between the fabric cover factor results

The results listed in Table 2 show the yarn spacing calculated by the digital image processing approach. Figure 8 shows the results of the image processing approach for the fabric cover factor compared to the estimated values that calculated from the measured data, i.e. fabric density and yarn counts. It is noticed that there is no much difference between both results (excluding results of sample no. 4). In our opinion, the image processing results of fabric density, projection of yarn diameter, yarn spacing and fabric cover factor tend to be more accurate because of considering the yarn projection in the fabric. However, some variations have shown up in the yarn count results for the fabric structures that have long float due to the yarn flattening which changes the projected yarn diameter. Therefore, it can be concluded that the image processing technique is able to analyze the fabrics that have warp and weft yarns with the same color or uni-color fabrics. The image processing approach was able to assign the densities of warp and weft yarns, the yarn spacing, diameters of warp and weft yarns and counts of warp and weft yarns. In addition, the developed approach successfully identified the different weave patterns. It can be predicted that the the developed approach will be able to identify wide range of patterns once it can recognize the yarns' boundaries and so the cross-over areas.

7 CONCLUSION

This work focused on identifying the pattern of the woven structure in addition to evaluating other surface characteristics utilizing digital image processing approach. The developed approach uses Wiener filter to decompose the fabric image into two sub-images each of them contains either warp yarn group or weft yarn group. The sub-images are further analyzed to outline yarns' boundaries and hence characterize fabric surface characteristics. Yarn diameter, yarn spacing, yarn count, densities in both directions and rational fabric cover factor are characterized. Yarns' boundaries are further used to identify the areas of interlace or the cross-over areas which processed to recognize the fabric structure. Six fabric samples are used in this study to evaluate the developed approach. The samples include three fabric structures with two constructions for each structure. The samples were analyzed manually using magnifier and the results were compared to the results of

the developed approach. The approach results showed good agreement compared to the pre-identified results for the samples having same color for both warp and weft yarns. On the other hand, the developed approach failed to analyze the sample that has extreme difference in colors of warp and weft yarns. The approach was not able to identify the yarns' boundaries of this sample and so the fabric surface characteristics. The large variation in colors of warp and weft yarn in this sample confused the image processing approach and gave false results by merging two adjacent yarns or splitting one yarn into two. The developed approach also gives us better understanding of how the weaving process could alter some of yarn's dimensions and hence gives more accurate results for yarn spacing and rational fabric cover factor.

Acknowledgement: *This work was supported by the research project funded by the Deanship of Scientific Research, King Abdulaziz University, Saudi Arabia.*

8 REFERENCES

1. Cybulska M.: Analysis of Warp Destruction in the Process of Weaving Using the System for Assessment of the Yarn Structure, *Fibres & Textiles in Eastern Europe* 5(4), 1997, 68-72
2. Pohle E.: Interlaboratory Test for Wool Fineness Using the PiMc, *J. Testing Eval.* 3, 1975, 24-26
3. Berlin J., Worley S., Ramey H.: Measuring the Cross-Sectional Area of Cotton Fibers with an Image Analyzer, *Textile Res. J* 51, 1981, 109-113
4. Thibodeaux D., Evans J.: Cotton Fiber Maturity by Image Analysis, *Textile Res. J.* 56, 1986, 130-139
5. Watanabe A., Kurosaki S., Konoda F.: Analysis of Blend Irregularity in Yarns Using Image Processing, *Textile Res. J.* 62, 1992, 729-735
6. Zhao W., Johnson N., Willard A.: Investigating Wool Fiber Damage by Image Analysis, *Textile Res. J.* 56, 1986, 464-466
7. Żurek W., Krucińska I., Adrian H.: Distribution of Component Fibers on the Surface of Blend Yarns, *Textile Res. J.* 52, 1982, 473-478
8. Cybulska M.: Assessing Yarn Structure with Image Analysis Methods, *Textile Res. J.* 69, 1999, 369-373
9. Masajtis J.: Thread Image Processing in the Estimation of Repetition of Yarn Structure, *Fibres & Textiles in Eastern Europe* 10 (4), 1997, 68-72
10. Wu Y., Pourdeyhimi B., Spivak M.: Texture Evaluation of Carpets Using Image Analysis, *Textile Res. J.* 61(7), 1991, 407-419
11. Jasińska, I.: Assessment of a Fabric Surface after the Pilling Process Based on Image Analysis, *Fibres & Textiles in Eastern Europe* 17(2), 2009, 55-58
12. Semnani D. et al.: Surface Roughness Measurement of Weft Knitted Fabrics Using Image Processing, *Fibres & Textiles in Eastern Europe* 19(3), 2011, 55-59
13. Mirjalili S.A., Ekhtiyari E.: Wrinkle Assessment of Fabric Using Image Processing, *Fibres & Textiles in Eastern Europe* 18(5), 2010, 60-63
14. Huang X., Bresee R.: Characterizing Nonwoven Web Structure Using Image Analysis Techniques, *INDA* 5, 1993, 13-211
15. Shady, E., et al.: Detection and classification of defects in knitted fabric structures, *Textile Res. J.* 76(4), 2006, 295-300
16. Zhang Y.F., Bresee R.R.: Fabric Defect Detection and Classification Using Image Analysis, *Textile Res. J.* 65, 1995, 1-9
17. Liqing L., et al.: Automatic recognition of fabric structures based on digital image decomposition, *Indian J. of Fiber & Textile Res.* 33, 2008, 388-391
18. Sezgin, M. and Sankur, B.: Survey over image threshold techniques and quantitative performance evaluation, *Journal of Electronic Imaging* 13(1), 2003, 146-165
19. Pierce, F.T.: The Geometry of Cloth Structure, *J. Textile Inst.*,28(3), 1937, 45-96

CHARAKTERIZACE STRUKTURY TKANIN ZALOŽENÁ NA ANALÝZE OBRAZŮ

Translation of the article
Image Processing Based Method for Evaluation of Fabric Structural Characteristics

Abstrakt: Pro určování strukturních parametrů tkanin a vazby je využito analýzy digitálních obrazů a Wienerova filtru. Pro analýzu je použito šesti různých skupin s různou strukturou a konstrukcí. Obraz tkaniny se rozkládá na dílčí obrazy obsahující buď útkové nebo osnovní nitě. Pro určení povrchových charakteristik a detekci struktury tkanin se používají hranice nití. Z analýzy obrazů se určují také dostavy resp. faktor zakrytí tkanin. Výsledky jsou porovnány s analytickými postupy výpočtu strukturních parametrů tkanin a vazby.

INVESTIGATION OF WARP STREAK PROBLEM IN A WOVEN FABRIC COMPOSED OF 100 % POLYESTER AIR TEXTURED YARN

Syed Zameer Ul Hassan[1], Jiri Militky[2] and Ali Asghar[3]

[1,2]Dept. of Textile Materials, Faculty of Textile Engineering; Technical University of Liberec, Studentská 2, 461 17 Liberec, Czech Republic
[1,3]Dept. of Textile Engineering, Faculty of Engineering, Balochistan University of Information Technology, Engineering and Management Sciences, Quetta, Pakistan
syed.zameer@buitms.edu.pk

Abstract: *Air-jet texturing is a well-established filament yarn processing technology that has been around for more than half a century. This study analyzed a serious warp streak problem in a woven fabric produced for car seats composed of 100 % Polyester air textured yarn. Yarn variability regarding stress-strain properties, structural behavior of two samples of yarn and the yarn diameter variations is being investigated. One of the yarn samples was producing these defects in the fabric and the other not producing this defect. Moreover the comparison of the influence of these parameters on both the samples is being monitored. Variation in the behavior of these samples is also observed.*
Keywords: *Air textured, Warp Streak, Yarn variability, Stress-strain properties.*

1 INTRODUCTION

The basic constructional element of a yarn and of any textile product is the fiber. The specific weight of a textile fiber and particularly its geometric properties determine the performance characteristic of a textile product from the view point of its bulkiness. In the majority of textile products two important functional properties are required: protection and thermal insulation. Both these can be satisfied by adequate bulkiness of the product.
In general a bulky product will have to be made of bulky raw material, i.e. fiber, yarn. Thus bulkiness has been traditionally one of the main requirements of textile manufacturers. As due to their geometric properties a great number of textile raw materials lack the necessary bulkiness, there have been efforts made since long ago to impart higher bulk to such fibers.
The synthetics having low specific weight and the extremely important inherent property of thermo plasticity makes them a good choice to be texturized and subsequently heat set (stabilized) in this textured configuration. For this reason synthetic fibers have become an ideal material for the production of high bulk textiles. The process in which the bulkiness of synthetic fibers, yarns and products is developed and increased is generally called “the texturing process”. Several techniques have been introduced for the increment of the bulkiness; some of them are Conventional process, False twist process, Stuffer box texturizing, Knit de knit texturing system and last but not the least is Air textured technology.
The production of air textured yarns was launched in late 70s at the Hedva n.p. in Liberec and the yarns have been marketed under the trade mark MIRLAN. The system is covered by a Czechoslovak patent No.106, 675. Air-jet textured yarns are produced from thermoplastic, cellulosic or nonorganic filaments yarns using a turbulent fluid, which is usually compressed air [1-3].
When the overfed filaments enter the texturing nozzle, they are carried along through the nozzle, blown out from the texturing end, and are formed into loops which are mutually trapped in the yarn structure by the effect of the supersonic and

turbulent air stream and forms a textured yarn structure. The supply yarn is normally wetted just before it is fed into the texturing nozzle by passing it through a wetting unit. Wet texturing improves the quality of textured yarn produced. Textured yarn is taken up at right angles to the nozzle axis by the delivery rollers located after the nozzle. Another set of take-up rollers, running at slightly higher speeds than the delivery rollers, may be used before the high-speed winders to apply tension to the textured yarn in order to stabilize the loops formed during the process. The textured yarn is then wound up by means of a high-speed winding unit [5].

The main principles of air jet texturing system are Overfeeding, Bending & Rotating, Wetting and Stretching. The main processing variables in air texturing are overfeed, air pressure, yarn wetting, stretch, operating condition, production speed, air-texturing jet, mechanical stabilization, heat-setting, yarn lubrication and package build. The variation of these parameters is believed to influence the final air textured yarn structure to varying degrees [4, 5].

Mechanical properties of polyester multifilament yarns are reasonably changed by air texturing. Breaking tenacities of polyester air textured sewing threads are markedly less than that of the raw polyester thread. This is due to core-wrap structure of the air-textured threads and the disordering of filaments of core threads during air texturing. Polyester threads are pretty less responsive to loop testing if compared with straight thread test than the raw polyester yarn. Air-pressure and overfeed in texturing are influential factors in respect of stress-strain properties [6].

Due to an increase in air pressure, the tenacity and breaking elongation of air textured yarns is reduced where as by increasing the texturing speed the yarn tenacity and breaking elongation are both dropped initially then begin to increase [7].

Textured yarns always show variation in their behavior. Variability can arise in textured yarns from many causes – in the feed yarn, in process conditions, or in subsequent handling and manufacturing. There may be differences in fiber linear density (Tex) and fiber internal structure, which then show up in bulk and crimp. The major problem is that very small differences in shade, which are not easy to pick up by analytical methods, can be detected by the eye, particularly in uniform shades of critical colors. These differences may be due to physical form, e.g. bulk differences affecting luster or variability in dye uptake. This consequence consists of faults called barre or streak in fabrics.

A difference in a single yarn from its neighbors may be of too small, a size to be resolved by the eye and so will not be detectable, but when several similar yarns happen to come together, the barriness will be objectionable. If each yarn is itself very regular, then differences between yarns are very apparent; but if the yarns have appreciable short term variability, which is not objectionable, then the differences between yarns are less apparent [8].

The main causes of streak during the texturing process may be due to the fluctuation of yarn temperature at the outlet of heater, irregular yarn and the mechanical structure of the final package [2, 9].

In this paper we analyze the above mentioned causes of barre in the woven fabric produced by 100 % Polyester air textured yarn by realizing the stress-strain properties, yarn diameter variations and the structural behavior of the yarns.

2 EXPERIMENTAL PART

The two samples of yarn provided by Fezko Company were compared. One sample was creating the warp streaks in the fabric and the other one without creating any streaks. Both samples were 100% Polyester air textured dyed filaments of 520 dtex. All the testing was carried out on the basis of comparison between these two provided samples:

- Yarn creating no streaks in the fabric, Sample A.
- Yarn creating streaks in the fabric, Sample B.

The force and elongation tests were being conducted on Instron 4411. The tests were provided at gauge length (500±1) mm, testing speed 250 mm/min and the specimen pretension of 0.260 N. The temperature and humidity of the lab was 22.6°C and 60% respectively. All the tests were processed with *blue hill* software. During the test 150 measurements were taken for sample A and sample B each and these parameters were obtained: Breaking Force [N], Elongation at break [%], Breaking Tenacity [cN/tex] and Young's Modulus [gf/tex]. Matlab and SPSS programs were used for the evaluation and graphical representation of these parameters.
The longitudinal view of both the yarns was observed using the Digital Microscopy Imaging, TESCAN. The yarn samples for this study were prepared precisely on SCD 030 (Balzers) quoted with gold and the images were taken at different scales; 2 mm, 500 µm, 50 µm and 10 µm.
The both samples of yarns were tested for measuring the diameter using NIS Elements. 850 images were taken during the test for sample A and sample B each. The dilation was carried out with the recommended length of 51 pixels and calibration was being done at 3.67 µm/pixel. These images were then processed on Matlab for the measurement of the diameter.

3 RESULTS AND DISCUSSION

The mean values of the measured parameters (Force-Elongation) are shown in the Table 1 and Table 2 for sample A and sample B respectively. It was seen that the standard deviation, variance and coefficient of variation is on the higher side in case of sample B.
The comparison of both samples for the relation between Force-Elongation at break and Tenacity-Elongation at break on the basis of the above results is shown in the Figure 1 and Figure 2, respectively. The variation and more dispersion of the values in sample B is quite visible as compared to sample A.

Table 1 The measured values of sample A

	Elongation at break [%]	Breaking Force [N]	Breaking Tenacity [cN/tex]	Energy at Break [mJ]	Young's Modulus [gf/tex]
Total No of Tests	150	150	150	150	150
Mean Value	26.58	16.04	30.85	934.90	154.58
Standard deviation	1.68	0.54	1.04	41.40	2.95
Variance	2.84	0.29	1.09	1714.31	8.72
Coefficient of variation [%]	6.34	3.38	3.38	4.43	1.91
Minimum value	23.23	14.49	27.86	839.90	144.40
Maximum value	31.92	17.27	33.21	990.53	160.95

Table 2 The measured values of sample B

	Elongation at break [%]	Breaking Force [N]	Breaking Tenacity [cN/tex]	Energy at Break [mJ]	Young's Modulus [gf/tex]
Total No of Tests	150	150	150	150	150
Mean Value	27.80	16.64	32.01	1276.89	154.57
Standard deviation	3.84	1.43	2.76	299.52	7.79
Variance	14.74	2.06	7.60	89713.56	60.61
Coefficient of variation [%]	13.81	8.61	8.61	23.46	5.04
Minimum value	16.69	11.63	22.37	491.04	141.87
Maximum value	33.02	18.22	35.03	1679.41	188.53

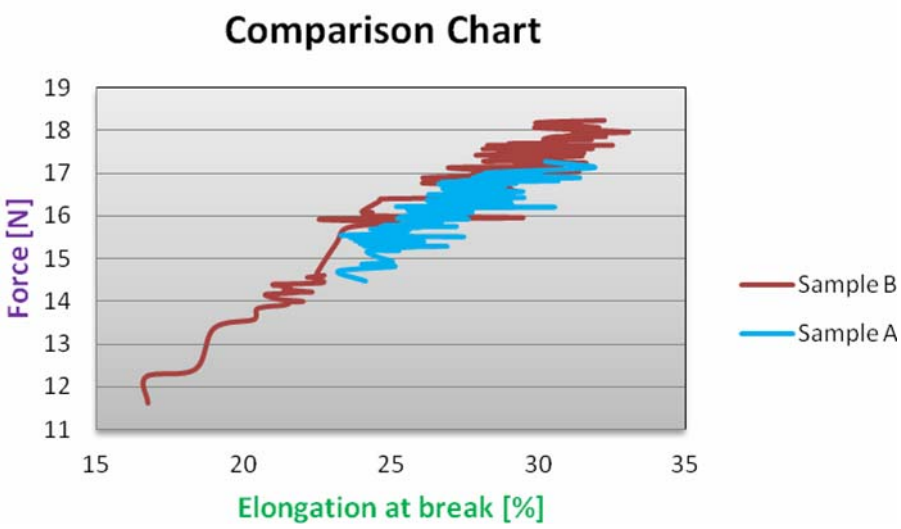

Figure 1 Comparison for Force and Elongation at break

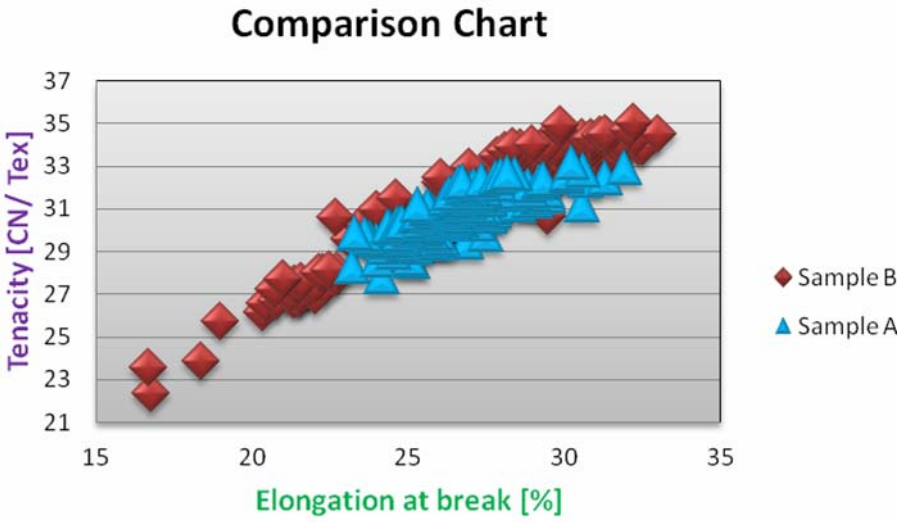

Figure 2 Comparison for Tenacity and Elongation at break

The histograms for force and elongation parameters with the relative frequencies are shown in the Figure 3 with sample A on the left hand side and sample B on the right hand side. The higher variation can be seen in case of sample B.

Finally the mean stress strain curve of both yarn samples was derived with the help of MATLAB as shown in Figure 4 and Figure 5 for sample A and sample B, respectively.

The difference of lower strength and lower elongation in the case of sample B is quite visible. The dotted line shows the gap between the minimum elongation and the mean value and we can observe the huge distance in sample B which is a sure sign of wide spread and variations in this yarn sample.

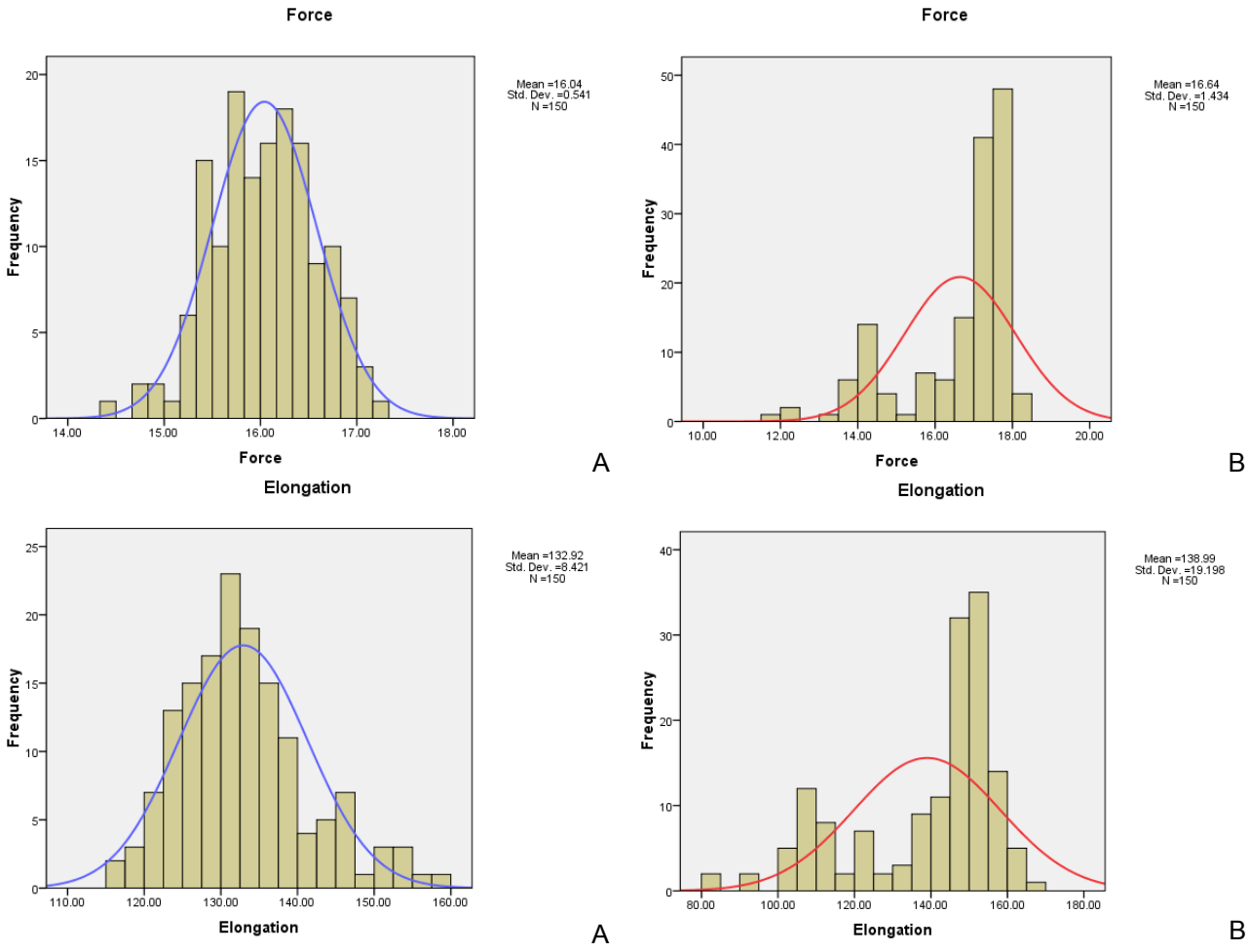

Figure 3 Upper row is comparison of the Force values with relative frequencies and the lower row is between Elongation values

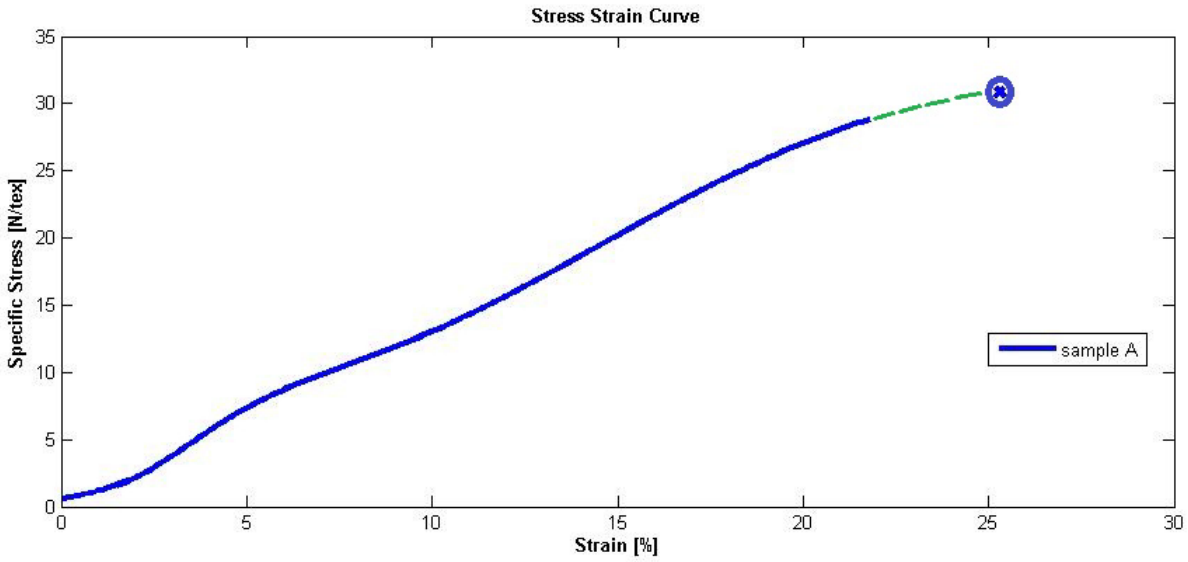

Figure 4 Mean stress strain curve of sample A

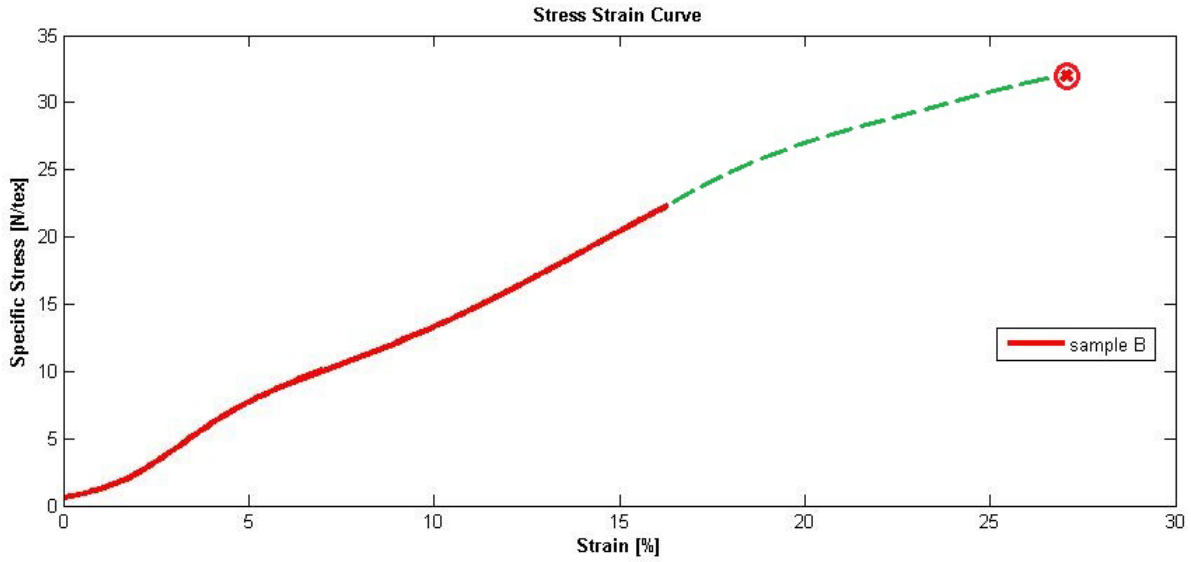

Figure 5 Mean stress strain curve of sample B

The images taken from the electron microscope were viewed in comparison of the sample A (left hand side) and sample B (right hand side). From the following Figure 6, it is quite obvious that the sample B shows quite different structural behavior of texturing. The bulk is more as compared to the sample A and we can see the arrangement of fibers not oriented and the helix angle is increasing at yarn surface where as in the case of sample A there is more orientation. If we compare (d) and (h), we can observe the scales and quite rough appearance of the fibers of the sample B where as in case of sample A there is smooth and rather clean surface.

The comparison of the calculated values for the yarn diameter is shown in the Table 3. The parameters Maxs (the longest possible distance between yarn boundaries), Mins (the longest possible distance between yarn boundaries) and Diameter D_1 (the real diameter of the cylinder where can be yarn) are calculated using Matlab program. We can observe the higher values and higher variation in sample B which shows more unevenness as compared to the sample A.

Table 3 Comparison of the calculated parameters of both samples

	Maxs [µm]		Mins [µm]		D_1 [µm]	
	Sample A	**Sample B**	**Sample A**	**Sample B**	**Sample A**	**Sample B**
Mean Value	601.912	597.847	370.268	384.352	637.507	640.254
Standard deviation	91.0538	93.7562	55.1604	58.2931	93.0204	97.3794
Coefficient of variation [%]	15.1274	15.6823	14.8974	15.1666	14.5913	15.2095
Upper Limit	608.234	604.352	374.103	388.406	643.965	647.003
Lower Limit	595.591	591.342	366.434	380.297	631.049	633.506
Median	601.88	601.88	370.67	385.35	634.91	645.92

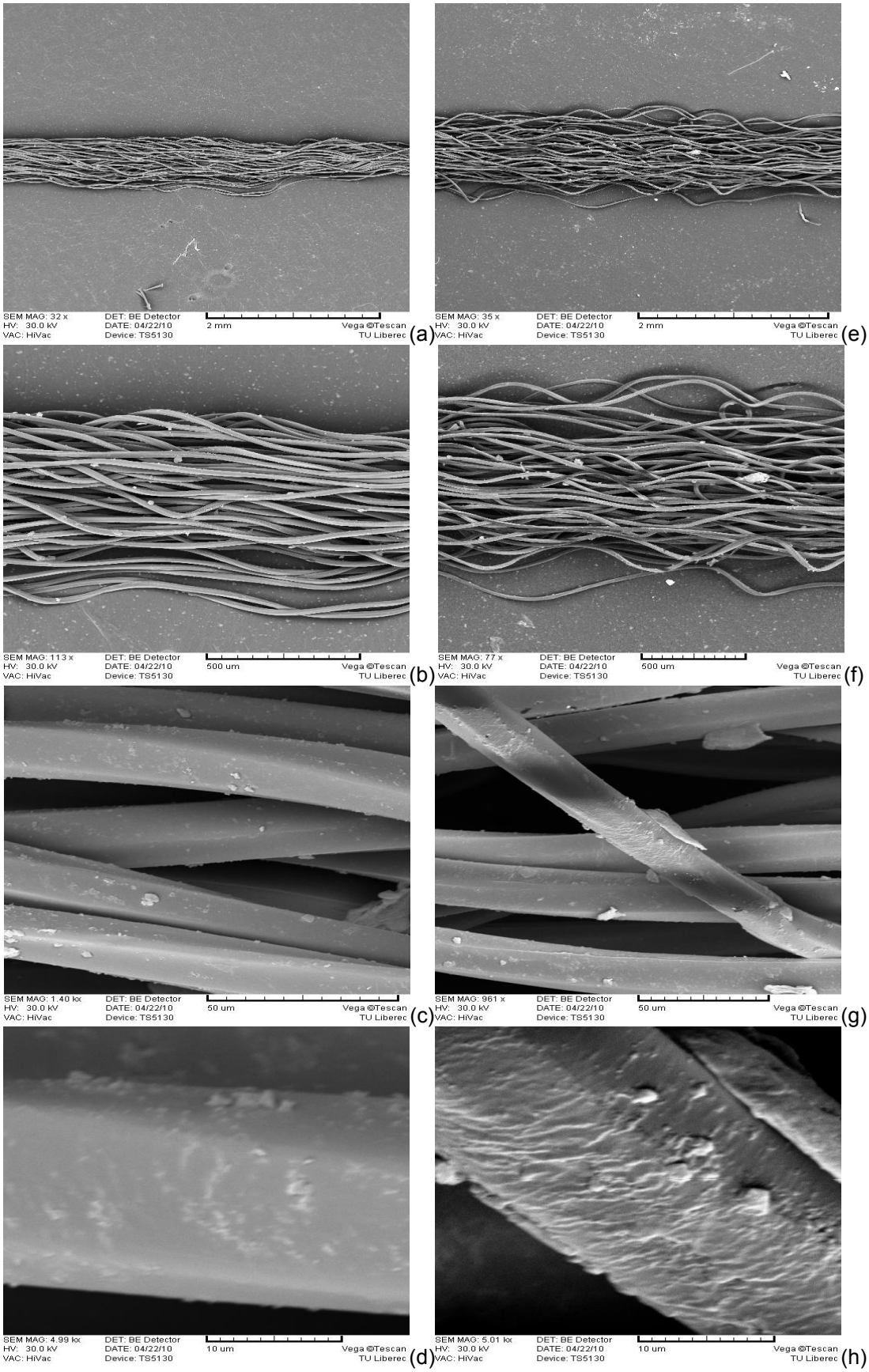

Figure 6 1Appearance of sample A on the left hand side at magnification (a) 2 mm (b) 500 μm (c) 50 μm (d) 10 μm and sample B on the right hand side at same magnification (e) 2 mm (f) 500 μm (g) 50μm (h) 10 μm

4 CONCLUSION

Mechanical properties of sample B show more variations as compared to sample A. Breaking tenacities, Breaking Force and Young's modulus values have a high rate of dispersion and more coefficient of variation as in the case of sample B, where as in sample A, these values show a lower dispersions. This variation in this typical stress strain behavior may cause variation in the subsequent process of manufacturing the textured fabric resulting in the form of visible streaks in the fabric. Moreover the irregular bulk, disorientation of fibers and the scales on the surface in the case of sample B may cause the streakiness also.

These variations in stress strain properties, structural geometry and the excess of dispersion in diameter in the case of sample B which is reported as defect producing yarn justifies the statement. These variations may be a source of indication regarding inappropriate texturing process. It is also concluded that sizing must be applied on the warping yarns to have a suitable even distribution of load during warping and weaving process.

For future work it is recommended to analyze the fabric containing the yarns responsible for this defect of streakiness regarding dyeing unevenness, shade variation and the mechanical properties.

Acknowledgements: *The Authors would like to thank Fezko Industry Strakonice, for their assistance in the process monitoring and arranging the yarn samples.*

5 REFERENCES

1. Piller B.: *Bulked Yarns,* Prague: SNTL Publishers of Technical Literature, 1973
2. Hes L., Ursiny P.: *Yarn Texturizing Technology,* Eurotex, 1994
3. Acar M.: Use of air jets in yarn texturing processes, *International Fiber Journal*, 1989
4. Rengasamy R.S, Das B.R., Patil Y.B.: Thermo physiological comfort characteristics of polyester air jet textured and cotton yarn fabrics, *The Journal of the Textile Institute* 100(6), 2009, 507-511
5. Dani N.P.: The Fundamentals of Air Jet Texturing, 2004
6. Jing Z., et al.: Investigation on Air Texturing Process for Diacetate Blending with polyester filaments, *Fibers and Polymers* 8(1), 2007, 84-88
7. Zauraite J., et al: The Dependence of Air textured PES Thread Mechanical Properties on Texturing Parameters, *Materials Science (Medziagotyra)* 13(4), 2007, 333-336
8. Hearle J.W.S., Hollick L., Wilson D.K.: *Yarn Texturing Technology,* Cambridge: Woodhead Publishing Ltd, 2001
9. Mahall K.: *Quality Assessment of Textile,* 2nd, Berlin, Springer-Verlag, 1993

SLEDOVÁNÍ ÚTKOVÉ PRUHOVITOSTI TKANIN ZE 100 % NÍHO POLYESTEROVÉHO VZDUCHEM TVAROVANÉHO HEDVÁBÍ

Translation of the article

Investigation of warp streak problem in a woven fabric composed of 100 % polyester air textured yarn

Abstrakt: Výroba vzduchem tvarovaného polyesterového hedvábí je známa více než půl století. V tomto příspěvku jsou analyzovány problémy spojené se vznikem útkové pruhovitosti tkanin určených pro automobilové sedačky, které jsou tvořené ze 100 % ního polyesterového vzduchem tvarovaného hedvábí. Pro zkoumání jsou použity dva typy tvarovaného hedvábí. Jeden, jehož použití vede ke vzniku útkové pruhovitosti je porovnán s druhým, který nevede ke tvorbě útkové pruhovitosti. Jsou porovnány vybrané mechanické vlastnosti, struktura a kolísání průměru obou typů. Je porovnána také variabilita vlastností těchto materiálů.